View metadata, citation and similar papers at core.ac.uk
brought to you by CORE
provided by Helsingin yliopiston digitaalinen arkisto

UNIVERSITY OF HELSINKI REPORT SERIES IN PHYSICS

HU-P-D95

SOLUTIONS FOR CLINICAL IMPLEMENTATION OF BORON NEUTRON CAPTURE THERAPY IN FINLAND

MIKA KORTESNIEMI

Department of Physical Sciences
Faculty of Science
University of Helsinki
Helsinki, Finland

Helsinki 2002

UNIVERSITY OF HELSINKI REPORT SERIES IN PHYSICS

HU-P-D95

SOLUTIONS FOR CLINICAL IMPLEMENTATION OF BORON NEUTRON CAPTURE THERAPY IN FINLAND

Mika Kortesniemi

Department of Physical Sciences
Faculty of Science
University of Helsinki
Helsinki, Finland

ACADEMIC DISSERTATION

To be presented, with the permission of
the Faculty of Science of the University of Helsinki,
for public criticism in the Small Auditorium E204, Physicum,
on June 28th, 2002, at 12 o'clock noon.

Helsinki 2002

ISSN 0356-0961
ISBN 951-45-8954-8
ISBN 951-45-8955-6 (pdf-version)
http://ethesis.helsinki.fi/
Helsinki 2002
Yliopistopaino

"Enough knowledge of the remarkable behavior of neutrons has been accumulated through physical research to enable the prediction of certain biological effects, and to see, in general way at least, certain therapeutic potentialities of this new kind of corpuscular radiation."

Gordon J. Locher,
July 1936

M. Kortesniemi: Solutions for clinical implementation of boron neutron capture therapy in Finland, University of Helsinki, 2002, 97 p. + appendices, University of Helsinki, Report Series in Physics, HU-P-D95, ISSN 0356-0961, ISBN 951-45-8954-8, ISBN 951-45-8955-6 (pdf-version).

Classification (INSPEC): A2940P, A2970, A8760M, A8770H, B7500, B7520C
Keywords: medical physics, radiotherapy, BNCT, dosimetry, kinetics, patient positioning

ABSTRACT

Boron neutron capture therapy (BNCT) is an emerging binary radiotherapy method which utilises epithermal neutrons in conjunction with a boron biodistribution to treat patients with certain malignant brain tumours. BNCT can also be described as neutron activated chemotherapy. Without the neutrons the boron compound is functioning as a non-toxic agent which has certain temporal behaviour with respect to its concentration within various tissues. A period of time can be specified when boron is preferentially located in the tumour cells and the healthy tissue has a lower boron concentration. Only during that specific time window the tumour is irradiated with epithermal neutrons, thermalising and interacting with the boron atoms. Thereby the non-toxic boron atoms in the cancer tumour cells are activated by neutrons, producing highly toxic alpha and lithium particles hence killing the tumour cells. The requirement for BNCT to be successful is to have a large enough amount of ^{10}B in the tumour cell and then to have a sufficient amount of thermal neutrons around, reaching the boron atoms and causing the boron neutron capture reaction to occur. Thus there are three important factors in a successful BNCT treatment: the boron biodistribution at a certain period of time, the epithermal neutron field with a certain energy distribution and in the end a carefully set position which brings the neutron field and the boron biodistribution optimally together. As a result, the desired therapy effect is acquired in the correct position.

According to ICRU (International Commission of Radiation Units and Measurements) the uncertainty of the dose to the patient in external radiotherapy should not exceed 5% and the recommendation from the literature is below 3%. That sets high objectives for reliability and accuracy in patient positioning in addition to the boron level definition and beam dosimetry in BNCT. Accordingly, the objective of this work was to 1) develop the dosimetry methods of the FiR 1 BNCT beam, 2) estimate the blood boron level after a boronophenylalanine fructose (BPA-F) infusion and 3) implement a system for patient positioning in the Finnish BNCT facility.

The FiR 1 epithermal neutron beam of the Finnish BNCT facility was assessed extensively using various dosimetric methods, phantom materials and geometries. Measured and calculated doses were compared to verify the beam source model and the treatment planning system. The blood boron concentration during the treatment irradiations was estimated with a bi-exponential function fit. The accuracy of the boron estimation was tested on nine patients with 290 mg/kg – 400 mg/kg BPA infusions. A custom-made treatment coach was developed and used in patient positioning with a beam aperture simulator and laser crosshairs. Three positioning methods based on angular settings and distance alignments were studied with respect to spatial accuracy. The effect of positioning uncertainty on the doses was studied

with simulations. The combined uncertainty of the physical dose was assessed by combining data from different relevant factors.

The calculated and measured doses agreed within few percentages. The uncertainty of the blood boron estimation was less or equal than 0.5 ppm (1-3% 1SD). The spatial uncertainty of patient positioning by using the default entry/exit point alignment method was 5 mm (1SD) corresponding to a beam angular deviation of 2.6 degrees. The effect of 5 mm positioning uncertainty to the target dose is below 5%. The combined uncertainty of the total physical dose without the boron dose is 7% (1SD) due to the uncertainties in positioning and in neutron and gamma dose determination. The boron dose introduces considerable extra uncertainty to the total physical dose uncertainty.

Dosimetry, boron estimation and patient positioning have a combined effect on the reliability of the eventual patient dose. Due to the uncertainties related to neutron interaction data the level of dose accuracy recommended by ICRU should not be directly applied in BNCT. There are still obvious improvements that should be achieved to reduce the existing uncertainties. The dosimetry system provides functional means for dose assessment but the accuracy of the total dose should improve. Importance of reciprocal verification between measurements and calculations is emphasised in complex geometries. The large uncertainty related to the boron distribution in different tissues is a commonly acknowledged objective for future research. However, the blood boron estimation presented in this thesis works efficiently and with appropriate reliability. The developed application combining boron estimation with operational beam data forms a coherent interface for the treatment process. The developed patient positioning system offers a functional solution in BNCT where the conventional methods for positioning are only partly applicable. The beam entry/exit mark alignment used as a default positioning method and the mark angular method provides the best selectable accuracy for patient positioning. Still, technical improvements should be developed especially for head fixation. The static fixation of the patient with the existing beam aperture geometry will remain a challenging task but the time required for the complete positioning can be reduced significantly. The methods covered in this work provide practical means for BNCT and have been established in test use and in actual treatment situations.

PREFACE

This Ph.D. thesis is based on the work done by the author in the Finnish BNCT project during the years of 1997 through 2002. Dosimetry work begun in May-June 1997 when thermal neutron responses were measured with a semiconductor Si(Li) detector in LFR (low flux reactor) and HFR (high flux reactor) beams in Petten (Holland). Thereafter an experimental dosimetry campaign was initiated to study the FiR(K63) epithermal neutron beam in 1997. The beam was characterised in air and in phantoms applying different phantom geometries and materials during 1997-1999. Dosimetry intercomparison was performed between the beams in Brookhaven BNL/BMRR (USA) and FiR 1 (Finland) in 1999. Twin ionisation chambers were used to determine the total neutron and gamma doses. Semiconductor Si(Li) detector were used to determine the relative lithium reaction rates. Technical equipment and software were developed as technical prerequisites for the dosimetry measurements e.g. the program for the three dimensional detector movements in the water phantoms.

In 1998 a bi-exponential function was chosen based on the published data to describe the blood boron concentration of the patient after a BPA-F infusion. An iterative gradient search algorithm was implemented for the bi-exponential function fitting according to the measured blood boron values. A software application utilising the bi-exponential model was created for clinical use to provide estimates of the average blood boron concentrations during the treatment irradiations. Later in 2001 the application was expanded to combine the operational beam data and the blood boron estimation as an active document interface.

During 1998-1999 a custom made treatment coach, beam simulator and coordinate system was planned and implemented for patient positioning and fixation in the Finnish BNCT facility. The spatial accuracy of the positioning system was determined with three alternative positioning methods in early 2002. The effect of the spatial accuracy on the doses was determined with SERA simulation in the spring 2002.

Sections of the work have been presented in six publications which include a report annex, two journal articles and three conference proceedings:

I. M. Kortesniemi, A. Kosunen, C. Aschan, T. Serén, P. Kotiluoto, M. Toivonen, P. Välimäki, T. Seppälä, I. Auterinen, and S. Savolainen, *Measurements of phantom dose distributions at the Finnish BNCT facility*, in *Frontiers in Neutron Capture Therapy*, M.F. Hawthorne, K. Shelly, and R.J. Wiersema, Editors. 2001, Plenum Publishing Corporation: New York. p. 659-664.

II. A. Kosunen, M. Kortesniemi, H. Ylä-Mella, T. Seppälä, J. Lampinen, T. Serén, I. Auterinen, H. Järvinen, and S. Savolainen, *Twin ionisation chambers for dose determinations in phantom in an epithermal neutron beam.* Radiation Protection Dosimetry, 1999. 81(3): p. 187-194.

III. P. Ryynänen, M. Kortesniemi, J. Coderre, A. Diaz, P. Hiismäki, and S. Savolainen, *Models for estimation of the 10-B concentration after BPA-fructose complex infusion in patients during epithermal neutron irradiation in BNCT.* Int J Radiat Oncol Biol Phys, 2000. 48(4): p. 1145-1154.

IV. T. Seppälä, M. Kortesniemi, L. Kankaanranta, P. Perkiö, I. Auterinen, and S. Savolainen. *Patient positioning according to dose planning in BNCT at FiR 1*. in *Medical & Biological Engineering & Computing*. 1999. Tallinn: IFMBE. p. 402-403.

V. T. Serén, M. Kortesniemi, C. Aschan, T. Seppälä, J. Lampinen, I. Auterinen, and S. Savolainen. *A tale of two beams - comparison of the radiation fields at the BMRR and FiR 1 epithermal BNCT facilities*. in *Medical & Biological Engineering & Computing*. 1999. Tallinn: IFMBE. p. 396-397.

VI. T. Seppälä, S. Savolainen, I. Auterinen, C. Aschan, P. Hiismäki, M. Kortesniemi, A. Kosunen, P. Kotiluoto, T. Serén, and M. Toivonen. *Determining and reporting the doses in the treatments of glioma patients in the epithermal neutron beam at the Finnish BNCT facility (FIR 1), Annex 9 - Dose Reporting, in: Current status of neutron capture therapy*, *IAEA Tecdoc-1223*. 2001, IAEA, Wien. p. 275-287.

The beam dosimetry part of this thesis (Chapter 3) concentrates on the dose determination in the ellipsoidal water phantom which has not been previously published. The boron distribution part (Chapter 4) presents new results of the bi-exponential blood boron estimation applied to nine patients with varying boron infusions. The patient positioning part (Chapter 5) describes the positioning and fixation system which has been introduced only briefly in the previous publication. The positioning accuracy study and the dose simulations in Chapter 5 provide unpublished data.

A monograph form was chosen for this thesis to join the studied methods relating to clinical implementation of BNCT in Finland. Some technical solutions facilitating the presented methods could otherwise have been left unpublished e.g. the head arc-fixation scheme (presented in Chapter 5) which is currently in preparation for patent application. The resulting manuscript provides a comprehensive description of the BNCT implementations in the areas of dosimetry, boron estimation and patient positioning. An estimation of the combined physical dose uncertainty is presented based on this description.

CONTENTS

ABSTRACT 1

PREFACE 3

NOMENCLATURE 7

1 AIM OF THE STUDY 9

2 INTRODUCTION 10
2.1 Radiotherapy 10
2.2 Conventional radiotherapy methods 11
2.3 BNCT principle and history 11
2.4 Neutron sources 13
2.5 Dose components 16
2.6 Beam dosimetry – the first objective 16
2.7 Treatment planning 18
2.8 Boron concentration in blood – the second objective 19
2.9 Patient positioning – the third objective 20
2.10 BNCT facilities 20
2.11 Radiobiological studies 21
2.12 Clinical trials 21

3 BEAM DOSIMETRY 23
3.1 Materials and dosimetry methods 23
3.1.1 Epithermal neutron beam 23
3.1.2 Detectors 25
3.1.3 Dose determination with ionisation chambers 27
3.1.4 Phantoms 28
3.1.5 Dose calculations 30
3.2 Dosimetry results 31
3.2.1 Neutron and gamma dose in ellipsoidal water phantom 31
3.2.2 Neutron and gamma dose in ellipsoidal and cylindrical geometries 35
3.2.3 Thermal fluences in ellipsoidal and cylindrical water phantoms 35
3.2.4 Gamma doses in ellipsoidal phantom displacement study 37
3.3 Dosimetry discussion 38

4 BORON CONCENTRATION IN BLOOD 45
4.1 Materials and boron estimation methods 45
4.1.1 Boron infusion and measurements 47
4.1.2 Estimation model 48
4.2 Estimation results 49
4.3 Boron discussion 51

5 PATIENT POSITIONING 54
5.1 Materials and positioning methods 55
5.1.1 Coordinate system 56
5.1.2 Fiducial marking in preparative positioning 57
5.1.3 Beam alignment 58
5.1.4 Positioning procedure 59
5.1.5 Fixation 60
5.1.6 Spatial accuracy 61
5.1.7 Effect of positioning accuracy on the dose 63
5.2 Positioning results 63
5.2.1 System implementation 64
5.2.2 Spatial accuracy results 66
5.2.3 Dose effect results 67
5.3 Positioning discussion 68

6 GENERAL DISCUSSION 73
6.1 Quality control 73
6.2 The treatment log 74
6.3 Uncertainty of the dose 76
6.4 Future of BNCT 77

7 CONCLUSIONS 78

ACKNOWLEDGEMENTS 79

REFERENCES 81

List of figures 93

List of tables 96

APPENDICES 97

NOMENCLATURE

1SD	One standard deviation
2D	Two dimensional
3D	Three dimensional
A150	Plastic substitute material for muscle tissue
BBB	Blood brain barrier
BNCEFNT	Boron neutron capture enhanced fast neutron therapy
BNCT	Boron neutron capture therapy
BNL/BMRR	Brookhaven National Laboratory/Brookhaven Medical Research Reactor
BPA-F	Boronophenylalanine fructose
BSH	^{10}B enriched sodium mercaptododecaborate
BUGLE	Coupled neutron and gamma ray group cross section library
CADSCAN	Water phantom system (Dosetek Oy)
CT	Computed tomography
CTV	Clinical target volume
CV	Coefficient of variation
DORT	Two dimensional discrete ordinates (deterministic) transport code
DVH	Dose volume histogram
EMA	Entry/Exit mark alignment method
FCB	Fission converter beam
FiR 1	Finnish research reactor located in Otaniemi, Espoo
FNT	Fast neutron therapy
GBM	Glioblastoma multiforme
GCP	Good clinical practice
GTV	Gross tumour volume
HFR	High Flux Reactor (Petten, Holland)
HUCH	Helsinki University Central Hospital
HUS	Hospital district of Helsinki and Uusimaa
IAEA	International Atomic Energy Agency
IC	Ionisation chamber
ICP-AES	Inductively coupled plasma atomic emission spectroscopy
ICRU	International Commission of Radiation Units and Measurements
IMRT	Intensity modulated radiotherapy
ISNCT	International Society of Neutron Capture Therapy
LET	Linear energy transfer
LFR	Low Flux Reactor (Petten, Holland)
MAP	Mark angles to plane alignment method
MC	Monte Carlo
MCA	Multichannel analyser
MCNP	General Monte Carlo N-Particle Transport Code
MDA	Mark distances to aperture alignment method
MRI	Magnetic resonance imaging
MRS	Magnetic resonance spectroscopy
NIM	Nuclear instrumentation modules
PET	Positron emission tomography
PGNAA	Prompt gamma neutron activation analysis
PMMA	Polymethylmethacrylate
PRV	Planning organs at risk volume

PSDL	Primary standard dosimetry laboratory
PTFE	Polytetrafluoroethylene (Teflon)
PTV	Planning target volume
QC	Quality control
RBE	Relative biological effectiveness
RSVP	Radiosurgery verification phantom (Phantom Laboratory)
SERA	Simulation environment for radiotherapy applications
SOP	Standard operational procedures
SSDL	Secondary standard dosimetry laboratory
STUK	Finnish Radiation and Nuclear Safety Authority
TAP	Transaxial plane
TE	Tissue equivalent
TEPC	Tissue equivalent proportional counter
TLD	Thermoluminescent dosimeter
TPS	Treatment planning system
UNSCEAR	United Nations Scientific Committee on the Effects of Atomic Radiation
VTT	Technical Research Centre of Finland

1 AIM OF THE STUDY

Boron neutron capture therapy (BNCT) is an emerging radiotherapy modality using a mixed epithermal neutron beam acting in conjunction with the boron biodistribution to treat patients with brain cancer. According to ICRU the uncertainty of the dose to the patient in external radiotherapy should not exceed 5% and the recommendation from the literature is below 3% [1-3]. That renders strong objectives for reliability and accuracy of patient positioning in addition to boron concentration prediction and beam dosimetry in BNCT.

The aim of this study is to

- develop the dosimetry system of the FiR 1 BNCT beam,
- provide an estimate of the blood boron concentration during the treatments,
- develop a patient positioning system for the static beam aperture of the Finnish BNCT facility.

These objectives are included in a more general objective which is the clinical implementation of BNCT in Finland.

2 INTRODUCTION

2.1 Radiotherapy

Radiotherapy means a clinical modality using the deterministic effects of radiation to kill the malignant tumour cells. The efficacy of the radiotherapy is based on the radiosensitivity of the malignant cells and the ability of the healthy tissue to recover from the effects of radiation. Treatment is directed to a defined target volume by a treatment planning system (TPS) [4-6]. Thereby a radiation dose is locally directed to the tumour tissue in amount which is assessed to be sufficient to eradicate the tumour but which does not cause intolerable effect on the surrounding healthy tissues. The separation between these two contradictory outcomes can be faint which is the reason for the common adverse effects of radiotherapy [6, 7]. The principle of the effects of radiotherapy on the healthy tissue and the tumour as a function of radiation dose is presented in Figure 1.

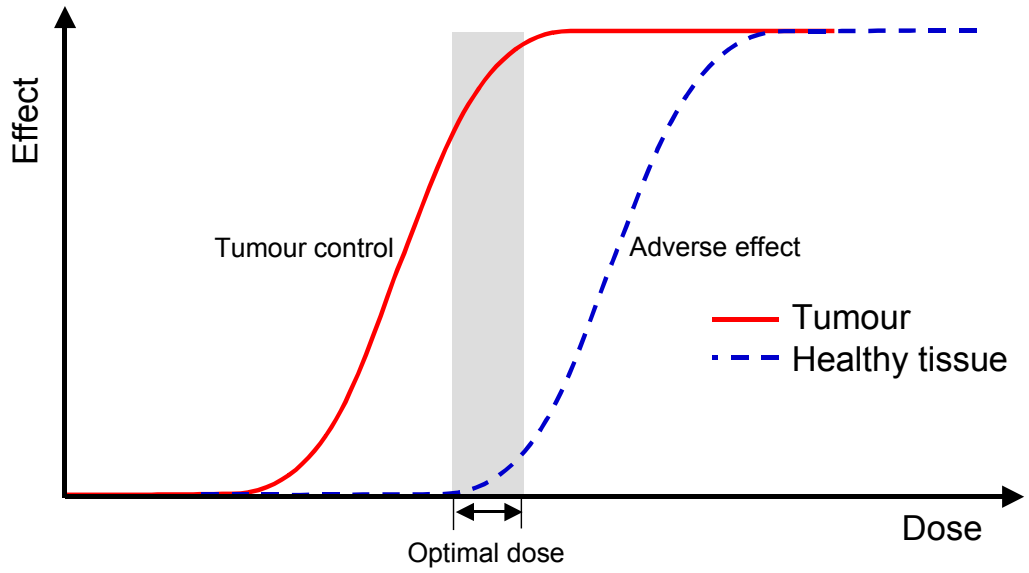

Figure 1. *The optimal dose for the radiotherapy application. The tumour tissue suffers from the radiation dose which is still tolerated by the healthy tissue. The width of the window sets the upper and the lower limit for the dose which is applied to the target volume.*

The separation between two efficacy curves determines the dosimetry window for the radiotherapy application. This window width is variable in each individual patient, normal tissue and with different tumour types. Furthermore, often the adverse effects start to appear in the healthy tissue before the desired eradication of the tumour occurs properly. Therefore the therapeutic dose should be administered with a high accuracy, enabling the fine balancing between tolerable healthy tissue damage and therapeutic efficacy. That balancing forms the basis for the accuracy recommendations of the absorbed dose in radiotherapy [1, 2, 6, 8]. The accuracy issue is emphasised in the entire area of dosimetric metrology as the traceability chain of the dose calibrations and measurements from the primary standard to the therapy applications should follow almost an unchangeable level of accuracy. Appropriate therapeutic dose accuracy is therefore at the level normally stipulated only for the measurements in established standard laboratory conditions [1, 8-10].

2.2 Conventional radiotherapy methods

Conventional external beam radiotherapy utilises high energy photon or electron beams as the most common form of primary radiation [11]. This kind of radiation is described as low linear energy transfer radiation since the energy depositions to the media in a form of ionisations occur only sparsely [12]. In the typical clinical settings these high energy radiation beams are created by linear accelerators or microtrons. Still a ^{60}Co gamma source or betaron for electron acceleration can be seen in some locations as an obsolete technique [7].

The required accuracy of the absorbed dose for radiotherapy is dependent on modern diagnostical and therapeutic imaging modalities, efficient treatment planning systems and especially accurate beam delivery techniques. These techniques include the beam technology itself but also the positioning solutions to realise the high accuracy of the target volume definition. The relative biological effectiveness of the ionising radiation is a function of the linear energy transfer (LET) which is unique to different types of radiation. Therefore the use of high-LET radiation instead of the conventional low-LET radiation may bring the same biological response but with a lower physical dose [12]. In fast neutron therapy (FNT) the high-LET radiation characteristics of neutrons have been utilised for many years. The few successful applications of FNT have focused on the treatments of inoperable salivary gland tumours, locally advanced prostate cancers and soft tissue sarcomas [13]. Proton beams has also been used as a form of high-LET external beam therapy [14-16].

Considerable development has occurred in external beam techniques since the earlier radiation sources. In modern external beam applications the patient dose distribution for the target volume and the surrounding healthy tissue can be optimised using multidirectional beams with modified shape and intensity [17]. One of the most important advances has been introduced by IMRT (intensity modulated radiotherapy) as a type of three-dimensional conformal radiotherapy which support specifically these complex beam delivery schemes [17-19]. The beam can be moved while the patient can be fixed in one position. The patient does not have to be in close contact with the beam structure which makes it easier to implement complex beam movements together with simple and comfortable patient positions.

2.3 BNCT principle and history

Boron neutron capture therapy (BNCT) is a binary radiotherapy modality which utilises epithermal neutrons together with a boron biodistribution for treatment of cancer. At the beginning the patient is given an intravenous infusion of a non-toxic ^{10}B-carrier compound which is then distributed in various tissues in the body. Then an appropriate interval time is waited when boron is preferentially concentrated in the tumour cells. During that specific time window the tumour with a higher ^{10}B-concentration than the surrounding healthy tissue is irradiated with epithermal neutrons, thermalising and interacting with the boron atoms. Thereby the non-toxic boron atoms in the cancer tumour cells are activated by neutrons producing highly toxic alpha and lithium particles killing the tumour cell. The requirement of BNCT to be successful is to have a large enough amount of ^{10}B in the tumour cell and then have a sufficient amount of thermal neutrons around, reaching the boron atoms and causing the boron neutron capture reaction to occur [20].

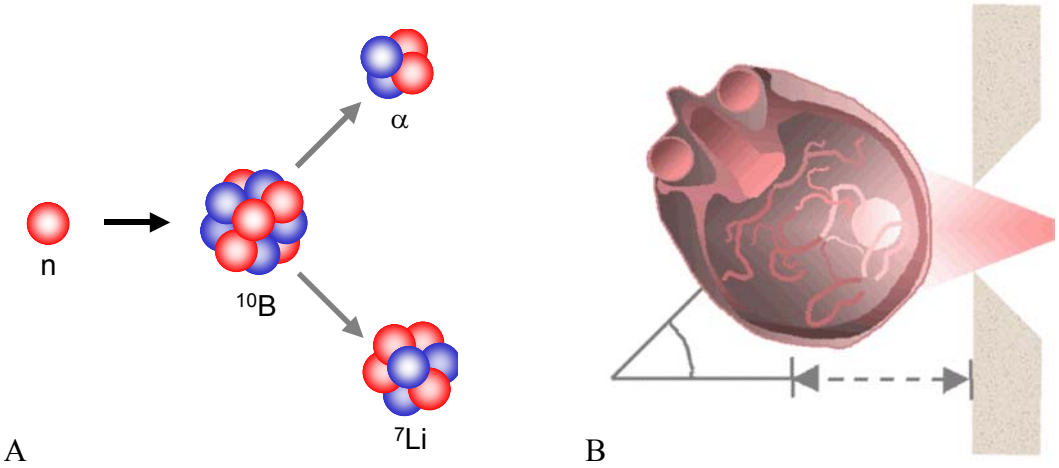

Figure 2. *The concept of boron neutron capture therapy presented in two levels. In A) the boron neutron capture reaction occurs where a neutron activates the boron-10 atom fission into highly lethal alpha and lithium particles with tissue track lengths of 9 and 5 µm, respectively. In B) the patient head is positioned into the planned location and angle with respect to the collimated epithermal neutron beam. The tumour has a higher boron concentration and is presented lighter than the surrounding healthy tissue which is presented darker. The intracranial vasculature functions as a channel for the intravenously infused boron carrier on its way to the tumour.*

The clinical idea behind the BNCT has been presented already in 1936 by Gordon Locher, soon after the discovery of the neutron in 1930 by Chadvick and noticing the remarkable cross-section of the ^{10}B isotope to slow or thermal (energy range of <0.1 eV) neutrons by a capture reaction in 1934 by Goldhaber. It was suggested that the high boron concentration within the tumour cell relative to the neighbouring healthy cell combined with thermal neutron exposure would result in a higher dose in the tumour cell [21]. Therefore the main method for targeting in BNCT would be the selective boron concentration instead of directing the beam as in conventional external beam therapy. In addition to the boron distribution also the directional neutron beam acts beneficially. The main advantages of BNCT are due to the synergistical effects of combining the idea of targeting principles of chemotherapy and the beam localisation schemes used in conventional radiotherapy. Those synergistical advantages according to IAEA are listed as follows [12]:

- Existing boron carriers are non-toxic substances without the neutron exposure as used in current concentrations.
- Biokinetics of the boron carrier can be fully utilised by the time interval between the infusion and the irradiation to optimise the boron biodistribution (the concentration difference between the tumour and the healthy tissue) during the treatment.
- Consequently, the primary neutron activated boron damage occurs only in the tumour and the directly adjacent healthy tissue.

There were occasional attempts to realise BNCT clinically in the earlier years but they did not yield results that were encouraging or would raise practical interest in further implementation. The first studies were carried out in BNL (Brookhaven National Laboratory, USA) and MGH/MIT (Massachusetts General Hospital, Massachusetts Institute of Technology, USA) between 1951 and 1961 using thermal neutron beams to treat patients with intracranial

tumours and specifically malignant gliomas. Gliomas were chosen because it has such a poor prognosis, and still does, even with the most modern therapy modalities. Thus even a modest success of BNCT in treating gliomas would be considered as indispensable technique compared with other choices. There were obvious adverse effects as scalp reactions and necrosis of the brain capillary. Furthermore, the original disease persisted as a result from an insufficient penetration of the thermal neutrons and a poor biodistribution of ^{10}B [22]. There was still an attempt to prove the efficacy of BNCT using a massive tumour debulking and an intraoperative irradiation but no evidence whatsoever were gained of prolonged survival that would encourage to continue the efforts. Thereafter the BNCT went on as intraoperative treatments in Japan where brain tumour and melanoma studies were carried out using thermal neutrons as in previous studies. This time some encouraging tumour regression effects were recorded by Hatanaka and Mishima in response to BNCT using two different boron carriers [23]. However, during the past decades the developments in chemistry, pharmacology, oncology, nuclear engineering and physics has rendered possibilities that could realise BNCT in a more advanced way [22, 24]. Focus has shifted into development and use of epithermal neutron beams (energy range of 0.5 eV to 10 keV) to solve the previous complications of an insufficient beam penetration [12, 24]. Also the development of new boron compounds and boron delivery schemes has a continuously increasing role in BNCT research [25, 26]. The growing interest in this field has fed an efficient international and interdisciplinary co-operation which is still required to gain proper resources for the BNCT to emerge as an acknowledged clinical application [24]. The phase I studies for toxicity and phase II studies for efficacy has to be proven successful before the phase III as randomised studies or any further steps can be taken. The future of current BNCT research projects may be questioned without such justification [12].

2.4 Neutron sources

The epithermal neutron beam for BNCT can be obtained by using a nuclear reactor or linear accelerator as a neutron source [12, 20, 27-32]. The current BNCT facilities use mostly the nuclear reactor approach while the accelerator based sources are still on the way to prove their technological applicability. Also the use of ^{252}Cf has been suggested as a highly compact neutron source although the tough obtainability and the half-life of 2.6 year of the isotope form some obvious shortcomings for its use [12].

The nuclear reactors used for research have core reflectors to enhance the power efficiency. In BNCT use the core reflector has to be modified in order to direct the maximal neutron flux to the preceding filtering and moderator assembly. This modification may involve additional fuel requirements in addition to the implementation of the reflector design to have optimal neutron circumstances in the reactor core [12].

The required neutron flux spectral features can be acquired by spectrum shifting (in thermal columns) and filtering (in beam tubes) where the spectrum shifting method is generally more efficient as described in flux-to-power characteristics. Filtering can still be used in addition to spectrum shifting to acquire the desired energy structure of the neutron fluence. The neutron intensity near the treatment position can be increased by using a fission converter in the beam line between the reactor core and the beam moderator elements [12, 33].

As only epithermal part of the neutron spectrum is desired the gamma radiation and the share of thermal and fast neutrons are tried to get minimal. Heavy materials such as Pb and Bi can

be used in shielding to block the incident reactor gamma rays but to let the neutrons through. Bismuth has still preferred characteristics in this respect compared to lead [12].

An overall filtration of the beam with respect to the neutrons can be realised with a set of thick layers of ^{60}Ni, ^{32}S, ^{10}B and enriched ^{54}Fe which act as a cross-sectional valley in the energy range of epithermal neutrons. Thus a coarse frame can be fixed to pass neutrons between 0.01 to 6-10 keV through the filter assembly. This approach is especially useful in neutron sources which apply filtering as a primary beam methodology [12].

In the reactors imbedding a thermal column the fast neutrons are moderated into lower energies by lighter mass moderator materials. Typically composite structures of Al, Al_2O_3 and AlF_3 have been proved to be useful although other choices are applicable as well [12]. Commercially produced Fluental™ developed in Technical Research Centre of Finland (VTT) has shown to be an efficient moderator material [34, 35]. Polytetrafluoroethylene (PTFE) also known as Teflon™ may be chosen in some facilities where a lower total neutron fluence is appropriate [12]. It has been studied in the MIT research reactor to evaluate the suitability of PTFE for use in MIT fission converter beam (FCB) [36].

The share of thermal neutrons in the beam is limited by using beam filtration. Cross sections with 1/v-dependence are utilised by choosing ^{6}Li or ^{10}B to deplete the lowest part of the neutron energies. At the slightly higher energies Cd is used to emphasise the 0.4 eV resonance energy although a high energy gamma radiation is adversely produced and cadmium oxide (CdO) represents a health hazard as a toxic substance [12].

Various approaches and materials are used in moderators which compact the neutron spectra to emphasise the desired epithermal energy range allowing the neutrons to drift deeper into target tissue and thus pass the skull to reach also the deep-seated tumours. The aim is to have the neutrons thermalising maximally in the precise depth and location of a tumour. Obviously, the precise characteristics of an optimal beam in individual treatment cases would be variable and dependent on the individual patient and target geometry. A practical trade-off is then required for static beams. However, use of an additional filtering that would be easily mounted could serve specific needs of individually managed beam penetration characteristics in different treatments [37].

In addition to the proper neutron beam spectra the beam intensity is also a significant factor regarding the practicality of the treatments. The boron concentration in the tumour and the beam intensity both affect the irradiation times and thus they must be carefully balanced for optimal treatment scheme. A weak intensity means a long treatment time which may extend beyond the tolerance limits for the static fixation of the patient and the reasonable operational conditions of the facility. The conventional radiotherapy fractions of about 10 minutes of duration are still applicable in patient treatments but any prolongation to approach an hour times is critical for the clinical acceptability and quality factors already from the positioning perspective [12].

The moderated epithermal neutron beams are collimated to present an optimal beam geometry for the patient irradiations. In BNCT the collimator has a dual task. Collimators that are included in the shielding structure reflect neutrons back in the direction of the beam whereas the outer collimator structure near the beam exit is designed to thermalise and capture the epithermal neutrons hitting on them. The consecutive emission of gamma radiation can be

minimised by using optimal materials in absorbing collimators [12]. As an example the collimator structure is visualised in the beam vertical cut in Figure 8 in Chapter 3.1.4.

The outermost beam structure before the patient contact is the beam collimator or an optional shutter. The shutters are used in the reactors which operate continuously or where the beam rising and shutting down can not be realised in adequately short periods of time as desired in BNCT irradiation concept. The beam shutter, radiation shieldings and other neutron beam related equipment typically weigh several tons and therefore careful considerations are needed about the floor loading in the reactor facility which is renovated for BNCT use [12].

Depending on the reactor type and beam geometry the core-to-patient distance should be minimised in order to maximise the flux-to-power ratio of the beam and thus to have an optimal beam intensity. However, the accommodation of various beam components including the moderator, shielding, collimators and beam shutters bring certain contradictions that have to be solved optimally for each individual beam. Therefore the technical beam design for BNCT is inevitably a challenging task and different types of beams each demand their own individual solutions for the optimal settings [12].

Beam monitoring controls the stability of the beam during the irradiations. Fluctuations in the reactor beam output resulting from deviations in the power level and other contributors in the irradiation circumstances should be managed and registered properly. ^{235}U fission chambers (with or without specific filters or shields) and ionisation chambers are examples of typical beam monitoring detectors measuring the neutron field components and the gamma radiation of the beam, respectively. The monitoring system should quantitatively determine both differential and integral radiation quantities covering the pulse rates, the total number of pulses, the pulse ratios describing the relative neutron energy distribution, and the beam position. Permanently positioned beam detectors are located around the aperture on the effective beam area, preferably in the main penumbral region. The incident neutron flux should be measured with an adequate accuracy irrespective of the albedo effects by interfering objects such as a patient in the beam target position. The beam position and symmetry are coarsely determined with each pair of detectors in equal distances but opposing locations relative to the beam axis. If the blood boron concentration is measured with a prompt gamma neutron activation analysis (PGNAA) telescope, the real-time boron analysis might also be combined with the beam monitoring system. The beam monitoring and the registration of the beam data should proceed reliably and continuously in all circumstances. Therefore a back-up electronic power supply is an essential part of a beam monitoring system [12, 38, 39].

In addition to the beam monitoring the intensity and spectral characteristics of the beam should be under proper quality control by using appropriate beam calibration and dosimetric techniques. Activation detectors are the primary method of beam calibration with a straightforward relationship between the measured reaction rates and the neutron flux under evaluation. Thermal neutrons can be measured practically by using semiconductor detectors with appropriate neutron converters. The gamma component of the beam is determined with non-hydrogenous ionisation chambers or TLD's. The beam dosimetry forms a fundamental basis for the BNCT operation and the technological framework of the modality [32, 40-42].

2.5 Dose components

The main therapeutic dose at the target volume in BNCT arises from the neutron capture reaction $^{10}B(n, \alpha)^{7}Li$. The resulting lithium recoil and alpha particles have track lengths of 5 and 9 μm, respectively, keeping the high linear energy transfer of the radiation exclusively in the boron containing cells [20]. The neutron capture reactions of hydrogen $^{1}H(n, \gamma)^{2}H$ and nitrogen $^{14}N(n,p)^{14}C^*$ contributes also at a significant level to the total dose of the patient [12, 32]. In addition to the capture reactions, elastic scattering between epithermal as well as fast neutrons and hydrogen nuclei are the other essential interactions of neutrons within the tissue producing recoil protons [12]. There is also gamma radiation produced by the reactor core with energy range of 0-15 MeV and the gamma radiation from the neutron capture of hydrogen reaction with energy of 2.2 MeV [43]. A vast majority of the ^{7}Li ions from the boron capture reaction are produced in an excited state. The de-excitation occurs instantaneously and a 477 keV gamma rays are emitted [12]. This minor gamma component is called consequently the prompt gamma radiation. Gamma radiation interacts and attenuates in the tissue mainly by Compton scattering and photoelectric effects [44].

Since the boron dose is the main therapeutic dose component and is solely responsible for the targeted tumour effect the remaining dose components should be minimised as not desired portion of the radiation dose. The total biological effect is a result of all dose components and consequently they all have to be individually assessed according to their specific relative biological effectiveness before they can be combined to calculate the total effect. However, in the case of BNCT the concept of relative biological effectiveness is far beyond of a use of simple biological weighting factors with respect to the physical dose components [12].

2.6 Beam dosimetry – the first objective

Beam dosimetry covers several issues considering the beam calibration and the beam characterisation issues. Beam calibration concerns the relation between the beam monitoring with respect to the reactor power and the dose determined in reference conditions. Dose determination involves experimentally acquired absorbed dose or neutron fluence in a specific reference position in a phantom preferentially in the depth of absorbed dose maximum. Beam characterisation involves measurements and calculations where the beam output is analysed with respect to the neutron fluences in different neutron energies and the spatial dose distributions in three dimensions covering the various dose components of the mixed beam. Proper assessment of all dose components is essential in order to determine the consecutive total biological effects of the irradiations [10, 12].

The gamma radiation of 2.2 MeV energy induced in the tissue from the $^{1}H(n,\gamma)^{2}H$ thermal neutron capture reaction of hydrogen constitutes the main part of the gamma exposure during the treatment in any living objects practically irrespective of any individual metabolical or biodistributive differences [45]. The direct gamma radiation from the beam constitutes the rest of gamma radiation to which the patient is exposed. The prompt gamma radiation of 477 keV from the de-excitation of the recoiling ^{7}Li ion is negligible with respect to the total gamma dose [12]. However, it is specific to the boron biodistribution in the target object and therefore possesses valuable information regarding the boron analysis purposes [46, 47]. The beam monitoring system includes a gamma sensitive ionisation chamber detecting the beam gamma component but not the gamma radiation which is induced in the target. Assessment of

the total gamma field to which the patient is exposed in treatment circumstances is therefore performed either prospectively by phantom studies or by in vivo studies relating directly to the individual irradiation under consideration [48].

The dose from the recoiling protons and the proton dose from the nitrogen capture reaction constitutes the main neutron dose components of an epithermal neutron beam without the contribution from the boron compounds in the target object or elsewhere [32]. The conventional neutron dosimetry methods like ionisation chambers, activation foils and TLD's have been used to determine these tissue dose components [42]. The boron dose component requires the use of boron containing detector for example a solid state semiconductor detector or a proportional counter used in microdosimetry where the boron has been doped in the tissue equivalent chamber wall material [49, 50]. However, the use of proportional counters has been limited to low reactor power measurements [51, 52]. A silicon diode based microdosimeters are highly potential in the BNCT use since all dose components in the mixed field can be measured on-line with a single small detector [53]. However, the optimal characteristics of the semiconductor detectors for BNCT are still under development. The construction of the detector includes a layer of suitable converter material attached to the surface of a p-n junction diode where the converted charged particles can be detected and measured [53-55].

General beam characterisation is made free in air without phantoms. In air the doses cover epithermal and fast neutrons in addition to the incident gamma rays. Such beam descriptions concentrate in incident beam performance surveys instead of evaluations of the treatment planning computational codes [12].

The absorbed doses from the neutrons cannot be measured directly. Therefore tissue kerma factors are applied to the determined neutron fluences to provide the desired dose quantities as the simplest case. The exact dose analysis from the primary measured quantity depends on the experimental method. Measurements with activation detectors and semiconductor diodes produce reaction rates and neutron fluence rates which are converted into doses by application of the kerma factors [32, 56].

Thermoluminescent detectors (TLDs) are applied in beam dosimetry both in the areas of phantom studies and in vivo use. Thermoluminescent materials can be used in wide dose ranges and the small size of the detectors and the lack of connecting cables extend the capabilities beyond the easily accessible measurement positions where the same holds also for activation detectors. Especially the in vivo measurements can be successfully applied using TLD's and the assumption of tissue equivalence is valid for most types of radiation [48, 57]. However, a successful application of the TL detectors in mixed fields requires knowledge of their responses to each dose component. Especially the variable neutron responses call for careful considerations and independent determination of the thermal neutron fluence [58].

Ionisation chambers measure primarily the electrical current or accumulated charge as determined according to the measurement mode and the electrometer. Environmental corrections including the polarity, recombination, ambient temperature and air pressure are taken into account in the recorded signal from the measurement. In the Finnish BNCT dosimetry chain the chambers are individually calibrated for absorbed dose to brain tissue in cobalt (^{60}Co) gamma beam. Difference in detector sensitivity between the calibration beam and the therapy beam is taken into account by assessing the relative neutron sensitivity of the tissue equivalent (TE) ionisation chamber. The relative neutron sensitivity is determined

according to general Bragg-Gray cavity ionisation theory following the ICRU formalism [59, 60]. The relative neutron sensitivity determination includes the stopping power ratios, absorbed dose conversion factors, mass absorption coefficient ratios, ion-pair production energies and kerma ratios. The spectral quantities involved in the relative neutron sensitivity assessment require the use of calculated neutron spectra from the transport simulations as the input data. Therefore the neutron dose determination with ionisation chambers is dependent on calculations. The measured gamma dose component and the recorded real-time beam monitor unit rate during the measurements are taken into account in the TE-detector signal and the consecutive neutron dose. In this study the relative neutron sensitivity of the gamma ionisation chamber constructed purely from non-hydrogen materials is assumed to be zero in all neutron energies [43]. Thus the gamma dose determinations does not require information of the neutron spectrum. The detector specific calibration coefficient in addition to environmental corrections and the beam monitor unit rates provide sufficient parameters for the determination of the absorbed gamma doses from the measured gamma detector signal. Neutron sensitivity of gamma detectors has been investigated in other studies where also non-zero values have been acquired [45, 61]. These contradictory results demonstrate that the assessment of relevant dosimetry factors in a mixed field is potentially sensitive to specific measurement set-up and thus careful considerations are required when analysing the acquired experimental data.

Taking into account the high complexity of the BNCT beam it is fundamental to have a proper characterisation of the beam and to implement a practical system for beam calibration. The first objective of this study was to develop the methods which were used to verify the calculated doses of the treatment planning system and to provide practical dose quantities for the dose assessment in BNCT in various cases of interest.

2.7 Treatment planning

A dedicated treatment planning system is required in BNCT to produce dose plans where all the mixed field characteristics of the epithermal beam have been taken into account. In Finland the patient is imaged by MR (1.5T Siemens Magnetom Vision) or CT scanner one to three weeks before the actual treatment for the dose planning. Modality sensitive external location markers (E-vitamin capsules) are set on the predefined anatomical positions during the imaging to mark the reference points of the head. The reference points are also tattooed on the skin. Gadolinium-DTPA is used as a contrast agent with the standard MR imaging sequence.

The contrast enhanced T1 weighted axial images are combined to form a 3D model of the patients' head. Thereafter the head model is typically segmented to specify the skin, the skull, the healthy brain tissue, the tumour and the target volume. The external markers are also identified to set the coordinate system for patient positioning. Furthermore, the tissue elemental composition according to Brooks is used in the dose calculations [62]. The dose to the target volume is prescribed and the beam directions are set according to an optimised dose plan. The neutron source and the head model is applied to the 3D Monte Carlo treatment planning software BNCT_Rtpe or SERA (INEEL/MSU, Idaho Falls/Bozeman, USA) to calculate the dose distribution within a patient. The total biologically weighted dose (D_w) for the patient is defined as a sum of four physical dose components each multiplied with a specific biological weighting factor according to equation [12]:

$$D_W = w_g D_g + w_B D_B + w_N D_N + w_n D_n, \quad (1)$$

where D_g is the gamma dose, D_B the boron capture dose, D_N the nitrogen capture dose and D_n the dose from epithermal and fast neutrons [12, 32]. The weighting factor for gamma dose w_g of 1.0 is generally assumed as the photons are acknowledged as reference radiation [3]. The boron weighting factor w_B of 3.8 is used for the target volume including the tumour, 2.5 for the skin and 1.3 for the normal brain tissue. The weighting factor of 3.2 has been used in BMRR and in Finland for both nitrogen and epi-fast neutron doses in all tissues. In the fluence-to-kerma conversions of the weighted doses the assumption of equal proportions of white and grey matter in the brain tissue composition was used according to Brooks' brain definition [62]. Thus the nitrogen concentration of 1.84 w-% and the hydrogen concentration of 10.57 w-% is assumed for the weighted nitrogen doses (relative to thermal fluence) and the epi-fast doses, respectively [63]. Alternatively, the ICRU brain composition can be assumed for dose determinations. In that approach a minor correction is made to the weighting factors according to the differences in the ratios of nitrogen and hydrogen in Brooks' brain tissue versus the ICRU brain tissue. As a result weighting factors of 2.68 for nitrogen capture w_N and 3.16 for recoil proton dose from the epi-fast neutrons w_n are acquired [32]. The unit for the biologically weighted total dose is Gy (W) where the W in parenthesis is used to emphasise the weighting whereas the physical dose components are expressed in Gy unit.

The dose as a function of the blood boron concentration is determined for the tumour, the target volume and the healthy tissue. The tumour-to-blood ratio of 3.5:1, skin-to-blood ratio of 1.5:1 and brain-to-blood ratio of 1:1 are assumed for the boron biodistribution [32, 64]. Upper limits are defined for the dose in each sensitive anatomical structure of the head model to protect the critical organs of the patient from the adverse effects [4, 5].

2.8 Boron concentration in blood – the second objective

Prior to the irradiation an infusion of ^{10}B-carrier (boronophenylalanine (BPA)) is given to a patient. BPA has a low solubility on its own and therefore it is rather used as a BPA-F, a fructose complex. The blood boron concentration is measured with ICP-AE (Inductively Coupled Plasma, Atomic Emission Spectroscopy) during the infusion and throughout the BNCT irradiations [65].

The boron concentration level affects directly the boron neutron capture reaction intensity and further the dose of the tumour and the brain. Therefore it is essential to have a reliable prediction of the blood boron concentration during the irradiation to accurately deliver the prescribed dose to the patient. However, there are considerable variations on the blood boron levels between separate individual patients despite the same infused amount of BPA-F. Also the blood boron measurements are applicable only at longer intervals and not at all during the irradiation. The gap between the measurements can be even 30 minutes. It is then necessary to implement a certain method to predict the blood boron level also between the measurement points and during the irradiation [66]. The second objective of this study was to develop a practical method to estimate the ^{10}B (BPA) clearance from blood for an individual patient with an increasing accuracy as more data points are available from the blood boron measurements.

2.9 Patient positioning – the third objective

The patient irradiation in BNCT is typically performed using two or more fields [12, 67]. Because of the static beam direction in BNCT all the required beam directions have to be facilitated by the patient positioning system. The beam cannot be moved and thus the patient has to be manoeuvred into all appropriate positions. The beam aperture in Finnish BNCT facility is basically a hole in the wall but the distance between the patient head and the beam port should be minimised to maximise the neutron field intensity and to minimise the lateral scatter. That brings a contradiction to practical positioning where the wall limits the space e.g. for shoulders. The most common beam position set-up is a beam directed to the lateral side of the patient head where the patient has to be set laying on his back with the head in a neck-bended position. However, the patient can be immobilised only into limited angles of static fixation. Hence the acceptable patient postures set the boundaries of tolerance which the positioning system has to extend without affecting the patient. That is a demanding task noticing that the means of traditional radiotherapy positioning cannot be directly utilised. The limited space around the treatment coach in the irradiation room sets mechanical and functional conditions that further restrict potential techniques. The third and the final objective of this study was to realise patient positioning in the Finnish BNCT facility in a way that is practical considering both the patient comfort and the various functional, spatial and dosimetric circumstances of the treatments. Furthermore, the system has to be assessed quantitatively for spatial accuracy and consecutive dose accuracy to set a level of positioning accuracy to be required in the BNCT practise.

2.10 BNCT facilities

The overall technological prerequisite for the treatments is a BNCT facility which is constructed to serve all the clinical operations and the technological circumstances of the actual treatment chain, keeping the neutron source as the core concept. There are currently nine BNCT facilities operating in the world, either in the clinical trials or in the preliminary research: four in Europe (Finland, Sweden, Holland and Czech Republic), one in the United States, Taiwan and Argentina, and two in Japan [12, 23, 68].

The Finnish BNCT facility in Otaniemi, Espoo, uses the FiR 1 reactor which is a light-water moderated 250kW Triga Mark II type nuclear reactor consuming uranium-235 as fuel. The FiR 1 reactor was taken into use in 1962 and operated as a research reactor until the late 90's when the construction of the Finnish BNCT facility begun on the site. The Fluental^{TM} moderator block was shortened from 75 cm to 63 cm to provide a high intensity epithermal neutron beam. The beam quality with respect to the high purity of epithermal neutrons was demonstrated with measurements and simulations. Thereafter the concrete shielding of the reactor was partly cut to let space for the patient irradiation room. The whole reactor building was renovated to provide full clinical facility including a room for the beam simulator, patient preparation and monitoring, BNCT control room, boron laboratory, technical areas and staff office rooms. The reactor facility was granted the radiation safety licence for clinical use in January 1999 after it was surveyed by the Finnish Radiation and Nuclear Safety Authority (STUK). The Finnish BNCT facility was taken into clinical use in May 1999 after extensive operational testing [34, 69].

2.11 Radiobiological studies

Before the clinical trials on humans the safety of the treatments was established by series of beagle dog (large animal model) experiments in 1998. Radiobiological studies were needed to further determine the properties of the FiR 1 epithermal neutron beam and to study the contributions of the relative biological effectiveness between the main dose components. The dogs were irradiated in FiR 1 beam using escalating doses in three dose groups without boron carrier and one group with BPA-F carrier to prove the safety margins to be used in clinical trials and to further characterise the boron enhancement of the dose. Reference irradiations were made in the 6 MV Linac photon beam to have comparable results. Irradiations in 6 MV photon beam had four dose groups corresponding to the FiR 1 beam dose groups. Changes in the brain were determined using MRI, gross morphology and histology samples. Specific responses and endpoints were assessed according to the dose-effect curves to further determine the RBE (relative biological effectiveness) for each endpoint. The most clinically relevant endpoint was chosen to be the contrast enhancement observed in sequential MR images. According to the results the RBE of the FiR 1 mixed epithermal beam in the dog brain was about 1.25 compared with 6 MV photons [70].

2.12 Clinical trials

About half of all primary intracranial tumours in adults are gliomas. More than half of all gliomas are malignant neoplasms to which there is no curative treatment available. The median survival in high-grade gliomas after aggressive conventional therapy including debulking surgery combined with external radiotherapy or chemotherapy is about 12 months [71].

The first Finnish phase I to II clinical trial (protocol P-01) began in May 1999. The goal was set to prove the feasibility of BNCT as a primary therapy for glioblastoma multiforme (GBM) patients. Patients have been treated in collaboration with VTT (Technical Research Centre of Finland) and HUS/HUCH (Hospital District of Helsinki and Uusimaa/Helsinki University central Hospital). The interdisciplinary core team consists of oncologists, neurologists, nurses, medical and radiation physicists, chemists and nuclear engineers. In addition, radiologists, pathologists, pharmacists, neurosurgeons and technical staff have been involved in the BNCT team. Before BNCT the patients have been in debulking surgery to remove tumour tissue and to confirm the diagnosis of glioblastoma. 18 patients with supratentorial glioblastoma have been treated in the first protocol until the end of the year 2001. The average age of the 11 males and 7 females has been 54 years. The average physical dose of the planning target volume and the normal brain tissue has been 30-61 Gy (W) and 3-6 Gy (W), respectively. The maximum average weighted dose to the normal brain tissue has been limited to 7 Gy (W) while the realised average weighted doses has been about 5 Gy (W). The weighted peak doses of less than 14 Gy (W) has been given to the normal brain while the physical peak doses have been below 11 Gy. Keeping the BPA-F dosages between 290 mg BPA/kg and 400 mg BPA/kg the average weighted planning target volume doses has been 47±7 Gy (W). Preliminary clinical results have ascertained the feasibility of BPA-F mediated BNCT with the given irradiation doses. The patients have been followed up after the treatment by observing neurological status, adverse effects and by MRI examinations (1, 3, 6, 9, 12, 18 and 24 months after BNCT). The patients have tolerated the treatments well and all have survived the first few months time following the treatments. 14 of the 18 patients have had repeated

surgery and/or additional radiotherapy for tumour recurrence. Currently (April 2002) the estimated 12-month overall survival for the first protocol is 61% [63].

The second clinical trial has also begun in Finland (protocol P-03) as a prospective phase I study for the patients with recurrent or progressive glioblastoma after conventional radiotherapy. Additional protocols are opening as the safety of BNCT is further established.

Among the recent BNCT clinical studies phase I/II trials have already been conducted in Brookhaven National Laboratory (BNL). The published clinical results have shown the safety and feasibility of BNCT with brain doses below 6 Gy (W) using BPA-F as a boron carrier. Palliation provided by a single fraction BNCT compares favourably with conventional treatment modalities such as fractionated radiation therapy and adjuvant chemotherapy which expose the patient to protracted treatment sessions and more severe adverse effects [72].

3 BEAM DOSIMETRY

In the beam dosimetry studies the neutron and gamma absorbed dose rates and the thermal neutron fluence rates were determined in air and in various phantom materials and geometries by measurements and calculations. The doses were quoted to ICRU brain tissue to have equivalence with the dose planning target tissue composition and to have compliance with the target tissue type of the BNCT treatments of brain tumours [43, 73]. Dose values were determined in various locations inside the phantoms and in-air, including measurements along the longitudinal central beam axis (depth dose curve) and perpendicular to it at 25 mm – 30 mm and 60 mm depths (dose profile curves). The neutron and gamma dose components were measured separately using twin ionisation chambers and thermoluminescent detectors (TLDs). Thermal neutron fluences were measured using activation detectors and a Si(Li) diode detector (relative distributions). All measured results were compared with the simulated results to verify the dose calculations and the computational beam model [42].

3.1 Materials and dosimetry methods

Measurements were arranged at the Finnish BNCT facility to study the epithermal neutron beam constructed in 1997 and operated by VTT. Extensive dosimetric information was acquired with the focus on the relevant dose quantities with respect to BNCT: gamma and total neutron doses and thermal neutron fluences. The dosimetry process chain is presented in Appendix 1 and in a modified form in the recent publication [42].

The TL and activation measurements have been described more detailed elsewhere [48, 57, 74-77]. This study has concentrated in the use of Si(Li) diode detector and especially the twin ionisation chambers in the dose assessment for BNCT. Phantom geometries were chosen according to resemblance with patient head dimensions and the practical aspects of the measurement techniques and calculational methods. Several dosimetry results have already been reported about the cylindrical phantom geometry with different phantom materials [42, 43, 48]. In this study, the ellipsoidal phantom geometry has a special focus as it has resemblance with human head and it also introduces more complex curvature geometry for the verification of the dose calculations. Therefore a special study concerning curvature region points with and without the ellipsoidal phantom displacement causing beam asymmetry was also performed. The data concerning the displacement study has previously been presented at the 9th ISNCT meeting [78].

3.1.1 Epithermal neutron beam

The FiR 1 research reactor was used as a neutron source operating at a 250 kW nominal power. The reactor core is situated in a water tank with a graphite reflector. In the renovated beam construction (K63) the initial neutron field is modified with a 63 cm thick Fluental^{TM} moderator block consisting of AlF_3 (69 w-%), aluminium(30 w-%) and LiF (1 w-%). The bismuth shield is used to pass the neutrons after the moderator but to block the gamma radiation from the reactor core and the neutron activated parts in it. The resulting beam set-up produces an isotropic, high quality epithermal neutron field with a total free-in-air intensity of 1.4 x 10^9 epithermal neutrons/s.cm^2 which is clearly above the recommended intensity threshold of 10^9 epithermal neutrons/s.cm^2 stated by IAEA [12]. The neutron field is highly

thermalised as it propagates into a tissue equivalent medium such as water. The relative neutron contributions of the three main neutron energies and the four dose components (gamma dose and three neutron energies) of the beam are presented in Figure 3. Natural lithiated polyethylene was used at the beam port for the base of the beam collimator discs. Enriched ^{6}Li-polyethylene was used in the innermost aperture collimator cone defining the beam outline and producing the optional beam diameters of 8, 11, 14, 17 and 20 cm for the treatments.

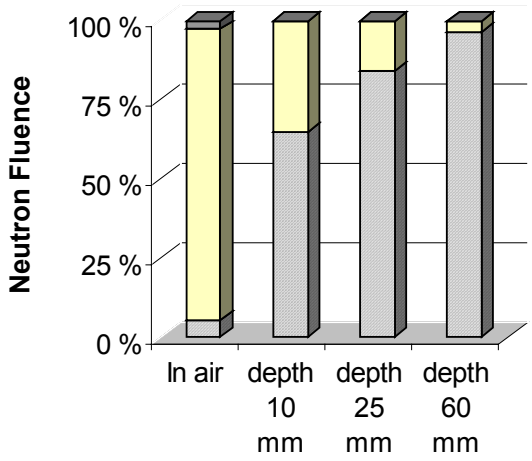

A

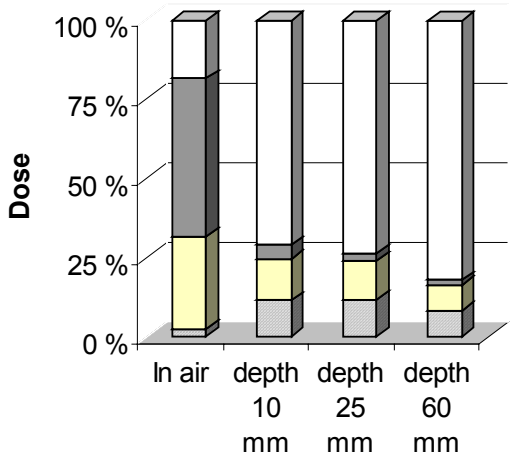

B

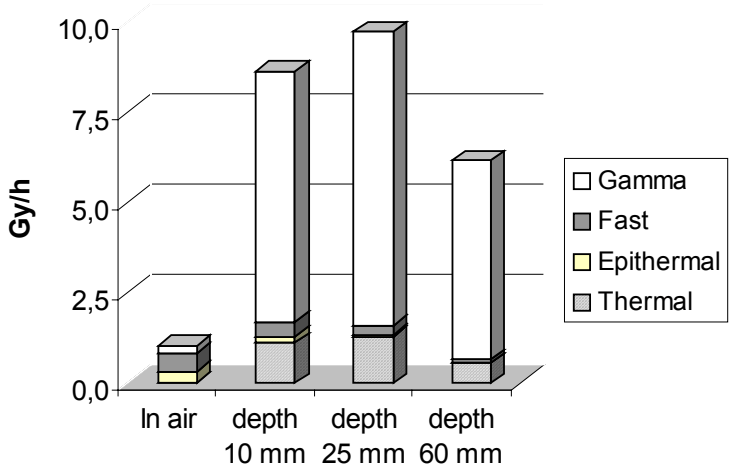

C

Figure 3. *The FiR (K63) BNCT beam components presented as the relative neutron field contributions to total neutron fluence (A), relative dose components of the total dose (B) and absolute dose values (C) in free beam and in three depths in the central axis of the cylindrical Liquid B phantom. The component colors are explained in C.*

3.1.2 Detectors

Diluted Au-Al and Mn-Al activation detectors (Ø 12 mm, thickness 0.2 mm) were used to measure the Au and Mn reaction rates, respectively. Diluted (1%) foils were used to avoid the self-shielding and mutual shielding of the detectors in the beam. The activity of the irradiated foils was measured with Ge detector. The SAMPO program was used to assess the saturation activities and to determine the Au and Mn reaction rates [75, 77].

Two-layer thermoluminescent detectors (purchased from TLD Niewiadomski & Co, Krakow, Poland) were used to measure the relative neutron fluence and the gamma dose. The neutron fluence was determined using detectors with thin active LiF:Mg,Ti layer for reduced self-shielding of thermal neutrons. The gamma doses were determined with LiF:Mg,Cu,P detectors with low sensitivity to thermal neutrons compared with gamma radiation [48, 57, 79].

A PN junction Si(Li) diode with an aluminium layer on p-type was used as a custom made thermal neutron detector. As a surface barrier detector it has a thin dead layer which is advantageous in charged particle spectroscopy use. The wafer thickness was 300 μm and the depth of the sensitive volume is dependent on the applied bias voltage and resistivity of diode material [54]. The diode was combined with a lithium converter where the reaction $^{6}Li(n,\alpha)^{3}H$ occurs producing alpha and triton particles which are detected on the diode with high efficiency [44, 54]. A layer of Li_2CO_3-glue mixture was used as a converter. The detector was covered with 1 mm aluminium and the interior behind the diode was filled with araldit epoxyglue to make the detector tissue equivalent [80]. The structure of the detector is presented in Figure 4.

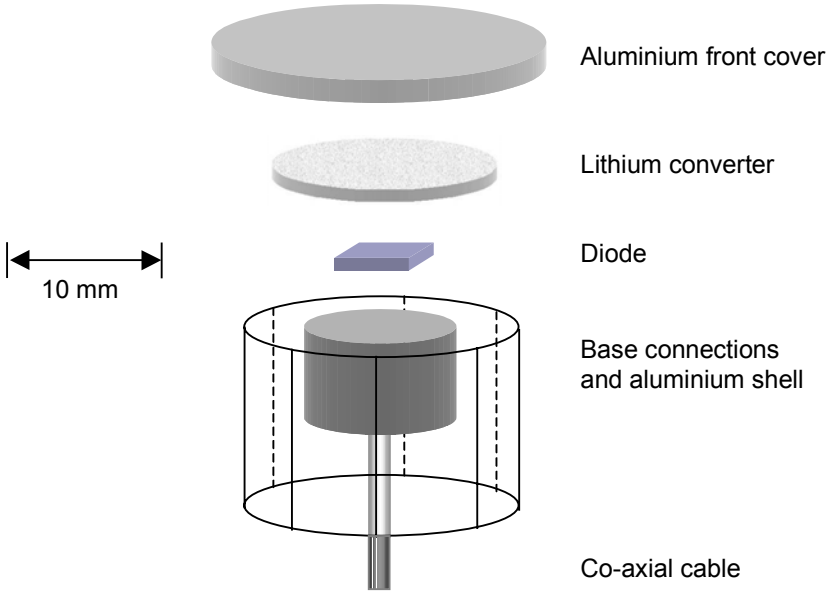

Figure 4. *The schematic structure of the Si(Li) diode detector used for the thermal neutron fluence measurements.*

The detector was used without a bias voltage (the bias voltage set to zero). The detected signal was transmitted through a charge sensitive preamplifier to a spectroscopy amplifier. An example of the resulting pulse spectrum is presented in Figure 5. The amplified signal was

observed and discriminated with a multichannel analyser (MCA) and the resulting pulses were collected with a counter card controlled by a computer program.

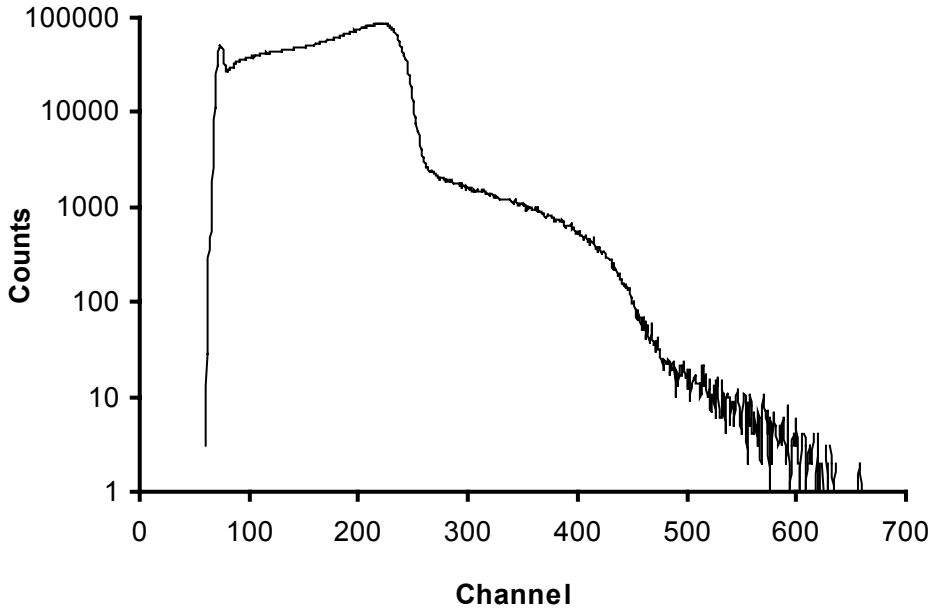

Figure 5. *The pulse spectrum of the Si(Li) diode detector in the central depth axis of the cylindrical PMMA phantom in the depth of 21 mm.*

A pair of tissue equivalent TE(TE) and non-hydrogenous neutron insensitive Mg(Ar) thimble ionisation chambers (manufactured by Exradin) were used in a current mode to determine the total neutron and gamma dose rates, respectively. Primary technical characteristics of the chambers are listed in Table 1. The twin chamber method has already been utilised in fast neutron therapy and it has also been used in dose determinations in other epithermal beams for BNCT [45, 81] in addition to the FiR 1 epithermal beam [42, 43]. Build-up caps were used with the chambers to produce an equilibrium of the charged particles in the gas cavity of the detector. The depths of the Table 1 are defined from the apex of the build-up caps to the geometric centre of the chamber gas volume which corresponds to the effective point. During the measurements in the liquid phantom the chamber was shielded by sub-millimetre thick rubber sleeves around the detector to make it waterproof. The stem of the chamber was further locked in a hollow tube and a silicon hose was used to lead the electrical cables out of the phantom liquid. The silicon hose connected the airspace between the rubber sleeve and the irradiation room. Thus the liquid pressure in the measurement location inside the phantom pool tends to exclude all air between the chamber and the sleeve. The chamber-tubing complex was then attached to the electronic detector transport mechanism. In the solid cylindrical PMMA (polymethylmethacrylate) phantom the chambers were inserted in the central canal of the phantom using special PMMA fitting parts to exclude air around the chambers and to attain the desired depths for the measurements.

Table 1. *The Exradin thimble TE(TE) and Mg(Ar) ionisation chamber characteristics.*

Chamber model	Wall and build-up cap material	Wall and build-up cap thickness (mm)	Effective point depth from the apex (mm)	Volume (cm^3)	Gas
T2	A-150 plastic	1+4	13.8	0.53	TE*
M2	Magnesium	1+2	11.8	0.53	Argon

**TE-gas composition: 64.4 vol-% methane, 32.4 vol-% carbon dioxide, 3.2 vol-% nitrogen.*

The gas flow system of the chambers included pressure gauges and rotameters to monitor and control the gas flow rate and the pressure. Methane based tissue equivalent (TE) gas mixture (CH_4 64.4 vol-%, CO_2 32.4 vol-% and N_2 3.2 vol-%) and extra pure (99.9999%) argon gas was used for the TE and Mg chamber, respectively. The ambient conditions were recorded for the temperature and pressure correction and the recombination and polarity effects of the collecting potential were tested to be taken into account in the charge measurements [82]. The Keithley 6517 (Keithley Instruments Inc, USA) and NE Farmer 2570 (Saint-Gobain Crystals & Detectors UK Ltd, England) electrometers were used in a manual mode to collect charge from the ionisation chambers.

3.1.3 Dose determination with ionisation chambers

The gamma and total neutron dose rates were determined from the measured readings using the ICRU formalism [59] where the doses related to the twin ionisation chamber measurements can be described by a pair of equations:

$$\begin{aligned} M_u N_{u,c}^{brain} &= h_u D_g + k_u D_n \\ M_t N_{t,c}^{brain} &= h_t D_g + k_t D_n \end{aligned}, \tag{2}$$

where h_u and k_u are the ratios of the photon sensitive Mg(Ar) chamber responses in the mixed beam of photons or neutrons, respectively, compared with the responses in the ^{60}Co calibration beam. Furthermore, h_t and k_t are the corresponding ratios for the TE(TE) chamber which has roughly equal sensitivities to the gamma and neutron components of the beam. M_u and M_t are the measured readings corrected for ambient and electrical conditions. $N_{u,c}$ and $N_{t,c}$ are the detector specific calibration factors to determine the absorbed doses to brain tissue in the ^{60}Co calibration beam for the Mg(Ar) and TE(TE) detectors, respectively. D_g and D_n are the absorbed photon and neutron doses which are to be determined. The doses were quoted to the ICRU brain tissue.

$N_{u,c}$ and $N_{t,c}$ calibration factors were based on air kerma calibration in the SSDL (STUK) ^{60}Co gamma beam. The chamber sensitivity in 2.2 MeV gamma energy was determined by an interpolation using the dose weighted mean energies of the ^{60}Co gamma beam and a 6 MV linear accelerator based photon beam [10]. The zero relative neutron sensitivity (k_u) was used for the photon sensitive Mg(Ar) chamber whereas the relative neutron sensitivity (k_t) of the TE(TE) chamber was determined in every measurement point according to the calculated neutron fluence and other spectral parameters using equation [59]:

$$k_t = \frac{W_p}{W_n} \cdot \frac{\left(S_{A150,TE}\right)_p}{\left(r_{A150,TE}\right)_n} \cdot \left(\frac{(\mu/\rho)_{brain}}{(\mu/\rho)_{A150}}\right)_p \cdot \left(\frac{K_{A150}}{K_{brain}}\right)_n \tag{3}$$

where subscripts p and n refers to the ^{60}Co photon calibration beam and the mixed epithermal neutron beam, respectively. In the first quotient the W_p value of 29.2 eV was used for the energy required of the ^{60}Co beam secondary electrons to produce an ion pair in TE gas. The corresponding value W_n for secondary charged particles of the neutron field was determined according to neutron energy from the data by Jansen et al [83]. For the stopping power/absorbed dose conversion factor ratio and the mass absorption coefficient ratio values of unity were used in the second and third quotient, respectively. The kerma rates of A150 (K_{A150}) and ICRU brain tissue (K_{brain}) were calculated from the weighted ICRU kerma factors and the calculated neutron fluence. The BUGLE (Coupled 47 Neutron, 20 Gamma-Ray Group, P3, Cross Section Library for LWR (Light Water Reactor) Shielding Calculations) energy structure used in the spectral calculations has only two energy bins in the thermal energy region. Therefore a separately determined weighting of the kerma factors was used in all BUGLE groups for the neutron dose calculations [43].

3.1.4 Phantoms

Phantom materials covered water, PMMA and brain tissue equivalent liquid (Liquid B). The relative elemental compositions of the phantom materials are presented in Figure 6. Liquid B has good conformity with the ICRU brain composition [84]. Water as a phantom medium has similarity with the brain tissue with regard to an attenuation and scattering features of epithermal neutrons. PMMA and water are commonly used as phantom materials in the photon dosimetry and in the BNCT dosimetry [85]. PMMA has 14% lower hydrogen concentration than water or Liquid B and consequently a lower gamma dose. However, the solid composition is appreciated in measuring practise [42, 85].

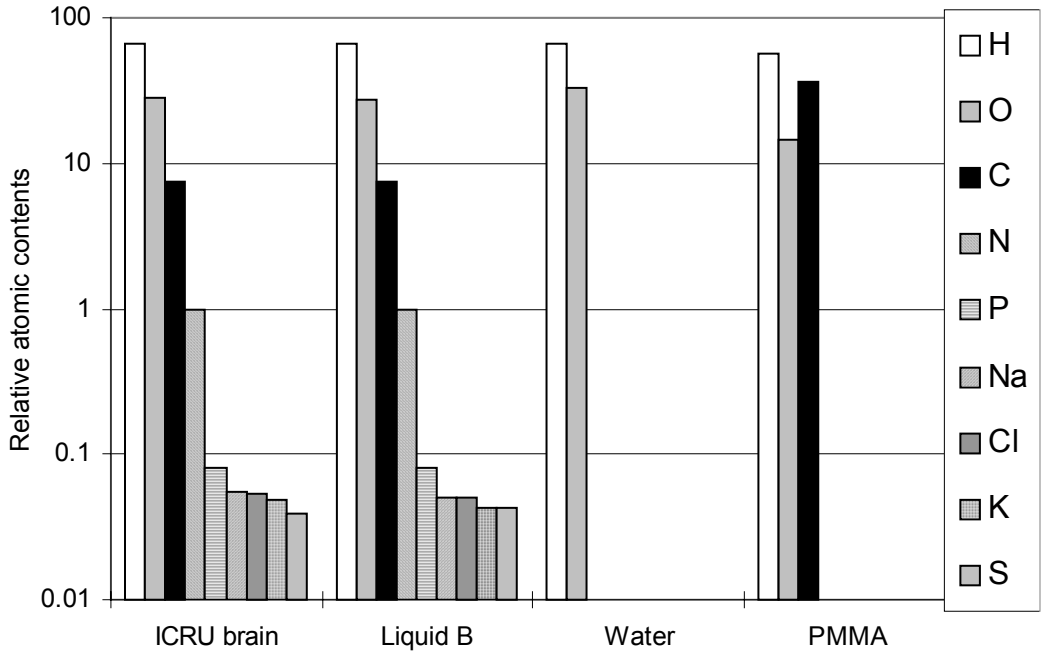

Figure 6. *The phantom materials and the ICRU brain elemental composition [84].*

The phantom geometries were chosen to present simple shapes to establish the dose calculations but also to have approximate resemblance with the real patient and

radiobiological object shapes and sizes. The phantoms are described in Table 2 and in Figure 7. The ellipsoidal phantom geometry is defined with equation

$$\left(\frac{x}{80}\right)^2+\left(\frac{y}{100}\right)^2+\left(\frac{z}{83}\right)^2=1 \tag{4}$$

where x is the lateral axis, y is the anterior-posterior axis and z is the superior-inferior axis. The measures are in mm. The ellipsoidal geometry presented here follows approximately the skull geometry of the Snyder head model [86]. The doghead phantom is shaped according to the large animal model of the radiobiological studies. The large cubic CADSCAN (Dosetek Oy) tank phantom could be used as a reference of an infinite scattering object.

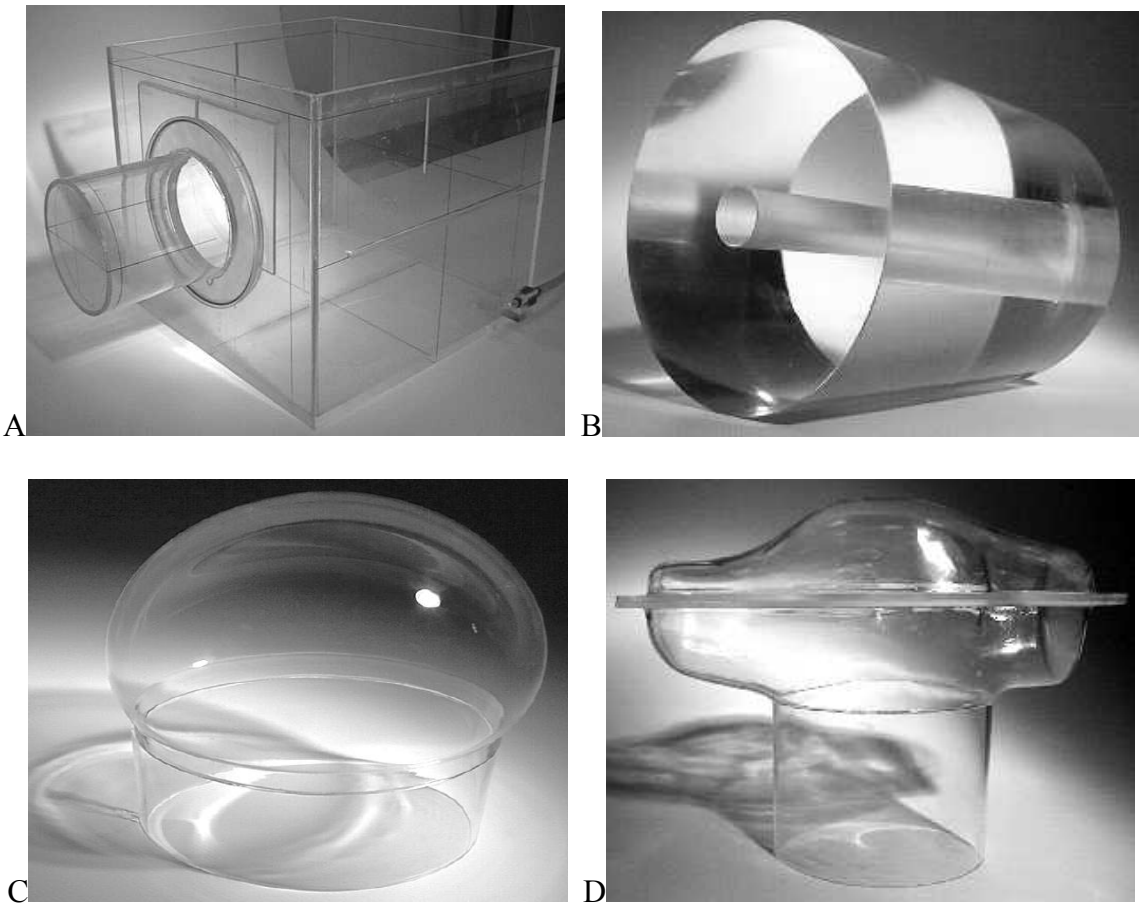

Figure 7. *The phantoms used in dosimetry studies at the Finnish BNCT facility; A) the liquid cylinder attached to the tank phantom, B) the solid PMMA cylinder, C) the ellipsoidal phantom and D) the doghead phantom.*

Table 2. *The phantom materials and dimensions.*

Name	Material	Geometry	Diameter (cm)	Length (cm)	PMMA wall thickness (mm)
Cylinder	Water and Liquid-B	Cylinder	20	20	5
Standard	PMMA	Cylinder	20	24	Solid
Snyder	Water and Liquid-B	Ellipsoidal	16	20	2
Doghead	Water and Liquid-B	Anatomical beagle head	12	22	2

All the measurements in the PMMA phantom were done along the central axis using special PMMA fittings to attain the desired depth from the phantom front surface and the beam. The PMMA phantom was used separately whereas the liquid filled phantoms were attached to the large cubic phantom tank where the detectors could be immersed in liquid (water or liquid B) and attached in the detector transport mechanism to be positioned freely in the phantom. A custom made computer program was used to control the detector position in three dimensions with 400 mm range in each orthogonal direction. The spatial accuracy of the 3D-mechanism linear motion was ±0.1 mm achieved with homoheteropolar stepper motors and miniature timing belts [87]. The overall measurement set-up and the beam construction is shown in Figure 8.

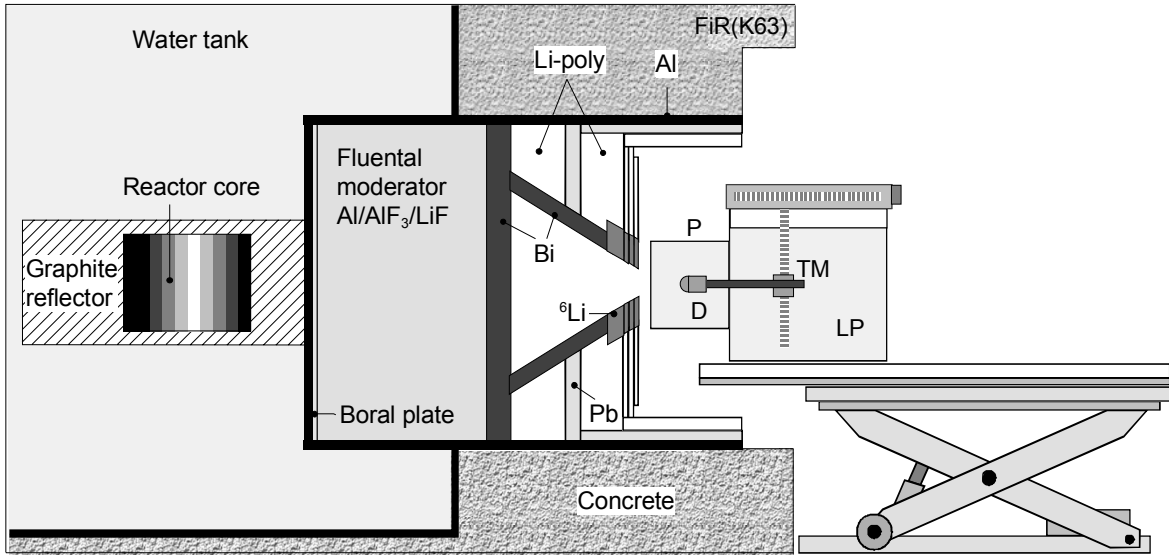

Figure 8. *The Finnish BNCT beam construction and the measurement set-up. The epithermal neutron beam is produced as the radiation from the reactor core and the graphite reflector is filtered through the boral plate, the 63 cm thick Fluental moderator and the bismuth shield. Finally, the beam is collimated by the ^{6}Li enriched aperture cone rings before the resulting neutron and gamma field is distributed and detected in the phantom (P). The phantom (not in scale) is attached to the large liquid pool (LP) and the detector (D) is moved in three dimensions using the computer controlled transport mechanism (TM).*

The stability of the beam output was monitored during the measurements. The reported doses and thermal fluences were corrected according to the ratio between the reference beam monitor pulse frequency and the observed beam monitor pulse frequency. The observed pulse frequency was determined as an average from the integrated pulses during each measurement. Thus all the dosimetry results were normalised according to the reference beam output.

3.1.5 Dose calculations

The FiR 1 epithermal beam was modelled with the deterministic two-dimensional discrete-ordinates transport code (DORT) using the 67-group (47 neutron + 20 γ) coupled P3 neutron-photon BUGLE-80 cross section library. The model which has a cylindrical symmetry in the horizontal direction was calculated in two parts. The first part includes the reactor core with the fuel elements surrounded by the graphite reflector and water. The forward biased core loading, where fresh fuel is located in the direction of the beam moderator block, was taken

into account in the model. The first part is usually not changed and thus it can be used as a source for the second part including the 63 cm thick Fluental™ moderator, the collimator set, the phantom and a part of the heavy concrete shield structure. Angular simulation of the beam was done using a forward-biased quadrature set (D-166) [75].

The dosimetry calculations for the cylindrical phantoms were based on the deterministic DORT code but the ellipsoidal phantom required the use of Monte Carlo based computations accomplished with MCNP (General Monte Carlo N-Particle Transport Code) and SERA (Simulation Environment for Radiotherapy Applications) code packages. The beam model was used as a source in the dose calculations providing absolute neutron fluence rates and neutron and gamma spectra in the free beam (in-air) and in the phantoms. The calculated beam intensity was adjusted according to the measured reaction rates based on the multifoil detector activations where different energy-dependent neutron cross sections are utilised in the measurement of the neutron spectrum [81]. IRDF-90 (International Reactor Dosimetry File) cross section library was applied to the DORT calculations of the neutron fluence rates to obtain the simulated reaction rates which were compared with the multifoil measured reaction rates [75]. The least-squares code (LSL-M2) [88] was used in the intensity adjustment of the DORT calculated neutron spectrum of the FiR (K63) beam resulting in a correction factor of -3.6% [43]. The dosimetry calculations were compared with measurements to verify the beam source model and the calculated dose components.

3.2 Dosimetry results

The dosimetry results concerning the measured (IC) and calculated (SERA, MCNP) neutron and gamma dose rates in the ellipsoidal phantom are presented in Chapter 3.2.1. The measured (IC) neutron and gamma doses in ellipsoidal and cylindrical geometries are presented in Chapter 3.2.2. The measured (Si(Li)-detector) and calculated (SERA) relative lithium reaction rates, thermal fluences and measured Mn reaction rates in the ellipsoidal phantom are presented in Chapter 3.2.3. Also the measured (Si(Li)-detector) and calculated (SERA) relative lithium reaction rates in the ellipsoidal and cylindrical geometries are presented in Chapter 3.2.3. The measured (IC) and calculated (SERA, MCNP) neutron and gamma doses in the ellipsoidal phantom from the displacement study are presented in Chapter 3.2.4.

3.2.1 Neutron and gamma dose in ellipsoidal water phantom

The relative neutron sensitivity (k_t) of the TE(TE) ionisation chamber (IC) according to the depth in the elliptical water filled phantom at the central beam axis are presented in Figure 9. The relative neutron sensitivities at the perpendicular direction to the beam axis were constant within 1% in the depths of 30 mm and 60 mm in the water filled ellipsoidal phantom.

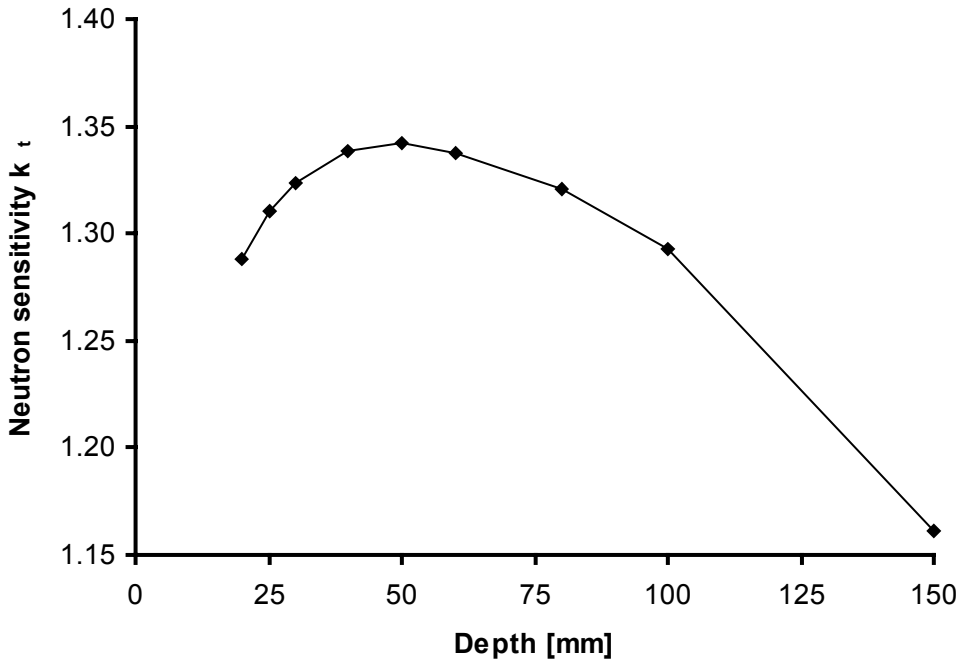

Figure 9. *The relative neutron sensitivity (k_t) of the TE(TE) ionisation chamber determined in the central beam axis according to the depth in the elliptical water filled phantom. The beam aperture diameter was Ø14 cm.*

The absorbed gamma and neutron dose rates in the central axis of the water filled ellipsoidal phantom are presented in Figure 10. The gamma dose measured with the Mg(Ar) non-hydrogenous ionisation chamber is compared with the MCNP and the SERA calculations in the upper set of curves. The neutron dose determined with twin chamber method is compared with the MCNP and SERA calculations in the lower set of curves. The error bars represent the uncertainty (1SD) of the measured dose.

The gamma dose rate determined at the perpendicular direction (dose profiles) as a function of distance from the beam central axis in the depths of 30 mm and 60 mm in the ellipsoidal water phantom is presented in Figure 11. The corresponding neutron dose is presented in Figure 12. The measured gamma and neutron dose rate values are compared with the calculated dose profiles from the MCNP and SERA simulations.

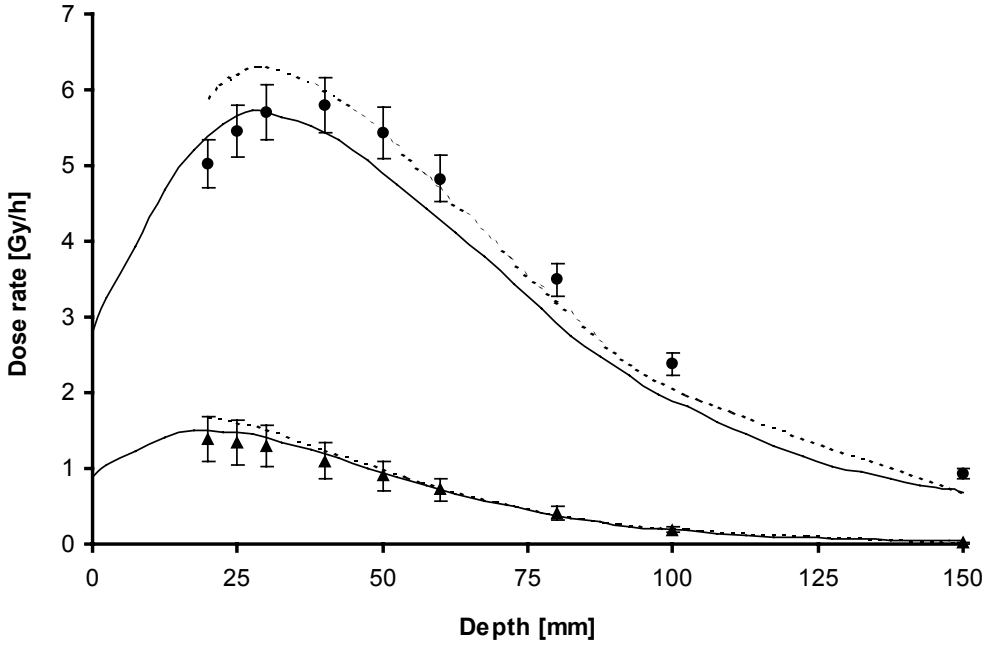

Figure 10. *The measured absorbed gamma (circles) and neutron (triangles) dose rate as a function of depth along the beam central axis in the water filled ellipsoidal phantom. The calculated dose from the SERA (solid line) and MCNP (dashed line) simulations are presented, respectively. The beam aperture was Ø14 cm. Error bars represent the uncertainty (1SD) of the measured dose.*

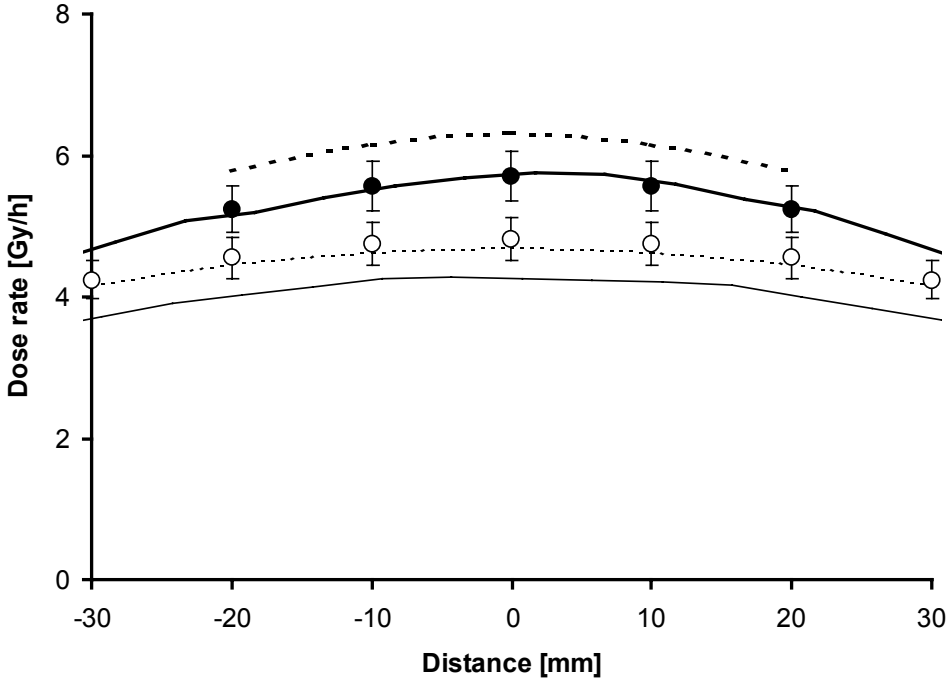

Figure 11. *The absorbed gamma dose rates at the perpendicular direction of the water filled ellipsoidal phantom. Distance is from the beam central axis. The calculated gamma doses from the SERA and MCNP simulations are presented as lines (SERA=solid, MCNP=dashed) and measured (IC) doses are marked individually as circles. Thicker lines and solid circles correspond to 30 mm depth. Thinner lines and empty circles correspond to 60 mm depth. The beam aperture was Ø14 cm. Error bars represent the uncertainty (1SD) of the measured dose.*

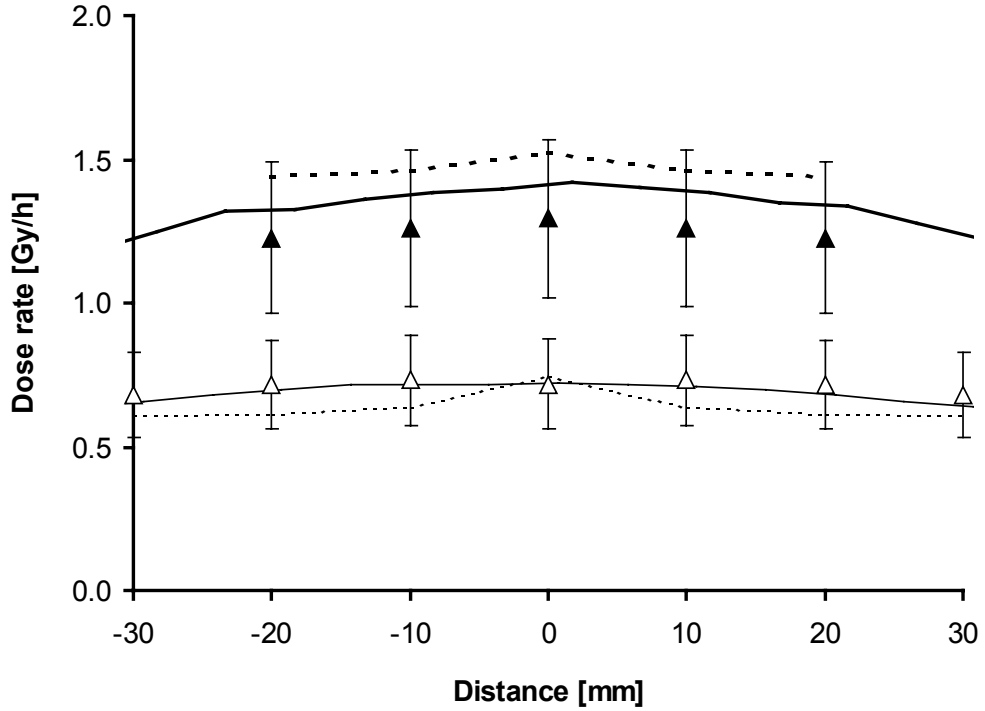

Figure 12. *The absorbed total neutron dose rates at the perpendicular axis of the water filled ellipsoidal phantom. The distance is from the beam central axis. The calculated neutron doses from the SERA and MCNP simulations are presented as lines (SERA=solid, MCNP=dashed) and measured (IC) doses are marked individually as triangles. Thicker lines and solid triangles correspond to 30 mm depth. Thinner lines and empty triangles correspond to 60 mm depth. The beam aperture was Ø14 cm. Error bars represent the uncertainty (1SD) of the measured dose.*

3.2.2 Neutron and gamma dose in ellipsoidal and cylindrical geometries

The measured gamma and neutron dose rates in the central axis of the water filled ellipsoidal and cylindrical phantom are presented in Figure 13 as depth dose curves. The gamma dose values measured with the Mg(Ar) non-hydrogenous ionisation chamber in the ellipsoidal phantom are compared with the gamma dose values in the cylindrical phantom in the upper set of curves. The neutron dose values determined with the twin chamber method in the ellipsoidal and cylindrical phantom are compared in the lower set of curves. The error bars represent the uncertainty (1SD) of the measured dose.

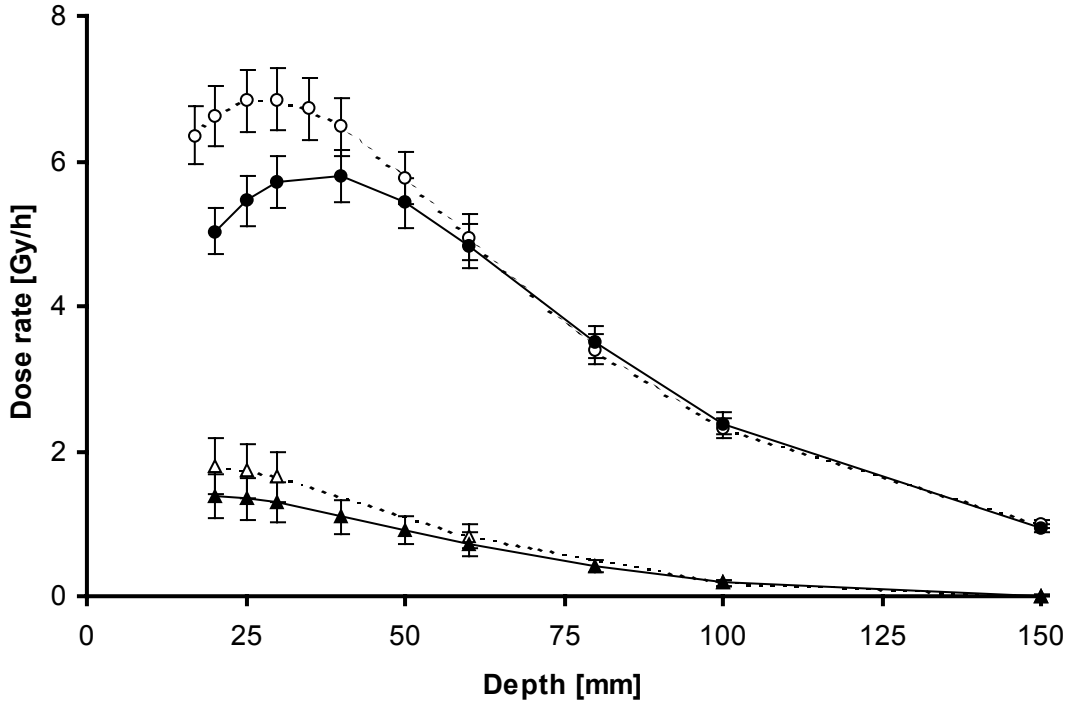

Figure 13. *The measured (IC) gamma (circles) and neutron (triangles) dose rates in the beam central depth axis in the water filled ellipsoid (solid symbols) and cylinder (empty symbols) phantom. The data from Kosunen et al. is used for the doses in the cylindrical water phantom [43]. The beam aperture was Ø14 cm. Error bars represent the uncertainty (1SD) of the measured dose.*

3.2.3 Thermal fluences in ellipsoidal and cylindrical water phantoms

The measured and calculated (SERA) lithium (^{6}Li) reaction rates, calculated (MCNP) thermal fluence rates and measured Mn reaction rates determined in the central axis of the water filled ellipsoidal phantom are compared in a relative scale in Figure 14. In Figure 15 the measured and calculated lithium reaction rates are compared in the beam central axis of the water filled ellipsoid and cylinder phantom geometries.

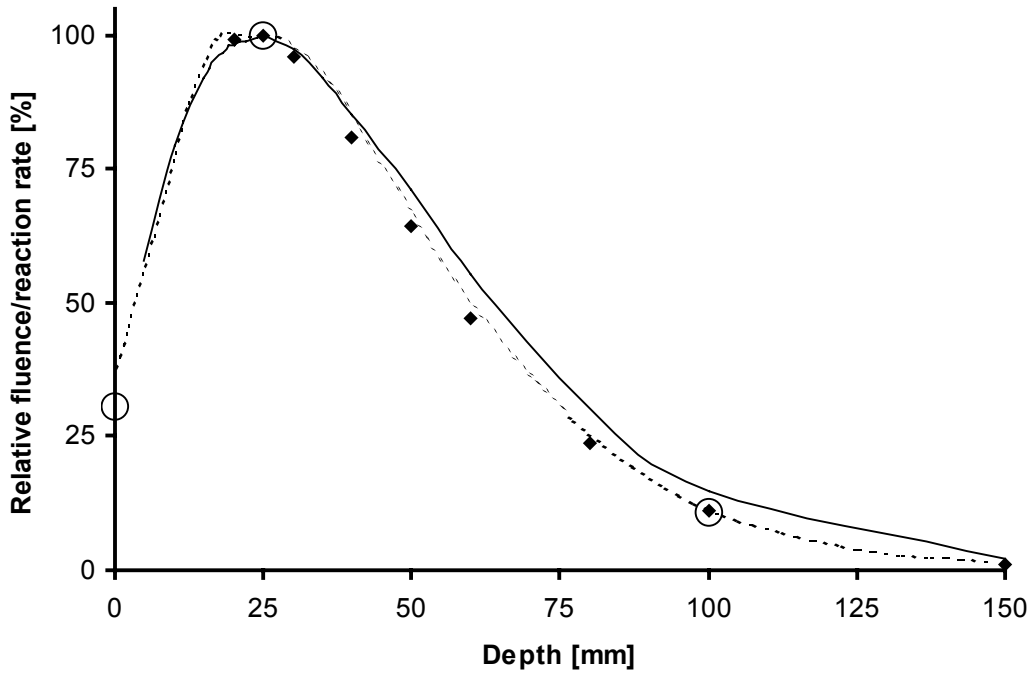

Figure 14. *The measured (solid line) and calculated (dashed line) relative lithium reaction rates, calculated thermal neutron fluence (diamonds) and measured Mn reaction rates (empty circles) at the beam central depth axis in the water filled ellipsoidal phantom. The beam aperture diameter was Ø14 cm.*

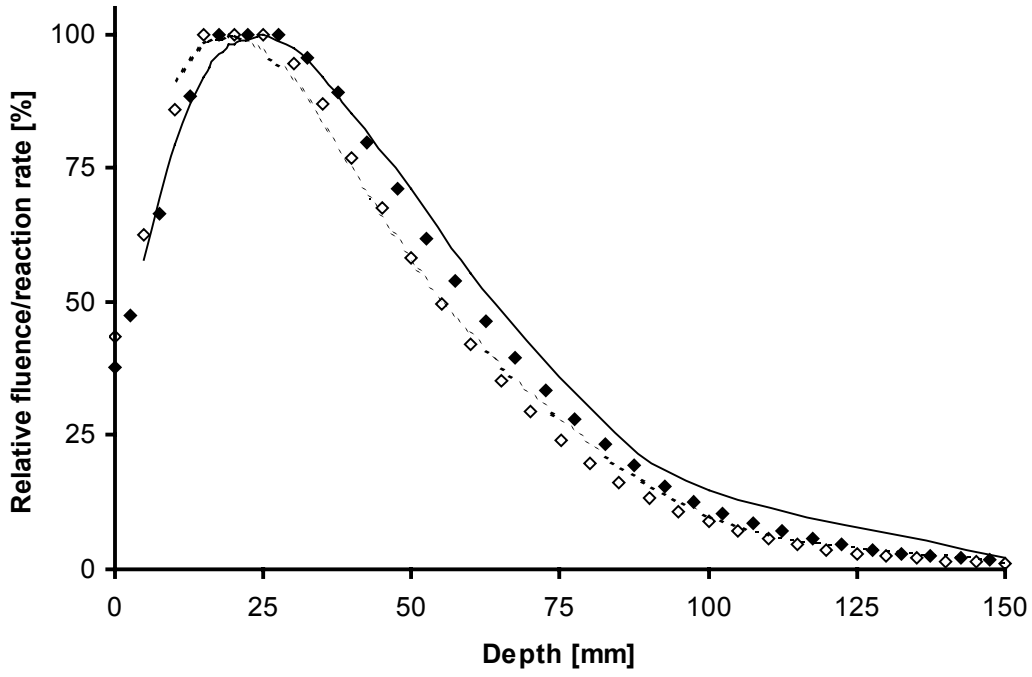

Figure 15. *The measured (lines) and calculated (diamonds) relative lithium reaction rates at the beam central depth axis in the ellipsoidal (solid line and diamonds) and cylindrical (dashed line and empty diamond) water filled phantoms. The beam aperture diameter was Ø14 cm.*

3.2.4 Gamma doses in ellipsoidal phantom displacement study

The gamma doses in the displaced and central phantom positions are presented in Figure 17 for the translated sagittal plane points corresponding to the approximate eye location in a human head. Points 1-3 correspond to the surface points located 40 mm in the perpendicular direction from the beam central axis. Points 4-6 correspond to the inner points located 20 mm in the perpendicular direction from the beam central axis. Points 3 and 4 were closest measured locations to the beam whereas the points 1 and 6 were the furthermost locations as presented in Figure 16.

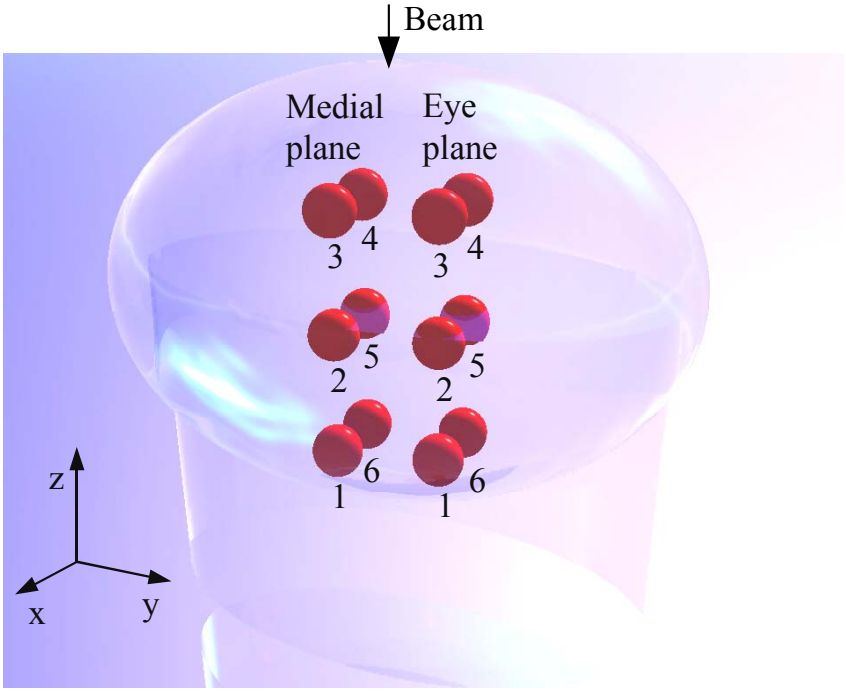

Figure 16. *The IC measurement points inside the ellipsoidal phantom. Two phantom positions were used for all the measurement points. The eye plane points were used in this study to determine the doses near the edge of the phantom with and without the beam asymmetry caused by the lateral phantom displacement of 35 mm [78]. The beam direction is schematically presented as an arrow.*

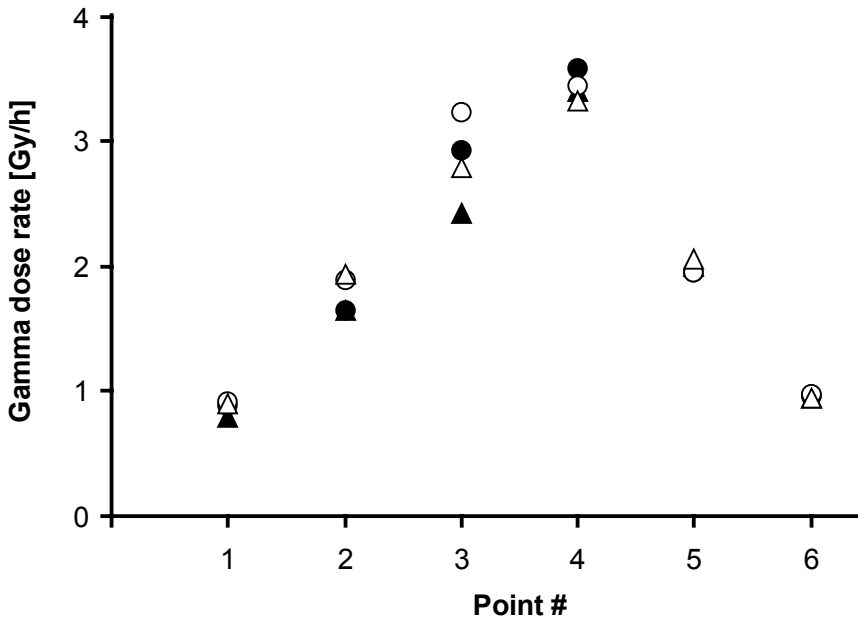

Figure 17. *The measured (IC, circles) and calculated (SERA, triangles) gamma dose rates in the specific locations in the water filled ellipsoidal phantom with two studied phantom positions (solid symbol for centre and empty symbol for displacement) in the translated sagittal plane points of the ellipsoidal phantom. The beam aperture was Ø11 cm [78].*

3.3 Dosimetry discussion

An extensive measurement campaign has been carried through in this work. The results presented here are mainly concentrated in the studies in the ellipsoidal water phantom. The ellipsoidal phantom was considered of special interest because it has resemblance with human head geometry. However, the dosimetry concerning the ellipsoidal geometry has practically left without reporting in the Finnish BNCT project. Much of the published dosimetry data has been acquired in the cylindrical geometry because it is simple and generally applicable in practical measurements and radiation transport simulations [42, 43, 82, 84, 89]. Especially the DORT model assumes cylindrical symmetry in dose calculations [90]. The dosimetry results described here are mainly measured with the twin ionisation chambers and Si(Li) diode detectors while keeping the main scope in the ionisation chambers studies.

An epithermal neutron beam introduces difficulties to the twin ionisation chamber method because the wide neutron energy spectrum requires determining the chamber sensitivities in all neutron energy ranges including the thermal energies [43, 61]. The thermal neutron energy range is covered in only first two groups of the BUGLE energy structure [91]. However, the relative neutron sensitivity of the tissue equivalent ionisation chamber as a function of neutron energy has maximum values in the thermal range as presented in Figure 18 [83]. The BUGLE library is obviously not an optimal cross sectional reference for BNCT since it was compiled for the reactor pressure vessel calculations of power reactors where the group cross sections are weighted accordingly. There is no cross sectional library available with weighting aspects specifically considered the mixed epithermal neutron fields in BNCT [75].

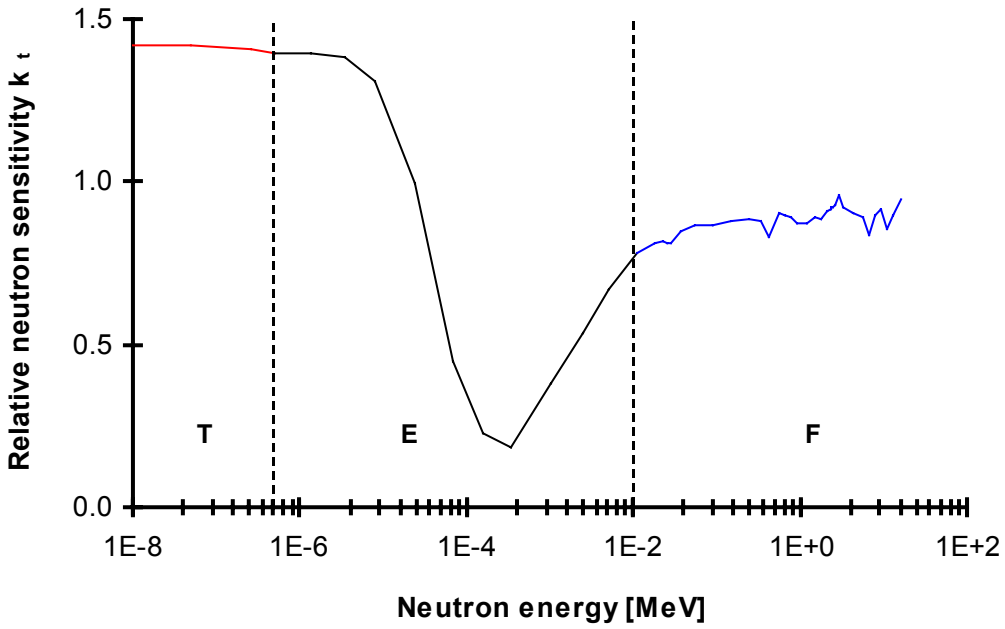

Figure 18. *The distribution of the relative neutron sensitivity k_t of the tissue equivalent ionisation chamber as a function of neutron energy presented in the BUGLE energy structure with 47 energy groups using the data of Jansen [83]. The thermal (T), epithermal (E) and fast (F) energy ranges are separated with dash lines.*

The kerma factors conceal the cross sections of elemental constituents of the medium where the absorbed dose is quoted. In BNCT dosimetry the absorbed dose is quoted in the ICRU brain tissue [32, 42, 43]. The major cross sections affecting the total dose are the neutron capture reactions of nitrogen and hydrogen and the neutron capture of boron when boron is included. Those cross sections are concentrated on the lowest neutron energies and generally the event probability is governed with the 1/*v* dependence which makes the thermal neutron energy range considerations crucial for the total dose reliability.

Taking into account the varying shape of the neutron energy spectrum with respect to the depth in the object volume the neutron kerma factors of individual values are required in each measurement position in each phantom setting. Therefore a weighting of kerma factors according to the neutron energy spectrum was done in all energy bins to increase the accuracy of the relative neutron sensitivities of the TE(TE) ionisation chamber. The determination of the relative neutron sensitivity relies on the calculated neutron spectrum. The BUGLE energy structure consisting of 47 neutron energy bins used in radiation transport calculations was expanded into 640 energy bin (SAND-II) structure using the POTOFINE program code [92]. Since the thermal region structure of the spectra cannot be determined from the BUGLE apportion consisting of only two thermal energy bins a general Maxwellian shape was assumed in the energy distribution of neutrons in the lowest thermal energies. This lowest energy spectrum was then joined to the expanded 640 binned spectrum at the neutron energy of 0.14 eV by scaling of the Maxwellian spectrum. Respectively, the neutron kerma factors defined by ICRU [73, 93] were converted into the same 640 group energy binning. In the lowest energies the ICRU data had to be extrapolated assuming the 1/*v* energy dependence mentioned above. Thereafter the kerma factors were compacted back into the BUGLE energy structure by weighting them according to the spectral abundance of neutrons in each energy bin. The FLXPRO code included in the LSL-M2 software package [88] was used in the

weighting procedure. The weighting of the kerma factors should have been done at each measured position, and in each phantom geometry and material due to the individual neutron spectrum in all those circumstances. However, that would require an overwhelming effort due to the large amount of measurements. Use of a common weighting spectrum determined at the depth of 2.5 cm in the cylindrical water phantom was considered sufficiently accurate to the determination of the relative neutron sensitivities in the neutron dose measurements [43].

The difference in the doses between the ellipsoidal and the cylindrical phantom geometries was anticipated. The geometry of the ellipsoid represents a curvilinear shape and a volume with considerably less water mass on the side of the beam. The volume of the ellipsoid is less than a half of the volume of the cylindrical phantom. Therefore there is also considerably less water for the radiative neutron capture of hydrogen to produce incident gammas at small depths in the phantom. Also there is less mass for photon scattering on the beam side of the ellipsoidal phantom compared with the cylindrical phantom geometry. That could explain why the gamma peak has shifted slightly deeper specifically in the ellipsoidal geometry. However, there is a clear discrepancy between the measured (IC) and calculated (SERA and MCNP) doses at the beam depth axis in the ellipsoidal water phantom. The measured gamma dose distribution at the central depth axis of the ellipsoidal water phantom in Figure 10 shows that the peak is located approximately in the 4 cm depth. Thus the measured results refer to a deeper gamma maximum than the calculated dose curves determined by radiation transport codes. The ellipsoidal phantom was attached to the large water tank (Cadscan pool). The presence of the large water volume (>100 litres) behind the ellipsoidal phantom could explain the discrepancy in its part. The gamma rays returning from the water tank contribute to the gamma dose distribution inside the ellipsoid with an opposing dose gradient compared with the original gamma field. The observation made by Wojnecki and Green supports the possibility of such contribution [94]. Deeper gamma maximum in the ellipsoidal phantom has been mentioned already in the previous publication [42].

The Mg(Ar) ionisation chamber, the magnesium build-up cap and the detector stem create a void in water relative to hydrogen concentration which creates perturbation to the local effective radiation field in the phantom [43]. The combined volume of hydrogen deficiency is 1% of the volume of the phantom. The detector stem creates an elongated air volume behind the chamber in the direction of the main gamma field gradient as shown in Figure 8 which potentially affects the central depth dose distribution. Furthermore, the SERA and MCNP calculations have considerable absolute discrepancy with each other. The absence of measured value in the depth of 3.5 cm obscures the exact location of the measured gamma dose maximum. Therefore additional studies in 2 cm and 5 cm depths with decreased intervals between measurement points should be performed.

Another perturbation effect may occur as a result of the finite chamber volume in the presence of a non-linear gamma dose gradient. The volume of the detector acts as a smoothing filter over the dose peak which is smaller than the effective chamber size and the effective point of the detector is shifted towards the gradient [3]. Due to the averaging the gamma dose peak can be underestimated (and the low doses overestimated) compared with the surrounding areas. On the other hand in the presence of a monotonically behaved dose gradient the effective point of the detector is likely to shift towards the dose gradient thus resulting in an overestimating smoothing effect. In the case of a linear dose gradient, the measured dose follows the gradient but because of the drifting of the effective point the measured values are biased upwards.

The measured gamma dose peak appears to be slightly smoother than the calculated maximum regions in the depth dose curve, thus presenting a possible averaging effect of the net chamber volume. However, the measured values do not display either overestimating or underestimating smoothing effects with respect to the calculations. The maximum gamma dose rates from the measurements equal that of the SERA calculations although the peak depth is different.

The measured and calculated gamma doses in the perpendicular axis agreed well in the 30 mm depth but in the 60 mm depth there was a clear discrepancy. The discrepancy is consistently of the same magnitude (about 10%) as in the depth dose curve in the same depth. An offset error in the detector position set-up was also considered as one possible error source that could have caused the observed discrepancy. However, the depth axis measurements and the profile measurements perpendicular to the depth axis were done with separate measurement sessions. In each session the detector position was reset by driving the detector build-up cap in contact with the vertex of the phantom. It is unlikely that the same offset error in detector positioning during the measurements would have occurred twice in two individual settings and with a same amount of spatial error.

The measured neutron dose distribution on the central depth axis and on the perpendicular axis in two depths (30 mm and 60 mm) agreed well with the calculated doses within the uncertainties of the measurements. The measured neutron dose profile in the 30 mm depth is about 10% below the SERA calculated profile which is between the measured and the MCNP calculated neutron profile. The gamma subtraction is the main source of uncertainty in the neutron dose determination with the twin ionisation chamber method in epithermal neutron beams [43]. The good agreement of the measured and calculated neutron dose implies that the gamma subtraction is done correctly in the measured TE(TE) detector signal. Thus also the neutron doses confirm the assumption that the measured gamma dose distribution is correct.

Summarising the difficulties relating to ionisation chamber dosimetry in BNCT the detector material (gas and the wall), size and neutron sensitivity are the most relevant factors. The detector size relative to phantom dimensions and the desired spatial resolution (due to the dose gradients) of the dose distribution should not be in conflict with each other. The finite size of the detector and its supporting structures always cause perturbation to some extent in the net mixed radiation field when the detector materials differ from the elemental composition of the phantom. Therefore acquiring a material equivalence between the phantom and the detector and minimising the detector size should also minimise the effective perturbation of the radiation field [43]. It would also facilitate the use of detector in experimental practise. The detector material should also resemble the dose reference material as closely as possible at least with respect to the nitrogen and hydrogen concentrations. Thus the ratio of kerma factors between the detector and the reference material would be close to 1.00 in all neutron energy regions.

The maximum of the relative lithium reaction rate measured with the Si(Li) diode detector and the calculated thermal fluence rate coincided within the phantom central depth axis region. The Li reaction rate relates mostly to the thermal neutron fluence rate as the detector efficiency for the fast neutrons and gammas is negligible and can be further reduced by using zero bias voltage [54, 80]. The Si(Li) diode detector is typically used in spatial measurements providing relative distributions. The structure of the detector has open features that can render it prone to environmental effects. The detector should be calibrated to produce absolute Li reaction rates and possibly to provide absolute thermal fluence rates. The sensitivity of the

detector requires lowered reactor power levels to maintain useful dead times in the measurements. This is due to the converter composition and thickness [80]. It is possible to construct a different converter which makes the detector suitable for the measurements using full reactor power corresponding to clinical BNCT irradiations. The custom made computer program can be used to perform the measurements automatically by controlling the diode acquisition together with the detector movements in three dimensions using the step motor based transport mechanism of the CADSCAN phantom system [87].

The use of semiconductor detectors has potential in future applications of BNCT dosimetry. There are several advantages in the use of diode based technologies as concluded in several studies [50, 53, 54, 80, 95]. Diode detectors are potentially cheaper than the conventional detectors which require highly specialised fabrication techniques. The same implies also for the diode detectors but the integrated circuit technologies form a massive area of industry that has momentum and resources for continuous technological development and large production quantities. Therefore the evolution of semiconductor based radiation detectors has various production platforms to choose its optimal niche. Diode detectors are also practical implementations in clinical facilities as they do not require demanding supportive systems such as gas flow rigs or high-voltage supplies. Measurements can be performed in real time without a need for additional readout or analysis timeouts. Different spectral components can be measured simultaneously with a high spatial resolution. The measurements are realised in solid state and thus there are no wall effects to consider. The possibility to construct multiple arrays of detection cells into a single detector assembly forms an obvious basis to improve the collection statistics. Considering the practical aspects further, the small size and operation at clinical beam power levels make the technology more feasible in routine use. The diode technology is also scalable from the methodological point of view. Devices can be manufactured with sizes and morphology of resemblance with living tissue cells. The BNCT applications could be further enforced by including boron dopant as specific concentrations and spatial distributions [50, 53, 95]. Various materials above boron can also be considered as implant substance. However, possible radiation damage and the consequential change in the detector sensitivity should be taken into account when assessing the feasibility of semiconductor technique in specific dosimetry applications.

There are at least two additional experimental methods for the BNCT dosimetry which are under preliminary evaluation in the Finnish project. Microdosimetry methods based on tissue equivalent proportional counters (TEPC) have been utilised already in the dose determinations of other epithermal beams [49, 96-98]. The proportional counter gas volume is filled with low pressure tissue equivalent gas so that the effective collective volume of the detector corresponds to site volumes of a typical cell (the diameter in the order of μm). The initial measured signal is amplified and analysed with a multichannel analyser (MCA) as in the diode detector measurements. The acquired pulse height spectrum is used to determine the single event spectrum as a function of lineal energy which can be considered analogous to linear energy transfer (LET) spectrum. Single event spectrum represents the distribution of the energy depositions in the simulated microscopic volume as a function of energy deposition magnitude. It can be used further to assess the (macroscopic) absorbed dose components of the BNCT beam. The detector can be calibrated using the proton edge as a distinctive landmark. The gamma dose forms a clearly visible peak in the measured single event spectrum. The separately determined gamma spectrum can be used to determine the shape of the gamma component in the combined gamma and proton single event spectrum. In the first approximations a known gamma spectrum form is fitted to the measured spectrum. Thus the overlapping tail of the gamma distribution and the proton part can be separated. The

absorbed dose equivalent values can be acquired by integrating the determined gamma and proton components individually. The fast neutron dose and the nitrogen dose cannot be distinguished from each other because the proton event spectra from both dose components are overlapped. However, using boron as a dopant substance in the counter wall material the boron dose component can be determined using two proportional counters: one with boron and another without it. Thus the combined gamma, neutron (proton) and boron dose determination with TEPC method resembles somewhat the twin ionisation chamber method. The dead times of the current detectors limit the TEPC studies into low beam intensities corresponding to few percentages of the normal clinical reactor power settings. This may introduce some uncertainty in the dose assessment. Miniature detectors could solve the problem but the required significant decrease in the sensitive volume bring cumbersome technical problems that need to be solved in order to develop functional applications for the current BNCT beams [99]. The assessment of the dose uncertainty with microdosimetry TEPC method is part of the current dosimetry studies in Finnish BNCT project and as a part of the EU shared cost project "Code of Practice for the dosimetry of BNCT in Europe" [100].

Polymer gels have also been studied as a potential method for the dose determination in epithermal beams. The BANG3-3Gy (MGS Research Inc, USA) gel packed in Pyrex glass vials have been introduced in the Finnish BNCT beam studies where the gel material is practically tissue equivalent in elemental composition and in density [101]. Thus all the relevant dose components occurring in tissues irradiated with the mixed field of epithermal neutrons are also reproduced in gel material. The response of the gel to the absorbed dose is the prolongation of the T_2 relaxation times. Thus the absorbed dose distribution in three dimensions can be determined with MRI scan using spin echo sequence to determine the T_2 relaxation time map. The gel studies were simulated with SERA code to evaluate the gel method and to make comparisons with calculations. The Mn-Al activation detectors and TL detectors were used along the gel measurements as a common practise to verify the calculational model. According to the preliminary results the measured and calculated dose distributions were in agreement. The gel dosimetry method can be particularly useful in BNCT by offering an excellent spatial resolution for the dose determination if the perturbation of the gel container walls turns to be negligible. However, such perturbation is not inherent to gel itself and thus the use of gel detectors is a potential new option for the BNCT dosimetry [102].

The position displacement study provided measured doses in the presence of curvature surfaces and the asymmetrical beam position [78]. The measurements and calculations agree that the doses are higher in the asymmetrical beam position on the beam side locations of the phantom as presented in Figure 17. For the asymmetrical beam the phantom was displaced 35 mm from the beam central axis. The same situation occurs in patient irradiations when an oblique beam direction is used. The beam line according to the entry and exit points is positioned by keeping both aspects of target volume doses and protection of the organs at risk in mind. Therefore the beam line is always a compromise where the symmetry issues are not among the most critical factors. However, they have an obvious impact on the dose which should be determined correctly by the treatment planning. According to this study the calculations and measurements were generally in a good agreement.

However, the results show that there are locations near the oblique surface of the phantom where the calculated and measured doses had considerable discrepancy irrespective of the beam asymmetry as shown in Figure 16 for the third measurement point. The boundary regions have already previously proven to be problematic dosimetry issues for calculational

codes and also for the measurements [10, 103]. Higher inconsistencies should be anticipated in such circumstances. Importance of reciprocal verification of measurements and calculations is emphasised as the geometry becomes more complex.

New studies using an antropomorphic head phantom should be performed based on the results of the measured and calculated doses in the ellipsoidal phantom. For example, a commercially available radiosurgery verification phantom (RSVP, Phantom Laboratory, Saalem, New York) could be a suitable candidate for realistic simulation of patient head geometry in future works.

4 BORON CONCENTRATION IN BLOOD

The principle of BNCT in targeting the high-LET radiation to the tumour at the cellular level is dependent on the boron (^{10}B) biodistribution. Within appropriate circumstances the dose to the target area should be strongly dominated by the boron dose [12]. The boron dose is calculated from the adjusted neutron fluences, the boron kerma factors and the boron concentration in the tissue [32]. The dose from the 477 keV prompt gamma radiation (from the ^{7}Li-recoil de-excitation) is negligible and furthermore it is summed into the gamma dose instead of the boron dose. The neutron fluence is acquired by dose calculations using the beam source model which has been verified by calculations and measurements when the beam has been characterised. The boron kerma factors are included in the treatment planning program and are based on the ENDF cross section data libraries [104]. The boron concentration in the tissue is estimated from the blood boron concentration during the irradiation by applying the assumed blood-to-tissue boron concentration ratios for tumour and healthy tissue. The assumed ratios of boron between the tissues and the whole blood are obtained from the literature [64, 105]. The ratios for BPA used in Finnish trials are as follows: 1:1 for the normal brain-to-blood, 3.5:1 for the tumour and target volume-to-blood and 1.5:1 for the skin-to-blood [64]. Thus the blood boron concentration is an essential parameter in each BNCT treatment as it scales the dose level in critical tissue and the tumour individually. The blood boron concentration is also an important parameter in itself because it affects directly the dose to the cranial vasculature. The boron estimation chain is presented in Appendix 2.

BPA has a low solubility on its own and therefore it is applied as a fructose complex BPA-F [106]. The use of BPA-F as a boron carrier has shown to be safe with i.v. infusions of 250-290 mg/kg of BPA [105, 107, 108]. The determination of boron concentrations in brain and other important tissue other than blood is currently not available since there is no practical means for non-invasive quantitative boron specific imaging during the treatment. However, there are studies aiming at the detection of BPA-F with magnetic resonance spectroscopy (MRS) and some imaging trials have already been carried out with a ^{18}F-labeled analogue of BPA imaged with positron emission tomography (PET) [109-114]. Earlier biological studies using ^{11}B as BSH complex in magnetic resonance imaging (MRI) and spectroscopy (MRS) have been reported already in 1988 [115].

4.1 Materials and boron estimation methods

A static infusion of the boron carrier is applied following a treatment with typically two consecutive irradiation fields. During the infusion the blood boron concentration increases and achieves its maximum value at the end of infusion. After the infusion the blood boron concentration starts to decrease according to bi-phasic clearance pattern [116]. A rapid fall is followed by a slowly tapering component. During the irradiations the blood boron concentration has already decreased significantly (40-50%) from its peak value. The blood boron level, the infusion phase and the timing of the irradiation fields are presented in Figure 19.

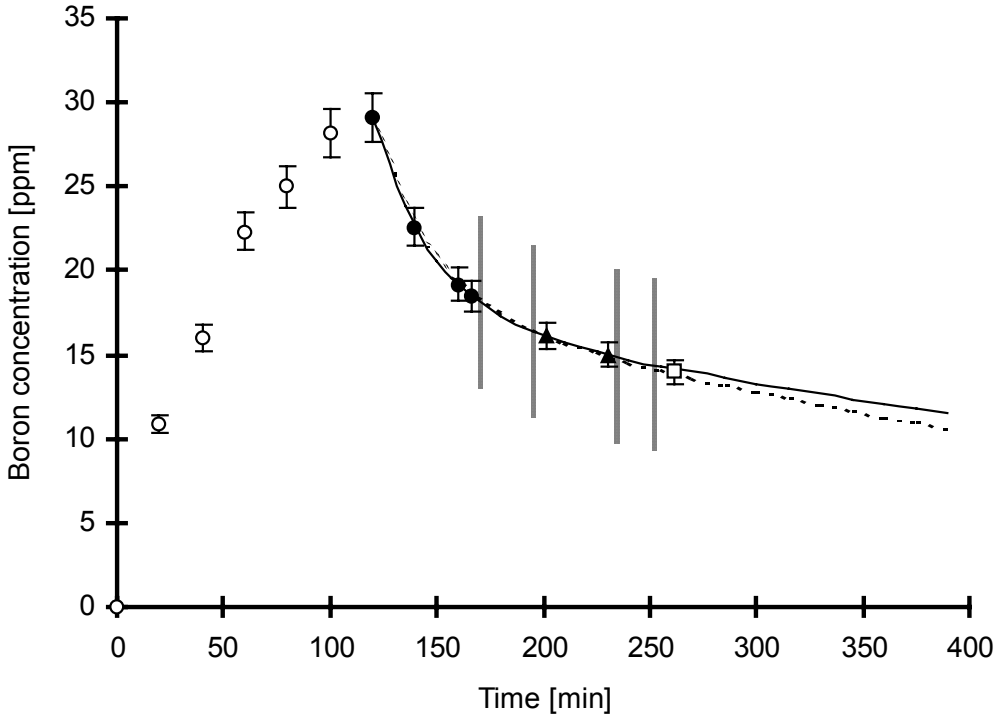

Figure 19. *The average blood ^{10}B concentration curve showing the BPA-F infusion and BNCT irradiation field phases of the Finnish clinical phase I trials. Standard (dashed line) and iterated fit (solid line) are presented with start and end indicators of the fields (vertical lines). Measured values during the infusion (empty circles), initial phase (solid circles) and intermediate phase (solid triangles), and after the treatment (empty square) are presented with individual symbols. Error bars represent the uncertainty of the measured values.*

There are several reasons why the determination of the blood boron concentration cannot rely solely on the measurements. The measured blood boron level as a function of time is only roughly obtained from the analysed blood samples. Sampling cannot be applied during the therapy irradiation where the knowledge of the blood boron level would be critical to have. There is considerable variation in the blood boron concentrations between individual patients irrespective of the same infusion scheme. Therefore an individual estimate for boron biokinetics is needed for each patient [66]. The objective for this part was to create an application which provides an on-line estimate of the blood boron concentration during the ongoing irradiation field. The proper quantification applies the standard kinetics and the updating real time blood sampling data before each treatment. The estimate of the boron concentration is needed prospectively before each irradiation field to set the irradiation time properly for the prescribed dose. Specifically, the first blood boron estimation uses the measured data points available before the first irradiation field and it is referred to as the *initial* boron estimation. The second blood boron estimation uses the measured data points available before the second irradiation field and it is referred to as the *intermediate* boron estimation. The last blood boron estimation when all the measured data points are available for calculation is referred to as the final estimation.

4.1.1 Boron infusion and measurements

The blood boron concentrations were measured from the blood samples with inductively coupled plasma atomic emission spectroscopy (ICP-AES) during the BPA-F infusion (290-400 mg of BPA per kg of total body weight) and after the infusion [65]. An interpolated average of the 12 protocol-1 patients of the Finnish phase I trial with respect to timing of the blood samples and analysed boron levels is presented in Figure 20. The blood boron data of those patients was used to determine the standard parameters of the estimation model used for the prospective boron estimation.

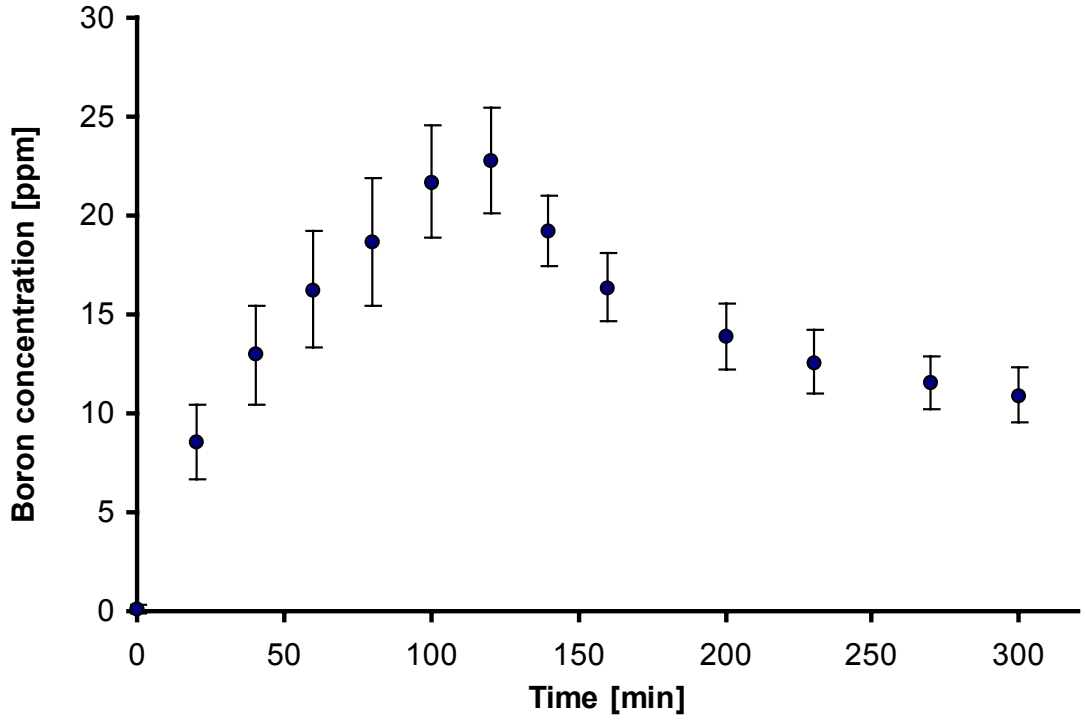

Figure 20. *The average blood boron concentrations of the 12 protocol-1 patients with 290 mg/kg of BPA infusions according to the interpolated boron data. Error bars represent the uncertainty (1SD) of the interpolated values.*

The treatments included two sequential irradiation fields, after a 120 min infusion of BPA-F where the blood boron concentration was continuously increasing. The first blood sample was taken before the infusion to lay the initial concentration value. Thereafter samples were taken typically in every 20 minutes until the end of the infusion. The maximum boron concentration was reached at the end of the infusion. Thereafter the boron amount in blood followed typically a monotonously decreasing bi-phasic clearance pattern [116]. During the clearance phase 2-3 blood samples were taken before the first irradiation field beginning about 50 minutes after the end of the infusion. Another 2-3 samples were taken between the irradiation fields and at least one after the second field.

4.1.2 Estimation model

The measured whole blood boron concentration provided the source data for each individual boron estimation. The temporal behaviour of the blood boron level was modelled with a bi-exponential function described by equation

$$c_B = a_1 \exp(-a_2 t) + a_3 \exp(-a_4 t), \tag{5}$$

where the background concentration of ^{10}B is assumed to be zero. The bi-exponential function was fitted according to the measured blood boron clearance data using the end-of-infusion maximum value and values thereafter for the calculations. Thus the measured infusion phase data was not used in this method. The first point (the peak value at the end of infusion) was applied to fixed half-lives determined from the previous clinical data consisting of 12 first patients in the first protocol of the Finnish clinical trials. In this default fit only the a_1 parameter was set as the exponential function was scaled according to the peak value. A weighting of $a_1=2.7*a_3$ was used according to a patient data as a default ratio between the coefficients a_1 and a_3. As there were more measured data available the fitting set a_1 according to the peak point and a_3 according to the last measured points keeping the fixed half lives constant. In addition to the default fit an iterative fit algorithm was also applied. A minimum of four measured points after the peak value (on the declining part of the ^{10}B curve) is required to apply the differential correction algorithm, based on the gradient search method of least squares to determine the values of the bi-exponential function parameters; a_1, a_2, a_3 and a_4. The default fit calculated so far was used as an initial approximation for the iteration algorithm. Parameters were adjusted by successive iterations to force the correction according to the gradient of χ^2 which is written as

$$\nabla \chi^2 = \sum_{i=1}^{n} \left[\frac{\partial \chi^2}{\partial a_1} \overline{a_i} \right], \tag{6}$$

where $\overline{a_i}$ is a unit vector for the a-parameter coordinate axis [117, 118]. The iterations were proceeded until the fit converged to the final solution. The iteration end condition was the fixed tolerance value of goodness of fit which was determined according to the χ^2 (Chi Square) test value. The iterated and default fit curves were plotted with the measured data points to the chart of the boron data interface.

The code of the bi-exponential fitting application was written in Visual Basic to operate as a MS Excel macro program with a clinical interface including an input of the parameters and a graphical readout of the boron estimation curve and the irradiation timing data. Updated irradiation schedules could be tested to have on-line estimations of the practical boron levels during the therapy irradiation fields. The estimation was developed further and finally the boron application was extended into a treatment log workbook where the boron data was combined with the beam data to work as an operational interface for the irradiations. The characteristics of the treatment log are described thoroughly in general discussion and examples are presented in Appendices 8-11.

4.2 Estimation results

The exponential half lives of the studied nine patients and the 12 patients used for the definition of the standard half lives are presented in Figure 21. The fast and slow half lives determined from the final fit calculated with the iterative algorithm have correlation of R=0.77. The regression function is:

$$T_{½\_slow} = 8.7 \cdot T_{½\_fast} + 175 \text{ min.} \quad (7)$$

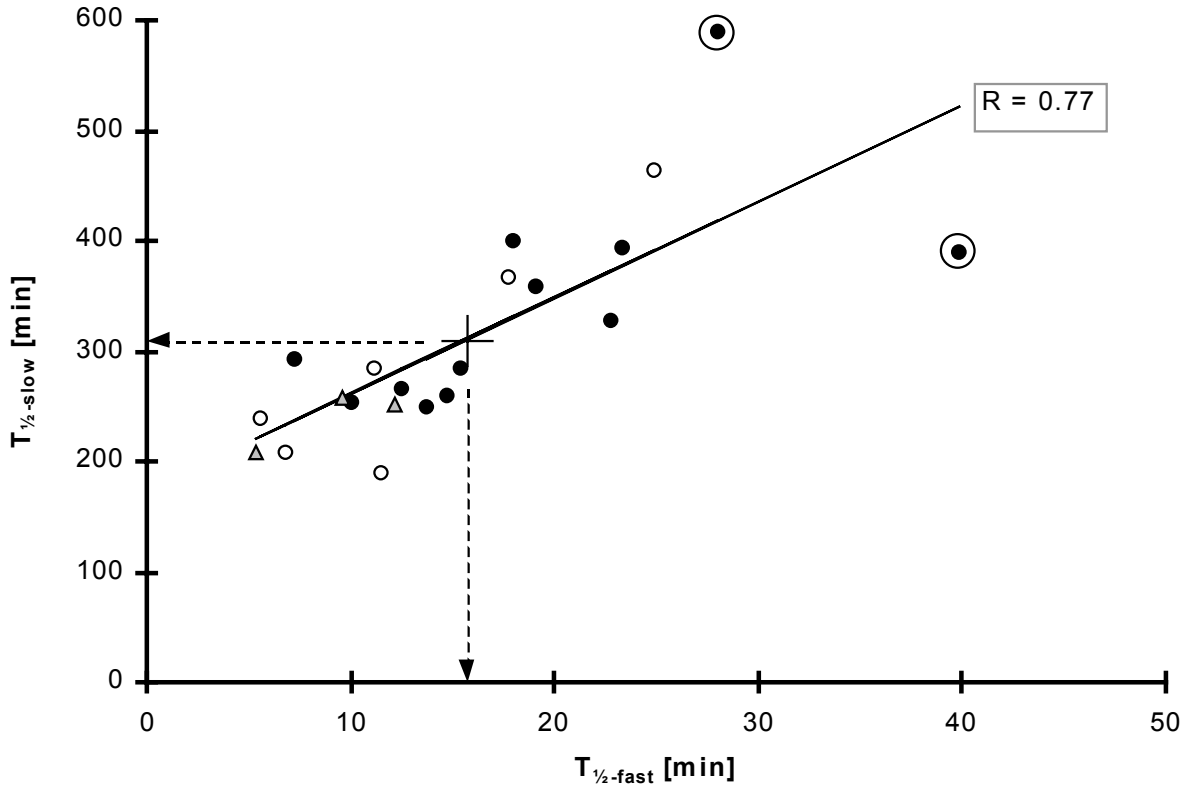

Figure 21. *The fitted half lives of the protocol 1 patients with 290 mg/kg infusions (black circles), protocol 1 patients with 330-400 mg/kg infusions (white circles), protocol 3 patients with 290 mg/kg infusions (triangles). The average half lives of the protocol 1 patients with 290 mg/kg infusions (excluding the two ringed circles) were used as defaults (cross and arrows). The BPA-F infusion time was 120 min. The regression line (solid) is plotted with the correlation coefficient R.*

The progression of bi-exponential fit as more measured data values are available is presented in Figure 22. The blood boron estimation data from the studied nine cases is summarised in Table 3.

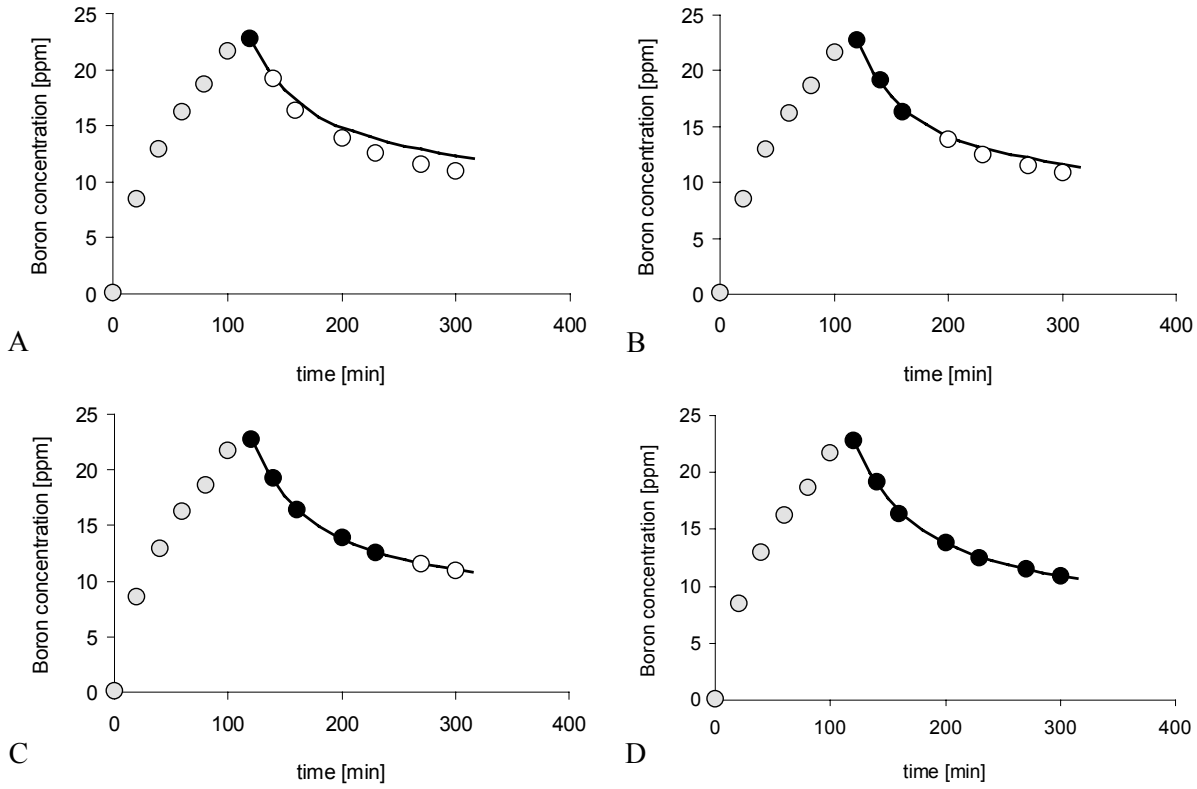

Figure 22. *The bi-exponential function fitting solutions for 1 (A), 3 (B), 5 (C), and 7 (D) blood boron values after the BPA-F infusion, determined from the interpolated average boron measurement data of the protocol 1 patients with 120 min (290 mg/kg BPA-F) infusions.*

Table 3. *Summary of the studied cases including the patient and protocol number, the infusion amount (BPA of total body weight), the normalised χ^2, the intrinsic standard deviation of the fit in ppm of boron and the half life values (fast and slow) of the bi-exponential fit.*

Patient #	Protocol #	BPA infusion (mg/kg)	Normalised χ^2	Intrinsic SD (ppm)	Half-lives	
					Fast (min)	Slow (h)
1	III	290	0.10	0.11	5.4	3.5
2	III	290	0.20	0.16	9.6	4.3
3	III	290	0.08	0.10	12.2	4.2
13	I	330	1.78	0.50	5.5	4.0
14	I	360	0.33	0.26	24.9	7.7
15	I	360	0.04	0.08	11.2	4.7
16	I	360	0.01	0.03	17.8	6.1
17	I	400	0.38	0.24	11.5	3.2
18	I	400	0.77	0.41	6.8	3.5

The normalised χ^2 of the boron estimations in the protocol-3 infusions (120 min and 290 mg/kg BPA-F) is 0.12. The normalised χ^2 of the boron estimations in the protocol-1 infusions (120 min and 330-400 mg/kg BPA-F) is 0.55. The change in the standard deviation of the fit from the final measured data as more measured values are available for fitting is presented in Figure 23.

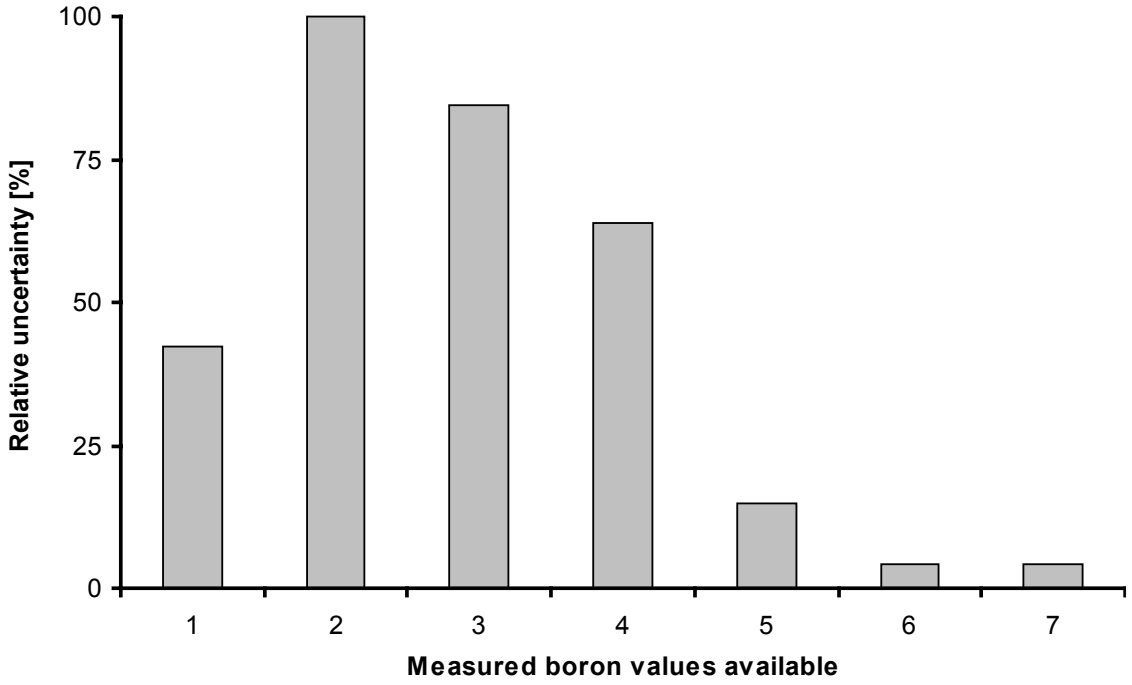

Figure 23. *The increasing accuracy of the boron estimation described by the relative uncertainty (1SD) between the updating fitting curves and the final measured (ICP-AES) boron concentrations determined from the interpolated average boron measurement data of the protocol 1 patients with 120 min (290 mg/kg BPA) infusions.*

The initial uncertainty of the blood boron estimation using the bi-exponential fit is 0.5 ppm (3% 1SD) and 0.4 ppm (3% 1SD) for the first and the second irradiation fields, respectively. The intermediate uncertainty of the blood boron estimation is 0.2 ppm (1% 1SD) and 0.4 ppm (3% 1SD) for the first and the second irradiation fields, respectively.

4.3 Boron discussion

The distribution of half lives including also the 12 patients used as a source data for the definition of the standard half lives presents a summary of the two main modelling parameters. Significant correlation was found between the fast and the slow half lives. Introduction of the new patients increased the previous correlation irrespective of protocol or boron (BPA) infusion amount which was gradually raised from 290 mg/kg up to 400 mg/kg. Therefore it could be useful to calculate the fast half life from the steeply decreasing phase including the peak sample point and the two consecutive points. This initial fast component would then be used together with the regression equation to determine the initial value for the slow component. Thus the initial fit before the first irradiation field could be performed with a higher accuracy.

The deviation of the initial fit and the intermediate fit from the final fit works as an indication of how well the standard parameter values of the bi-exponential function describes the blood boron characteristics in each individual case. The deviations collected from the nine studied cases are used to calculate the general standard deviations describing the uncertainty of the predicted average blood boron concentrations during the first and the second irradiation field. Half of the studied cases could be estimated with deviations below 0.5 ppm.

The χ^2 value is used specificly in each estimation to measure the goodness of fit between the bi-exponential curve and the measured blood boron values. It also serves as a tolerance definition for the iterative algorithm. The standard deviation between the fit curve and the sample values provides more general description about the coincidence of the model predictions and the experimental values having their own uncertainty. It was used together with a normalised χ^2 parameter to make comparisons between individual estimations. Normalisation was used to make χ^2 values independent of the number of sample points which was variable within different patients.

The standard deviation of the sample vector around the fit curve describes the uncertainty of the measurements assuming the bi-exponential model for the blood boron biokinetics. That uncertainty is also present in the initial and intermediate estimates in a form of standard error of the mean. While assessing the accuracy of the boron estimation this sampling uncertainty component is taken into account when calculating the initial and intermediate uncertainties. It is slightly lower in magnitude than the mean deviation of the retrospectively determined intermediate estimate of the first field from the final estimate of the first field when the samples after the second irradiation field are taken into account. The initial estimation is less accurate than the intermediate estimation because the smaller number of measured data is then available to calculate the fit. According to the studied cases, the intermediate fit is already very close to the final fit with respect to the level of uncertainty. The combined uncertainty of the blood boron estimation approaches asymptotically the final standard error of the mean which was calculated to be about 0.1 ppm. These results confirm the validity of the presented bi-exponential model in describing the blood boron biokinetics for BNCT using the BPA-F as a boron carrier.

The estimation algorithm is relatively sensitive to fluctuations of the measured blood boron data. Therefore the sparse number of measurements in the initial phase are used only to scale the predefined standard curve in the initial fit. As the amount of measured data increases the modifications of the decay coefficients become more reliable. At the present, the model does not use the infusion data to specify the initial clearance characteristics. The infusion phase could be modelled with another exponential modification. It could be a helpful addition to the present algorithm to set the maximum boron level at the end of the infusion if there were no measured data available from that specific moment. Furthermore, a regression analysis between the infusion model parameters and the clearance model parameters could provide means for more reliable predictions especially for the initial boron estimation before the first irradiation field. However, the infusion data is prone to the same fluctuations as the clearance phase data. Therefore the minute changes in the blood boron concentration during the static infusion are likely to stay unnoticed for the few sample points on the steeply rising part of the boron concentration as a function of time.

The boron values of the 13th patient (330 mg/kg of BPA) of the first protocol features a transient plateau slightly before the second irradiation field which is not included in the bi-exponential model. The curve is shown in Figure 24. A similar plateau or even a peak is observed also in the biodistribution studies with extended infusion times [119]. The reason for the plateau is not known but it may be due to an enterohepatic circulation from the liver and intestines. Therefore the initial predictions of the average boron levels in both irradiation fields are prospectively underestimated. Accordingly, the intermediate fit provides retrospectively an overestimated average boron level for the first irradiation field because the final measured blood boron values after the second field are not yet available. The non-

monotonous clearance pattern affects the goodness of fit and the standard deviation between the sample points and the fit curve. The normalised χ^2 value in this specific estimation is 7.5 times higher in comparison with the average of the other estimations and the standard deviation is 2.9 times higher, respectively. This single case increases the average standard deviation value between the samples and fit within the population by more than 20%.

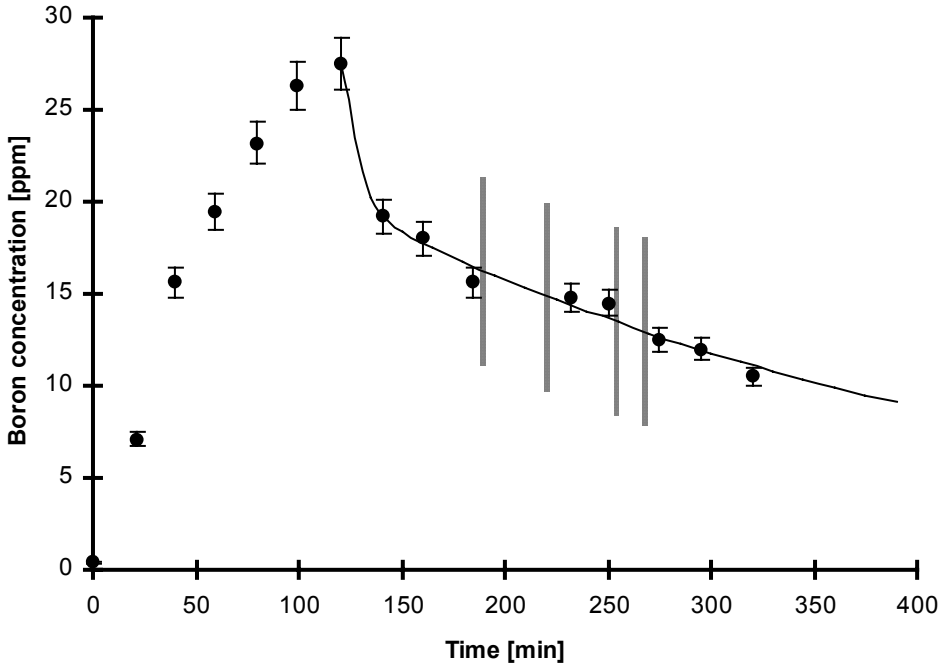

Figure 24. *An example of a clearance phase with a transient plateau. The measured (ICP-AES) blood boron concentrations (solid circles) and the bi-exponential fit (solid line) calculated from the clearance phase data points. Start and end indicators of the fields are presented as vertical lines. Error bars represent the uncertainty of the measured values.*

The ninth patient had a maximum blood boron concentration that was 50% higher than the other patient with 400 mg/kg BPA-F infusion and over 90% higher than the patients with 290 mg/kg BPA-F infusions. The average blood boron concentration remained at a high level also during the irradiations. Fluctuation between the two adjacent intermediate measurement points with 10 minutes gap was 10% which corresponds to the ICP-AES analysis uncertainty of 5% expressed as a coefficient of variation (CV) [65]. Such variabilities and irregular responses have to be tolerated because the measurements and individual physiology of the patients always conceal unknown factors.

It is anticipated that there are always some cases where the bi-exponential model is not justified. To what extent this model can be used will be seen in future studies where the infusion schemes will be further developed. Obviously the boron concentrations and the infusion times will be adjusted to get more favourable ratios between the healthy tissue and the tumour [116, 120]. When the boron biodistribution in other tissues than blood is further analysed there might be enough knowledge to introduce also more complex ways for boron delivery than the currently used static intravenous infusions [12]. Also other models for the boron prediction have been developed [121]. Thus the bi-exponential model used in this study provides only one plain yet practical tool for the blood boron level prediction in BNCT.

5 PATIENT POSITIONING

Conventional applications of patient head positioning appear mostly in radiotherapy and cranial surgery. The region of interest can be exposed to operation without a need to visualise the rest of the head or the body. In surgical methods the patient must be firmly attached to the optimal position for a reliable support. However, the support may cover relatively wide parts of the head to secure the static position and still enable surgical operation. Robust steel frames can be used for that purpose. In radiotherapy applications an external beam is directed to the patient according to the treatment plan. The beam gantry has elaborate movement abilities which facilitate exposures from continuous multiangular ranges without a need for patient movements. The distance from the beam aperture to the patient can be several tens of centimetres. Therefore the space around the patient is not very limited by the beam aperture or gantry structures. The patient can typically lie on his/her back while the treatment is carried out. The radiation is required to penetrate the fixation structures and thus the use of steel structures is prohibited. The fixation solutions used in photon radiotherapy cover thermoplastic masks, stereotactic frames, hardened polyurethane foam moulds and vacuum cushions [122-124].

Patient positioning in BNCT is required to facilitate the multiple field treatments reliably. Due to the fixed beam direction the patient instead of the beam has to be manoeuvred to the specific position for proper treatment. The treatment time may extend to 40 minutes which calls for extra comfort in addition to security in patient immobilisation. The ICRU authorisation of the dose uncertainty sets the fundamental level of accuracy also to patient positioning. The neutron field intensity of the FiR 1 epithermal beam decreases rapidly with the distance from the beam aperture and therefore the patient head and the clinical target volume should be as close to the beam port as possible, rendering an important constraint to the positioning concept. Finnish BNCT facility has a collimated beam which is directed horizontally to the irradiation room. The flat beam aperture construction practically necessitates patient positioning in contact with the plain of wall. The multiple irradiation fields indicate clearly distinct patient postures in each field but the optimal timing of the irradiation concerning the boron distribution requires a precise and compactly paced routine which is realised only with a specially developed positioning system dedicated to BNCT use. In addition to the geometrical and temporal aspects the fixation methods have to take account also the specific requirements of the epithermal neutron field. The fixation materials will be exposed to neutrons but they must pass them without getting activated themselves. These constraints rule out many lightweight materials that would be otherwise successfully utilised in fixation structures. As a result the patient positioning in BNCT turns out to be anything but trivial and the development of functional applications require several steps of experimental verification and testing.

There are only a few published reports of patient positioning in BNCT [125-127]. Each clinical project has used custom made solutions applying mostly stereotactic frames and mask techniques in head positioning and fixation which is contradictory with the close beam aperture requirement. Application of the experiences based on conventional patient positioning is very limited in BNCT field. Usefulness of different positioning methods is highly dependent on the specific facility settings, treatment characteristics and experience of the staff. Alternative methods can be argued as in conventional radiotherapy positioning [128].

5.1 Materials and positioning methods

The irradiation room and beam aperture dimensions set criteria of the amount of participating persons in patient positioning. Considering the space requirement of the coach the space utilisation limits the active contribution into two persons. However, the immobilisation alone requires that attendance and thus the complete positioning structure had to be further developed to facilitate the actual process of obtaining the proper patient coordinates.

Patient positioning for the BNCT treatment is optimally done in a separate simulation room to reduce the time spent in the irradiation room [125, 126]. The floor plan is presented in Figure 25. The simulation room also provides additional working space for positioning. A beam mock-up of identical dimensions with the beam port, selectable aperture collimator diameters and laser coordinate system is needed in the simulation room to provide authentic circumstances and accurate transfer of treatment co-ordinates between the two rooms.

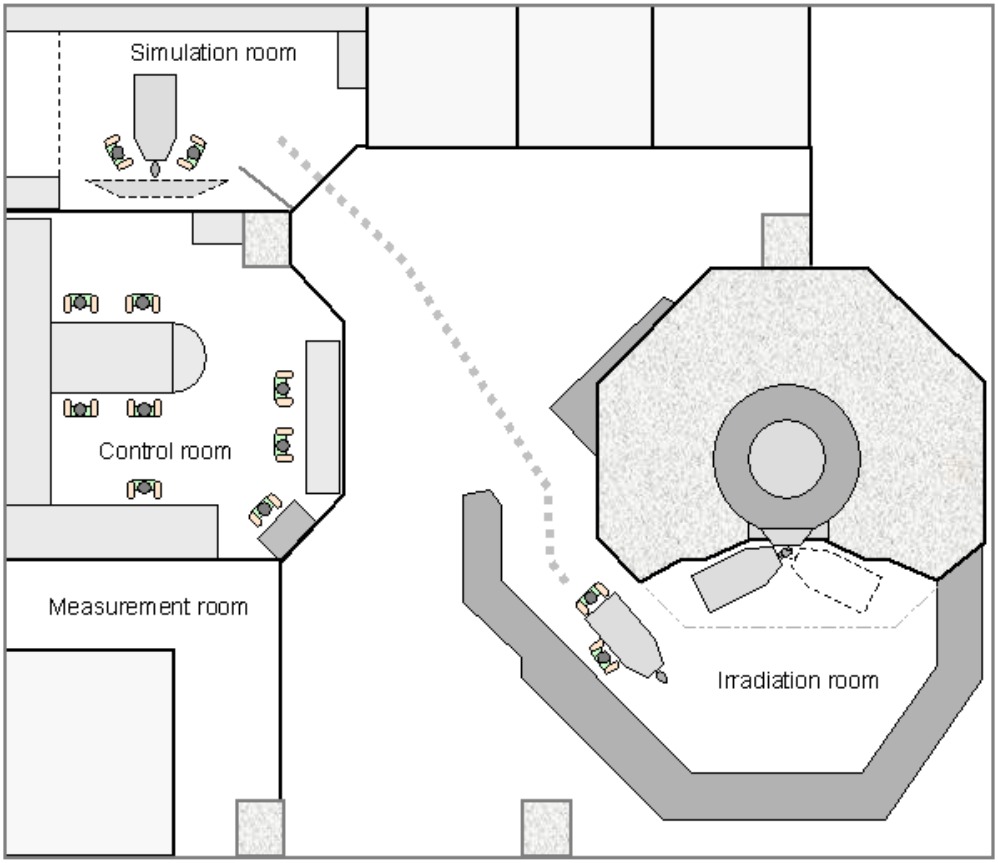

Figure 25. *The floor plan showing the irradiation room and the simulation room of the Finnish BNCT facility.*

Patient positioning is done on the treatment coach which has optimised dimensions according to the geometry of the beam aperture and the surrounding structures and according to patient dimensions to provide reliable support for the body, head and the additional structures used for patient immobilisation. The body is supported with a solid table top and a separate head support is designed to minimise the need for space near the beam port.

Patient transport from the simulating room to the irradiation room is done with the patient in the final treatment fixation on the treatment coach. The coach was equipped with wheels to

create a mobile assembly. The stability of the fixation is supported by having a smooth and short route with minimised amount of thresholds and vertical swells between the rooms. Also an adequate size and appropriate elasticity of the coach wheels assures smooth progression. Solid rubber wheels with a diameter of 15 cm were chosen to facilitate the coach transport and assure a rigid positioning environment. A docking feature with an angular scale was applied to provide a lateral isocentre and lateral angle settings for the coach. The position of the docking base was aligned to a specific distance from the aperture plane and along the beam central axis. An orthogonal laser coordinate system was created with multiple laser crosshair aligned according to the centre of the beam aperture. A construction laser alignment device in addition to spirit levels, steel straight angles, measuring tapes and bullet lines were used to provide comprehensive means for the alignment of the laser coordinate system and to check its equivalence between the irradiation room and the simulation room.

5.1.1 Coordinate system

The irradiation room and simulation room coordinate origin was defined as the point in the centre of the beam port. A crosshair laser aligned according to the beam central axis opposite to the beam direction was used to define the beam axis and the coronal and sagittal reference planes of the coordinate system. In the simulation room two opposing laser crosshairs were used to match the marked entry and exit points on the patient head with the beam central axis. Additional crosshair lasers were positioned on the top and on both sides of the beam to designate the transaxial plane, converging with sagittal and coronal planes at the isocentre located in the beam central axis at a specific distance from the beam aperture plane. As a result the simulation room has five orthogonally mounted laser crosshairs affiliating the triangulation of the target point: two lateral, one vertical and two beam axis (back-pointer and front-pointer) lasers. The irradiation room has four lasers: the vertical and the beam axis (back-pointer) crosshairs and the two lateral lasers defining the horizontal (coronal) plane of the beam. The resulting coordinate system is presented in Figure 26.

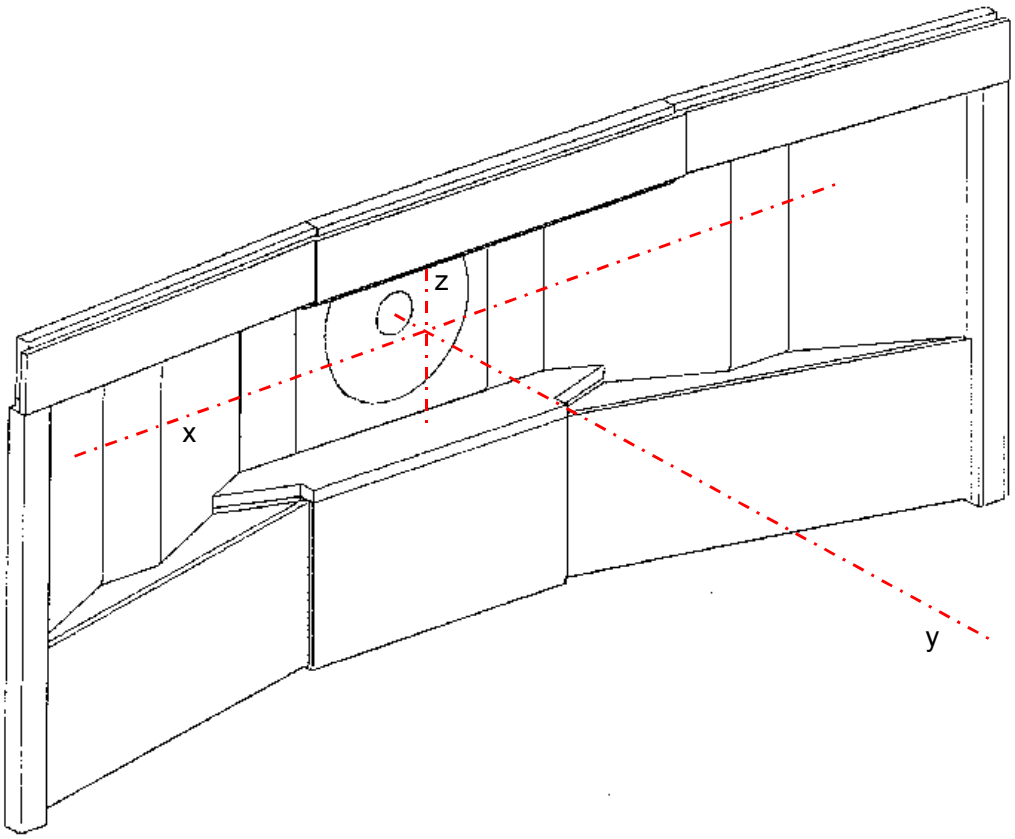

Figure 26. *The coordinate system with respect to the beam aperture. The transaxial plane is defined with the x/z-axis, the coronal plane is defined with the x/y-axis and the sagittal plane is defined with the y/z-axis if the patient is located on the y axis in a supine position. The y axis is located on the beam central axis.*

The floor surfaces were prepared with special structure to form an accurate horizontal plane. In the simulation room a conductive plastic topping was used as the floor material. The coach wheels direct considerable pressure to the floor as the weight of the heavy structure coach and the patient on it is directed to the small contact area under the wheels. Therefore the irradiation room required a special composite tiles with neutron absorbing materials inside a metal frame to form a steady floor for the coach. The floor geometries of the two rooms were tested according to co-planarity with each other. Thus the equivalence of the positions based on the rotational and translational identity of the coordinate and angular settings was assured.

5.1.2 Fiducial marking in preparative positioning

Prior to the treatment planning MRI the head of the patient is marked according to anatomical locations with fiducial marks on anterior, right lateral and left lateral points (TAP-marks; transaxial plane marks) with a surgical pen. Thereafter the vitamin-E capsules are attached to the fiducial points and to the vertex with a glue tape to make them visible in MR images. The patient head is imaged using a 1.5 T Siemens Vision MRI scanner with T1 weighted imaging sequence to produce 3 x 19 slices with 5 mm slice thickness as three continuous uniform stacks from the vertex capsule to the neck as shown in Figure 27. The images are segmented during the treatment planning program to create a 3D-model of the head. The beam directions and entry/exit points are defined according to the dose plan in the coordinate system set by the

fiducial mark locations. The beam coordinates are transferred from the dose planning coordinate system into the positioning coordinate system.

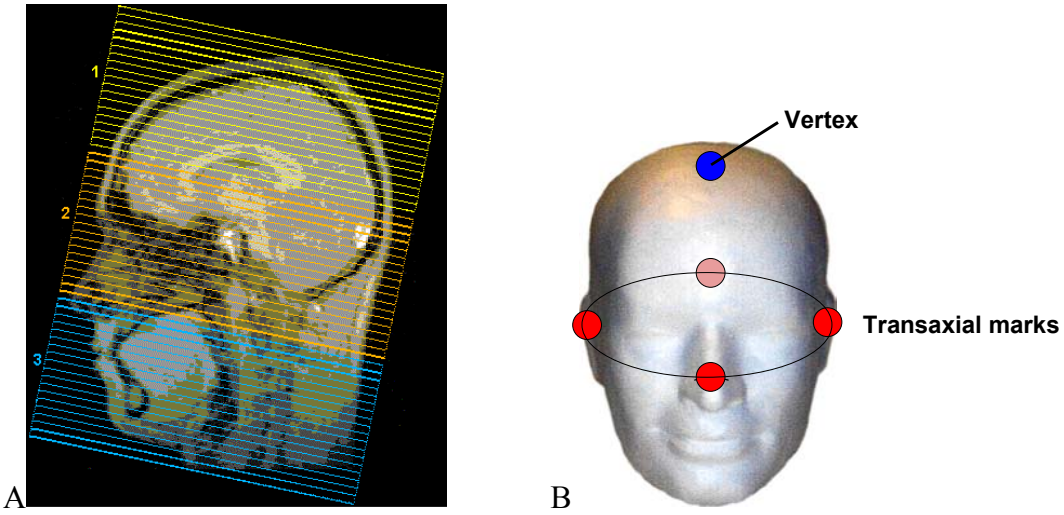

Figure 27. *A) The sagittal MRI head image and three image stacks covering the head and B) the locations of the fiducial marks on the head model.*

The beam entry point for the cranial tumours is located typically in a well accessible location on the patient head. The exit point is located on the opposing hemisphere in the case of a lateral field. In the case of an occipital field the exit point is cast on the frontal region e.g. on the patient face. However, in the cranial field where the beam entry point is near the vertex of the head the exit point can be located in the neck or body regions where the exit point can not be localised because the treatment planning covers only the head. Preparative positioning begins when the patient is set in the zero position on the treatment coach where the transaxial fiducial marks are aligned according to the transaxial, coronal and sagittal laser lines. When the zero position is achieved the patient head is fixated with vacuum forms (PAR Scientific, Denmark) and glue tapes to hold the exact position and the coordinate system of the coach is reset to define the positioning origin. The vertex point is marked on the scalp. As a result the lateral and anterior marks are coplanar in the transaxial plane. Similarly, the anterior, posterior and vertex marks are coplanar in mid-sagittal plane and the vertex point and both lateral marks in the mid-coronal plane. Thereafter the laser lines and coach movements in 3D are used to locate the beam entry/exit points of irradiation fields on the patient head which are then marked on the skin for the actual positioning. Two separate zero positions (back and side positions) may have to be used to mark the lateral and the occipital beam points successfully. One of the transaxial marks will be hidden in the side position and thus the vertex point is used to compensate the missing point when defining the alternative zero position.

5.1.3 Beam alignment

The beam alignment methods were considered in order to find an optimal method for each specific positioning case. The beam directioning in the absence of the exit point was considered in particular. The method compensating the direct alignment of the visible entry and exit points could be done with setting the distances of the fiducial marks with respect to the beam aperture plane. However, there are at least three points and three distance settings, respectively, to attain the correct beam direction. Every parameter make an additional

contribution to the uncertainty of the position. Therefore the number of necessary parameters were minimised into two angles instead of three distances. The beam parallel laser crosshair in simulation room has additional rotational ability to enable the angular control of the transaxial plane around the beam axis. The patient head can be turned according to the rotational laser crosshair to attain the desired transaxial angle. The angular setting can be limited only to the transaxial plane when the transaxial fiducial marks are kept aligned on the transaxial plane. The corresponding transaxial angle is marked with α whereas the lateral (coronal plane) angle is marked with β as presented in Figure 28. The lateral angle adjustment is realised with coach docking angle settings and the head support angle can be used to facilitate the extreme lateral angle typical in the lateral fields.

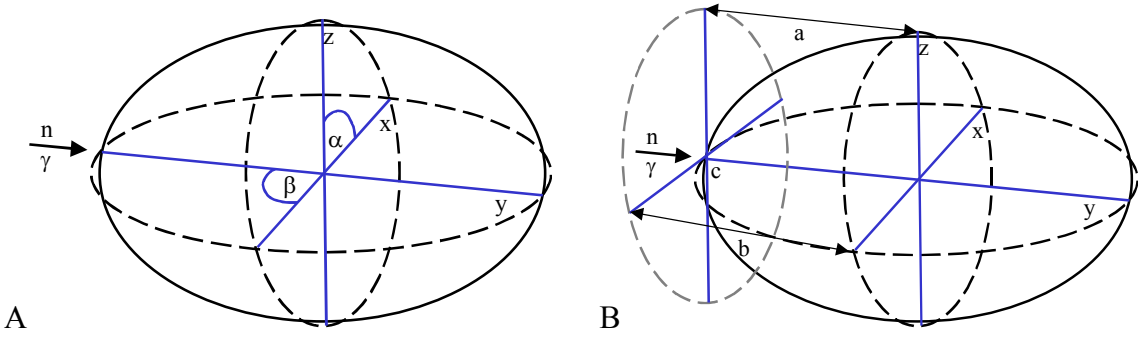

Figure 28. *A) The beam alignment with two angular settings. The transaxial plane corresponding to head turn is rotated α degrees. The coronal plane corresponding to coach rotation on the lateral plane is moved β degrees. B) The beam alignment with three distance settings (a, b, c) of the beam side fiducial marks with respect to the aperture plane.*

The maximum lateral angle required in positioning is 90 degrees which must be realised as a combination of the lateral angle settings referred to above. The maximum coach docking angle is 60 degrees and so the missing 30 degrees should be contributed by patient head positioning. However, the maximum patient head-neck bending angle in static fixation is only 15 degrees. The rest, 15 degrees, must then be arranged by optimising the patient body position on the coach.

5.1.4 Positioning procedure

During patient positioning the planned beam directions are realised by manoeuvring the patient head position with respect to the beam. Larger vacuum form is used to support the body and the small custom made vacuum form is used for head support. In the positioning phase the head form is used semi-hard to enable the needed modifications in the head position. Diagonal or side body positions are typical for both the lateral and occipital fields. The beam simulator is present from the beginning to facilitate the quick approximation of the correct position and for the definition of the available free space.

In the entry/exit mark alignment (EMA) method the head is aligned according to the beam laser crosshairs so that the entry and exit marks are centred in the beam axis. The position is accomplished when the distance of the head to the beam target plane is adjusted. Due to the circular beam shape the head angle can be chosen freely as far as the beam alignment remains valid.

In the mark angles to planes (MAP) method the correct beam direction with respect to the head is acquired by the rotational laser and the coach lateral angle setting. The beam exit point is not visible and so the proper direction has to be found by an alternative method. The zero position is acquired normally. Thereafter the rotational laser is turned into a planned transaxial angle. Keeping the zero position otherwise intact the patient head is turned into the rotated transaxial angle by aligning the transaxial marks according to the rotated laser crosshairs and keeping the vertex point of the head on the beam central axis crosshairs. The transaxial marks have to be maintained in the transaxial plane implemented by the lateral and top laser lines. Thereafter the patient head is fixated to keep the correct axial angle and the coach in its part is turned around the docking isocentre into the correct lateral angle. With these two angular settings the final beam direction is realised with a minimum amount of extra measurements and presumably without additional spatial uncertainty. The beam entry point is centred on the beam crosshairs and the head is brought into contact with the beam target plane, 1 mm outward from the beam aperture plane.

In the mark distance to aperture (MDA) method the distances of the three fiducial marks are measured to the beam aperture plane. Patient head is manipulated to achieve the specific distances defined in the treatment plan. The direct measurement of the distances requires the fiducial marks preferentially chosen from the beam side of the head. When those points are not visible or otherwise not applicable the straight angle ruler has to be used for the marks opposing the beam. Thereafter the entry point is centred according to the beam axis as in MAP method.

When the planned position is accomplished the vacuum forms are hardened and sealed until the irradiation. Also the laser lines corresponding to both irradiation fields are marked on the patient head and to the vacuum forms with a specific colour for each irradiation field. The angular and translational settings of the coach are written down. The vacuum form locations on the coach top are marked and the entry and exit beam views in addition to the general positioning view are documented with digital camera. Thus the positions for both irradiations are reproducibly acquired.

5.1.5 Fixation

The documented coach settings are reproduced in the simulation before the patient irradiation. The vacuum forms prepared during the previous positioning phase are set on the coach top. The vacuum form of the head is typically already attached to the head support to form a singular rigid ensemble. The patient is laid in the vacuum form and the correct head position is reproduced by aligning the beam marks of the head according to the laser lines while the beam aperture simulator is locked in position. The immobilisation is secured with Velcro tapes around the patient body and with a non-flexible glue tape for the complete head fixation. While the patient remains fixated the treatment coach top is centred for safe transportation. The coach and the patient are then transported from the simulation room to the irradiation room. The coach is locked in the docking base and the electrical connections are attached to AC power and control lines of the irradiation room. The planned beam direction is acquired by rotating the coach about the docking isocentre to attain the correct lateral angle. The coach wheels are then locked to fix the angle. The treatment coach top is moved laterally for the proper beam position. The final positioning presented in Figure 29 is verified according to the beam marks on the patient head and the laser lines. The proper distance of the entry point from the aperture plane is checked with 1 mm thick plastic plate.

Figure 29. *The final positioning in an actual patient treatment.*

5.1.6 Spatial accuracy

The spatial accuracy of positioning was studied to establish the positioning system and to compare the existing positioning methods. The study was performed using a solid head model (RSVP head phantom, Phantom Laboratory, Saalem, New York) and the three alternative positioning methods. The transaxial and vertex points were marked on the head model similarly as with the patient treatments in the phase I clinical trials. Additionally, six independent beam entry and exit points were marked on the head model to specify the objective beam lines. The external markers (vitamin-E capsules) were attached with a glue tape on all marked points for the MRI scan as presented in Figure 30. The head model and the attached markers were imaged using a 1.5 T Siemens Vision MRI scanner with a T1 weighted imaging sequence and 5 mm slices throughout the head. The images were transferred to BNCT TPS for segmentation and beam localisation to determine the entry and exit point co-ordinates and the corresponding beam angles.

Figure 30. *The antropomorphic head phantom (RSVP) with a part of the E-vitamin capsules shown on the fiducial mark locations corresponding to the transaxial, vertex and six beam entry/exit points used in the spatial accuracy study.*

The movement accuracy of the coach was tested using 0, 40, 80 and 120 kg loads on the coach and performing 10 cm coach movements in positive and negative directions along the x-, y- and z-axis of the coach base. The movements were realised according to the coach spatial console. The centre location was fixed according to the origin of the laser planes. The distances of the peripheral locations were verified with a ruler and return to central origin was assured with lasers after each movement. According to the measurements, the spatial uncertainty of the coach movements was less than 1 mm.

The planned entry and exit points from the TPS were marked on the head using the normal pre-positioning procedure where the orthogonal laser cross-hairs and coach movements are used to locate the points on the patient head surface in the zero position. The distances of the planned entry and exit points from the original entry and exit points were measured separately in x, y, and z directions. Thus the initial spatial uncertainty of the positioning system was determined.

The total spatial accuracy of patient positioning was determined using three different methods. In the Entry-Exit mark alignment method (EMA) the entry and exit points were simply aligned according to the beam axis cross-hair lasers. Therefore the EMA accuracy is by definition the same as the initial accuracy of the positioning system. In the mark angle to plane method (MAP) the transaxial and coronal (lateral) plane rotations were used to acquire the desired beam direction. In the mark distance to aperture method (MDA) thin PMMA rods with proper lengths were used to measure the distances of the fiducial points to the beam aperture plane. Thereafter the entry point was centred according to the beam axis in both methods.

5.1.7 Effect of positioning accuracy on the dose

The dosimetry effect of the spatial uncertainty of positioning was studied with phantom simulation. Two spherical volumes of 310 cm^3 and 56 cm^3 simulating the target volume and the tumour, respectively, were positioned in the ellipsoidal phantom near the thermal dose maximum in 15 mm depth from the lateral surface. The volume was chosen according to the average of the protocol-1 clinical target volumes and tumour volumes. The phantom was first positioned in the central location and the dose distribution of one direct ipsilateral beam was calculated with SERA treatment planning program. Thereafter the phantom was moved 5 mm off the beam axis and the dose distribution was calculated again. In both positions the dose profile curves were obtained in the lateral depth axis of the phantom directed through the target and the tumour volume centre points. Dose distribution was also obtained in the perpendicular axis at three depths corresponding to the ellipsoidal centre point of the phantom, the target volume centre point and the tumour centre point. The two phantom positions, the target volume and the tumour are illustrated in Figure 31. Between these two positions the calculated doses were compared.

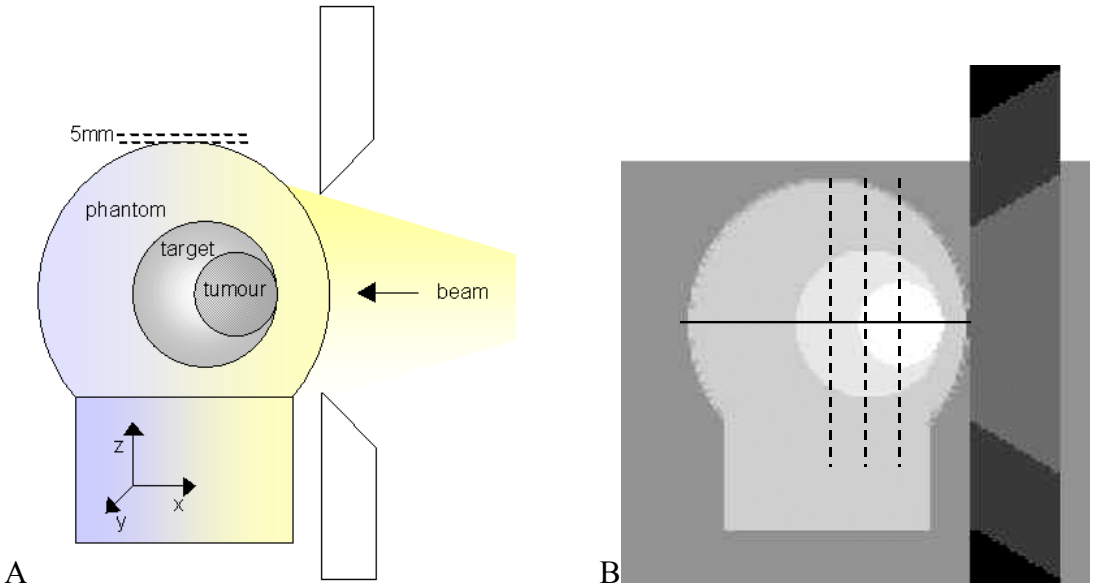

Figure 31. *In A, the ellipsoidal phantom is positioned laterally on the beam central axis and at 5 mm off-axis. The spherical target volume and the tumour were positioned near the beam side surface of the phantom at the location of thermal fluence maximum. In B, the SERA simulation image shows the central position and the dose profile lines in the lateral depth axis (solid line) and in the perpendicular axis at three depths (dash lines).*

5.2 Positioning results

The positioning system was realised for the Finnish BNCT facility. The system implementation is described in Chapter 5.2.1. The spatial accuracy of patient positioning was assessed using the implemented positioning system and applying three different positioning methods. The spatial accuracy results are presented in Chapter 5.2.2. The effect of spatial accuracy on the dose was evaluated with SERA radiation transport calculations. The resulting dose curves are presented in Chapter 5.2.3.

5.2.1 System implementation

The treatment coach and the beam aperture simulator was manufactured in Finland by TE-PA Medical Ltd (Lemi, Finland). The coach and the simulator structure was based on welded rectangular steel tubing. Transparent, clear PMMA was used in mobile beam aperture simulator surfaces for optimal visibility also from the other side of the beam. Step-motors were used in electrical controls of the coach positions in three dimensions. Digital display of the positioning coordinates with resetting and miscellaneous functions was combined with the coach transport mechanism in addition to the remote control with a continuous adjustment of movement speed in each individual (x, y, z) direction. Carriage was equipped with wheels including a 3-state direction lock with a foot control. The diameter of wheels was 150 mm and hard polyurethane coating was used for rigid transport characteristics. The coach top was rendered with apache wood to provide a lightweight, robust and an easy-to-clean surface for body support. Painted circular steel tubing without a chrome coating was used in the head supports with individual height measures. Feasibility to attach any commercial head support to the coach was also made possible. The laser system was purchased separately. The rotational laser crosshair in the simulation room was realised by combining a laser crosshair with a rotational base with an angular scale and a locking feature. Low activation in the clinical neutron field settings was verified for all parts by neutron beam activation tests.

Basic measures of the treatment coach is as follows: width 910 mm, height 900 mm, length 1950 mm (+ 300 mm head support) as presented in Figure 32. Coach weight is 120 kg and the maximum patient weight is limited to 170 kg. Coach movement ranges were as follows: side movement range 400 mm, longitudinal movement range 300 mm, vertical movement range 300 mm. Angular movement ranges of the head support and the coach are 180 and 120 degrees, respectively. Lateral movement range of the head support is 400 mm.

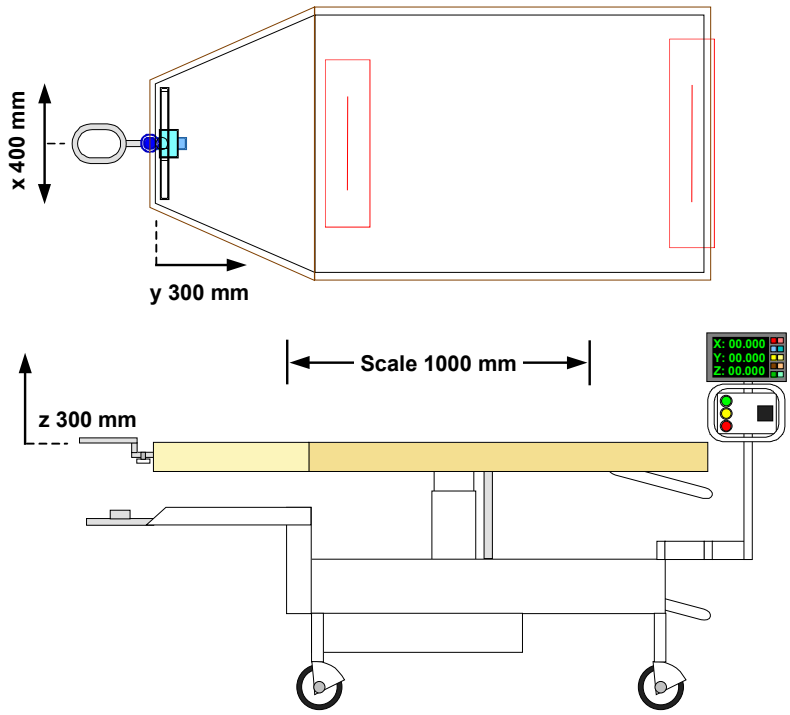

Figure 32. *The treatment coach dimensions and movement ranges in x, y, and z directions.*

The coach with an antropomorphic model positioned for lateral and posterior fields are presented in Figures 33 and 34, respectively. The treatment coach attached to the beam simulator using the docking feature and a head fixation is presented in Figure 35.

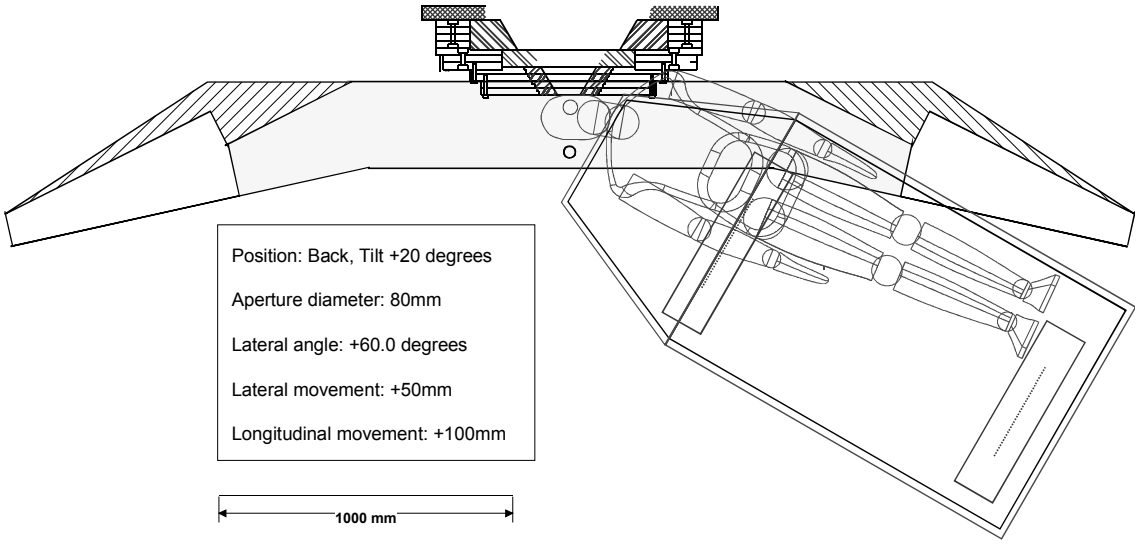

Figure 33. *The coach and the anthropomorphic model positioned for the lateral field. In practical positioning the semi-lateral body posture is used to fit patient shoulders on the beam side.*

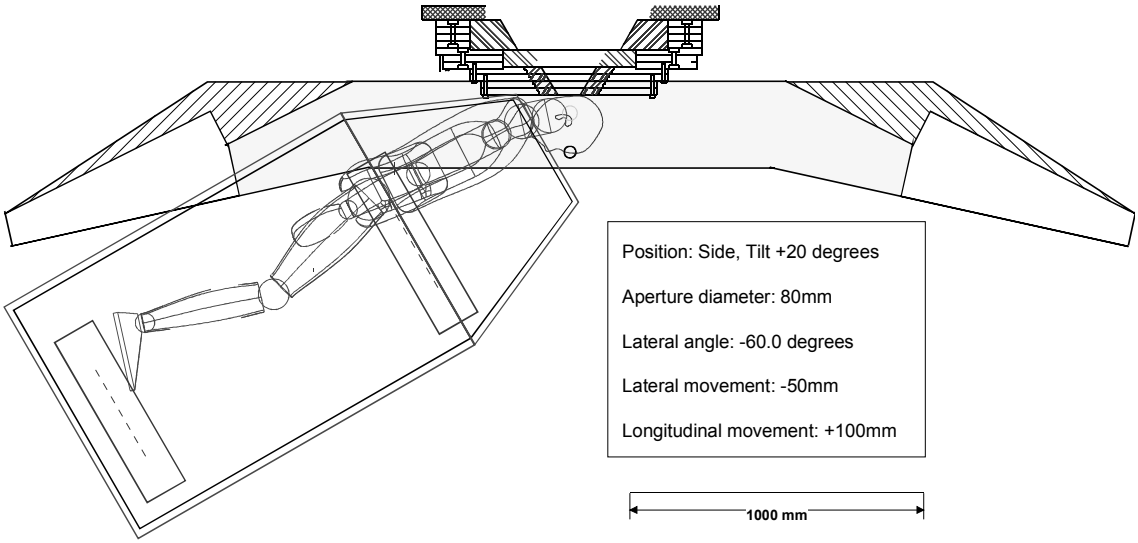

Figure 34. *The coach and the human model positioned for the posterior field.*

Figure 35. *The treatment coach (A) and the beam simulator system (B). The coach is attached to the docking base (C). In the small image the head model has been positioned for the vertex field using vacuum cushion fixation.*

5.2.2 Spatial accuracy results

The acquired target point and the angular deviations from the beam central axis of each method were measured and the corresponding standard deviations were calculated to determine the total positioning uncertainties. The percentage values were calculated from the target point spatial uncertainties and the average entry-exit point distance which was about 200 mm. The results are presented in Table 4.

Table 4. *The spatial and directional uncertainties of the three positioning methods: the entry-exit mark alignment (EMA), the mark angle to plane (MAP), and the mark distance to aperture (MDA).*

	Standard Deviations		
	EMA	MAP	MDA
Target Hit	2.3 %	3.1 %	4.7 %
Target Hit	5 mm	6 mm	9 mm
Beam Angle	2.6 deg	2.8 deg	4.5 deg

5.2.3 Dose effect results

The total dose in two studied positions (central and 5 mm displacement) in the lateral depth axis (parallel to the beam axis) is presented in Figure 36. The total doses in the perpendicular axis at the three depths are presented in Figure 37. The doses include also the boron dose component. The difference between the target volume and the tumour doses in the two studied positions was 0.1% in the perpendicular axis at the depth of 40 mm (tumour axis). The difference of the phantom doses in the two positions corresponding to the normal brain doses was less than 5% in the tumour axis. When covering all regions (phantom, target volume and tumour) the difference in the dose was 1.5% in the tumour axis. Biased locations off the beam central axis acquire increased differences between the two positions with respect to the dose rates.

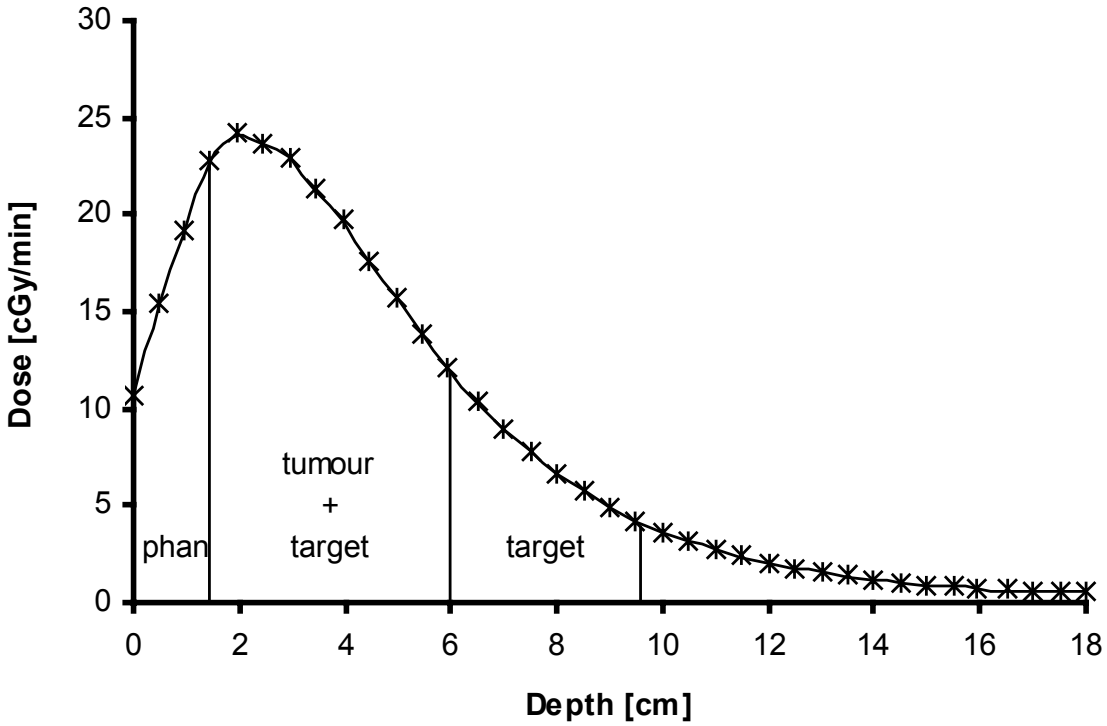

Figure 36. *The total dose in the lateral depth axis directed through the ellipsoidal phantom, the target volume and the tumour centre points. The solid line represents the central dose profile whereas the crosses represent the doses in the same points but at the 5 mm displaced beam position.*

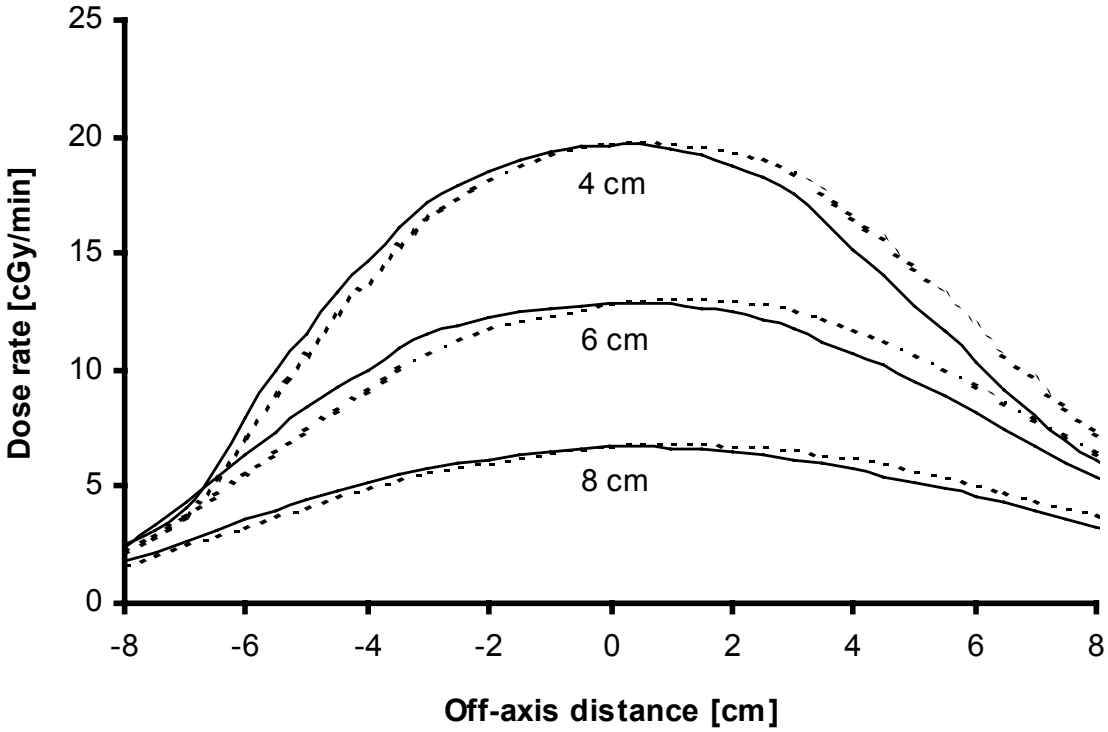

Figure 37. *The total doses in the perpendicular axis at three depths corresponding to the ellipsoidal phantom (8 cm), the target volume (6 cm) and the tumour (4 cm) centre points. The solid lines represent the central position dose profiles whereas the dash lines represent the 5 mm displaced position dose profiles.*

5.3 Positioning discussion

Patient positioning is implemented for the Finnish BNCT treatments using the mobile treatment coach equipped with controlled patient movements in three dimensions. Beam alignment is implemented with angular adjustments using the lateral coach docking angle and transaxial rotational laser crosshair. The time required for the first positioning trials extended into several hours. According to increasing experience during the first protocol-1 patient treatments the positioning time reduced at a level of about three hours. As the positioning procedure could be further developed the positioning in the latest patient treatments have been accomplished in less than two hours including the preparative phase where the beam entry and exit points are localised on the patient head. At the same time, the number of positioning staff has been minimised to two persons. An example of a positioning schedule is presented in Table 5 and the positioning process chain is described in Appendix 3. The fixation and final positioning in the irradiation room is performed just before the treatment irradiation. The pre-shaped vacuum forms from the preparative positioning day are used for quick reproduction of the proper patient position. The fast boron kinetics does not allow delays in the final positioning and fixation as the optimal irradiation to attain the prescribed therapy dose to the patient is obtainable only during a restricted time window. Realised final positioning is done in about 20 minutes before the first irradiation field and during the intermediate time between the first and the second irradiation field.

Table 5. *The realised positioning schedule for an immobile 64-year-old male patient.*

Time	Elapsed time	Event duration	Event
12:50	00:00	-	Patient arrives to the positioning room, coach is ready
13:10	00:20	00:20	Zero position is ready
			Beam points are being located by 3D-movements
13:15	00:25	00:05	1-field beam *entry* point located and marked
13:17	00:27	00:02	2-field beam *entry* point located and marked
13:20	00:30	00:03	1-field beam *exit* point located and marked
13:22	00:32	00:02	2-field beam *exit* point located and marked
			All beam points located, return to zero position confirmed
			Treatment positions are being acquired
13:45	00:55	00:23	1-field position is ready
14:08	01:18	00:23	2-field position is ready
14:15	01:25	00:07	Positioning completed, patient is retrieved to hospital

times in hh:mm

Pre-positioning begins with the zero position where the transaxial marks are aligned according to laser planes using the 3D-movements of the coach. The patient head is then fixed temporarily and the co-ordinate system of the coach is reset to place an origin in the zero position. Thereafter, the 3D-movements of the coach are used to acquire the beam entry and exit points one by one. Typically, for a bi-directional treatment two zero positions have to be used because only the entry and exit points of the lateral field can be located on the back position. That introduces considerable extra time in pre-positioning. However, it is difficult to develop a head fixation system which would expose the whole cranial area for the beam point localisation. Such method requires a fixation that would be based on neck and probably on the jaw region support. Possibly an upright position would then be used because an optimised support would be needed from each direction to secure the fixation.

Treatment typically consists of one lateral field and one posterior or cranial field. Posterior or cranial fields usually require a lateral body position for comfortable beam alignment. Lateral fields usually call for careful body adjustment between the lateral and diagonal positions. The most practical way to attain the optimised body orientation is acquired by using the aperture simulator together with the treatment coach to provide realistic spatial boundaries. Correct body positioning is essential because then the head is already very close to the correct beam alignment and thus the head position requires only minor further modification. Another important consequence is the increased patient comfort. The optimal body position ensures that the prolonged static fixation during the irradiation sequence is more easily tolerated and maintained.

The entry/exit mark alignment method is a straightforward procedure where the points are merely centred on the beam central axis laser crosshairs. This manipulation is done by keeping the head in contact with the aperture plane, thus accomplishing the final position as soon as the alignment is completed. An additional thin plastic plate is used to evaluate the distance of the entry point which is located in the centre of the beam port to the beam aperture plane. According to regular dose planning scheme, a millimetre gap is left between the aperture surface plane and the head apex. The resulting virtual surface is called the beam target plane. Optionally, a ruler is used in some cases to determine the distance in posterior fields where the curvature of the head forces the entry point further from the beam target plane. Otherwise a thin part of the scalp might become slightly intruded inside the beam port.

The total positioning uncertainty is presented in Table 4. The external marker positioning uncertainty was 1 mm according to the approximate measurement during the imaging phase of the study. The estimate for the zero position uncertainty was 2 mm. The spatial uncertainty involved in segmentation was estimated to be about 2 mm. The contribution from the coach 3D-movement mechanism was 1 mm which includes the laser line widths. The only source of error that is left over is the geometrical error from the MRI scan. The total spatial uncertainty of the EMA method according to measurements was found to be 5 mm. By assuming that all the mentioned sources of errors are independent of each other the spatial error of the imaging is 3 mm. An imaging uncertainty of that magnitude is also excepted according to the published imaging accuracy data concerning the spatial and geometrical distortions in MRI [129, 130]. It is still noteworthy that the concluded spatial accuracy concerns only the phantom situation where the surfaces are solid and the test object is practically a rigid body. Only the external markers were somewhat flexible because of the liquid filled content of the used vitamin-E (Aesol) capsules. In the normal patient treatment situation the skin of the head introduces a clear and probably also significant source of positioning inaccuracy. The scope of this study was focused on the determination of the accuracy of the positioning system and consequently on the rating of the existing positioning methods. The acquired spatial accuracy of 5 mm can serve as an initial reference level of the positioning uncertainty for the later studies. However, in future studies the effective positioning accuracy using a real test patient throughout the positioning chain should be examined.

The EMA has been used for positioning in the most BNCT irradiations in Finland because of ultimate simplicity, minimal amount of positioning time and sources of uncertainty. It is clearly the most accurate method as shown by the positioning accuracy study. The two alternative methods (MAP and MDA) have to be used when the EMA is not applicable. That can occur when the beam is directed gaudally through the neck. Then the beam exit point will not be located on the head area. The accuracy of the MAP method is proven to be better than the accuracy of the MDA method. Therefore it is chosen to be the secondary positioning method in the BNCT trials. The MAP method will be used for the beams where the beam exit point is located below the patient neck.

According to the dose simulation study the 5 mm translational positioning error introduces less than 1% difference with regard to the dose of the target volume and the tumour. The ellipsoid phantom corresponding to normal brain volume acquired less than 5% difference. Translational positioning error corresponds to the maximum error related to the positioning uncertainty where the entry and exit points are both deviated in the same direction with respect to the central beam axis. Strongly biased localisations of the beam are not performed in treatment plans. Thus the effective uncertainty of the dose due to the spatial uncertainty of positioning is most probably below 5%. However, 5% value will be quoted to allow total physical dose uncertainty estimation in variety of treatment circumstances.

Usefulness of the simulation room and the beam simulator has been recognised also in other studies [125, 126]. In the Finnish positioning system this usefulness is further enforced by creating a transparent mobile beam aperture simulator on wheels. Thus the various phases of positioning can be optimised either with or without the beam aperture simulator present with the reference laser coordinate system. Therefore the practical working space around the patient can be optimised in each step of the positioning procedure.

The head fixation using vacuum form and tapes attached to the head and the head support has provided acceptable means for the current treatment trials. However, it is still a prototype level solution which should be improved to allow more steady fixation and faster positioning routine in future treatments. The shape of the head support can be developed to be more comfortable. The steadiness can be increased by substituting the current fairly loose metal tubing in the head support socket with a robust precision profile tube. The vacuum form of the head can be made smaller and attached with Velcro strips to the head support base.

The most critical part of the current head fixation is the immobilisation of the top of the head to avoid rotating movements. In order to improve the steadiness of the fixation in that particular respect an arc fixation concept is proposed as presented in Figure 38. The tightening screws of the upper and middle part of the arc drive the anatomically shaped soft wedges. Wedges with rotational ability are used to secure the head fixation firmly by pressing them against the glabella and the vertex of the head in the zero position. The wedges can be reciprocally changed according to the head position. Another wedge is larger with a cupping shape to keep the vertex or the temporal region of the head firmly in position. Several different wedges with optimised geometries can be used according to specific needs in different alternative positioning schemes.

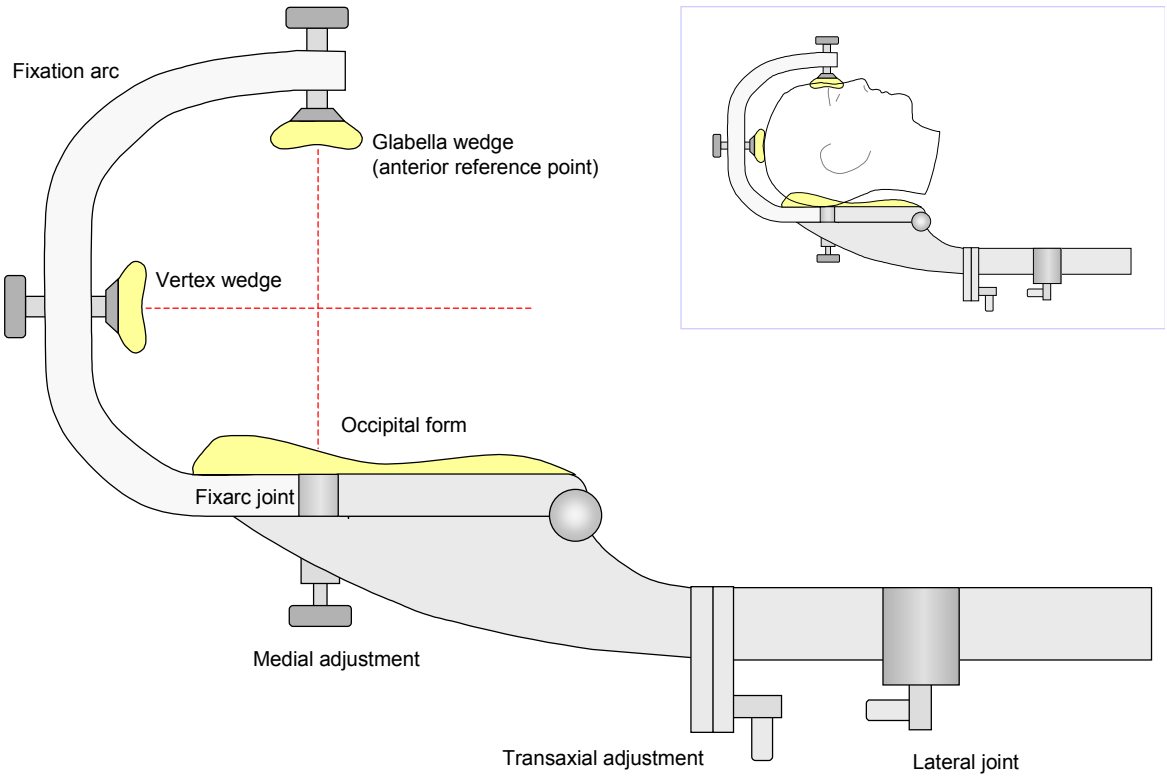

Figure 38. *The arc method for head fixation in BNCT. Soft anatomically shaped wedges are used to secure the head fixation. The arc can be turned aside to allow various beam alignments. The medial and transaxial adjustments provide accurate angular settings of the head while maintaining the fixation. In the small image the head is included in the fixation scheme.*

The lower part of the head support includes a transaxial rotation setting with an angular scale. The rotational feature is added to provide precise angular modifications of the head around the longitudinal axis while maintaining the fixation of the head. Such feature has been lacking from the present positioning system. Another angular setting can be realised with an additional structure of bi-planar plates. Between the plates, a wedge screw is used for vertical raise to realise medial adjustment with limited angular range. The arc structure above the medial adjustment plate has a joint which enables the turning of the arc aside to allow different head positions and to provide space for the beam aperture in changing beam alignments. The arc method also provides valuable additional free space for the head fixation as the head remains practically uncovered. Thus the patient monitoring can be performed with improved visual contact to the patient. The arc is also completely reusable without separate costs for individual positionings. The arc method for head positioning and fixation is currently in preparation for patent application.

6 GENERAL DISCUSSION

As the BNCT treatments are further established among the other therapy modalities they require well defined quality parameters to validate the individual treatment settings systematically and to make them comparable with each other. Therefore a code of practise in BNCT has been initiated among the European BNCT facilities [100]. The quality control of the Finnish BNCT project is fairly well defined on the procedural level. However, the comparability of the specific quality figures needs further effort until the results of the international co-operation are implemented locally.

Various approaches and solution for the clinical implementation of the BNCT treatments were initially defined as specific processes which are effectively independent of each other. As the operation approaches the clinical routine there will be an increasing need for synergy and practicality of the treatment sub-procedures. As an initiative example, the treatment log application combining the boron estimation with the operational beam data is discussed later in detail. Combining the real time beam monitoring data and an automated scram utility to the existing treatment log would further expand the practicality of the application.

The ICRU recommendation of the dose uncertainty serves as a fundamental motivator for the implementations presented in this work. The combined uncertainty of the present BNCT dose is therefore estimated. On the other hand it is worthwhile to consider the applicability of the existing radiotherapy dose uncertainty recommendation for BNCT practise. There are several factors that render BNCT doses with different perspective from what is intended by the ICRU statement. Thus it may not be justified to judge the BNCT dosimetry according to current recommendations. Instead, dedicated recommendations should be developed specifically for BNCT.

6.1 Quality control

Quality control of the BNCT treatments in Finland is supported by continuously updating general guides (the YO-documents) and operational guides (the TO-documents). There are also specific operational forms (the TK-documents) that work as practical documentation and executive level handouts of the quality assurance flow. Those documents subdivide into all individual speciality groups and contain the description of all the necessary precautions and steps of actions when realising the treatments at the Finnish BNCT facility in Otaniemi. Thus they serve as practical standard operational procedures (SOP) library for the Finnish BNCT project. Material suppliers and other co-operating partners e.g. the HUS pharmacy that prepares the BPA-F solution for infusion have their own SOP documents and quality systems which are neatly jointed into general quality control flow. The clinical BNCT scheme is governed by the existing clinical trial protocols (P-01 and P-03). The medical operation is depicted adequately at the protocol level and thus let more detailed actions fall within the good clinical practise (GCP) and the normal operational practise of the hospitals.

The quality control flow is summarised in the graph in Appendix 6. It has also been presented in an initial form at the 9th ISNCT meeting [131].

6.2 The treatment log

The boron estimation application was extended into a treatment log workbook by including the positioning data and the beam data with the modified boron data sheet which was previously used only for the bi-exponential fit. Thus the treatment data could be collected in a coherent way and the documentation could be automated as far as it is possible while using the current operational procedures and general operational guides. The treatment process of the Finnish BNCT project is presented in Appendix 5.

The positioning data is a memo of the realised positioning settings. The most time consuming part of positioning is done on the day before the irradiations. The scheduling data of the realised positioning phases were recorded to observe the efficiency of the continuously elaborating positioning schemes. The documentation of the attained positioning settings of the treatment coach was also included in the treatment log were it is directly available during the final positioning. The deviations of the final position from the beam lines are also documented for the follow-up of the stability and reproducibility of the positioning in actual patient treatments.

The actual treatment procedure with regard to the treatment log begins on the beam data sheet where the aperture size and the beam weighting is defined for the first irradiation field. The aperture sizes are manually defined for each field but the field weighting is determined as a percentage for both fields according to the weighting of the first field. Also the basic treatment information as the protocol, the patient code and the date is stored in this sheet but linked automatically on the other data sheets.

The blood boron data is updated continuously according to the measured boron concentration values from the blood samples analysed with ICP-AES. Also the patient specific infusion parameters are calculated according to patient weight and infusion amount. After the infusion the blood boron concentration starts to decline and the time window of the beginning of the first treatment field gets fixed within few minutes accuracy.

The estimated start-up time and duration of the first irradiation field is updated in the beam data. The duration is based on the table of irradiation times which is provided by the treatment plan. The proper duration is chosen from the table in the treatment plan according to the initial boron estimation for the first field.

The boron estimation is calculated as an integral from the bi-exponential fit. When the integration time limits (irradiation start and stop times) change, so does the value of the average boron estimate. The change in the boron estimate may further change the irradiation length and so forth. There is an obvious negative feedback between the boron estimate and the irradiation length when the dose is kept constant according to the dose prescription.

The effective duration of the irradiation is calculated by the normative beam monitor pulse frequency from the neutron detector one (fission chamber “N1” for thermal and epithermal neutron energy range) according to the total number of beam monitor counts. The dose planning system provides the table of planned irradiation times according to the reference pulse frequency which is the set reference level for the nominal 250 kW reactor power. The practical pulse frequency is typically slightly higher than the reference pulse frequency. Thus the practical irradiation times tend to be slightly shorter than the planned irradiation times. By keeping the beam monitor counts as the decisive dose quantity the realised dose becomes

independent of the inevitable minute changes in the reactor power. Obviously, that would not be the case if the dose would be realised according to the irradiation length in time.

If the primary beam monitor counter failed there would still be two other fission chambers (N2 and N3) and a gamma ionisation chamber left to determine the termination of the irradiation (scram time) according to the total amount of corresponding monitor counts. If the PC program for the counters failed, there is a secondary system and a NIM counter system continuously working in parallel as a backup. In addition the irradiation length in time is still monitored with radio controlled clocks and digital countdown watches.

Usually the last blood sample is taken right before the irradiation. The ICP-AES blood boron concentration analysis takes few minutes to run and therefore the boron result will be ready for the estimation program when the irradiation is already running. The change in the estimated average blood boron value may well change the effective irradiation time and so the irradiation length is typically still changing as the irradiation is going on. The updated irradiation parameters are calculated automatically and the beam scram time is estimated within ten seconds accuracy.

The normative beam monitor pulse frequency is monitored and registered into the beam data during the irradiation. Thus the estimated treatment times are produced with the best possible accuracy according to the real irradiation conditions. During the treatment field, the patient is continuously monitored with three video cameras (one close-up view and two descending general views) for the general appearance, breathing and position, and with a heart beat and blood oxygen level probe for primary vital signs. The scram time is registered in the beam data. After the irradiation, the beam monitor counts are acquired until the patient is detached from the treatment position and the beam aperture.

After the irradiation, the realised beam monitor counts are registered in the beam data and the discrepancy with the planned beam monitor counts is displayed as a percentage value. The post-irradiation blood sample is taken as soon as possible and the corresponding analysed value is used in the updated boron estimation for the first field. If the estimate changes significantly, the corrected value and the corresponding revised irradiation length in time (according to the dose planning timetable) is used as a revision input for the beam data of the first field. A correction factor for the second irradiation field is calculated from the realised beam monitor count percentage and from the possible boron estimation (and following irradiation time) data revision. Thus the uncertainty of the first irradiation field caused by the uncertainties in the boron estimate and the scram moment will be compensated in the duration and the corresponding beam monitor counts of the second irradiation field to realise the total prescribed dose as accurately as possible. During the second irradiation field, the amount of analysed blood boron data has increased. Consequently, the uncertainty of the boron estimate is significantly lower ensuring a reliable boron value from the dose planning point of view.

As the second irradiation has finalised the last blood boron sample is acquired and the analysed value is used in the last boron fit to provide the conclusive boron values for both irradiation fields which are registered among the other realised treatment related data. All the essential treatment data acquired in the treatment log is combined to provide the treatment summary. The actual treatment log data sheets are presented in Appendices 8 to 11.

6.3 Uncertainty of the dose

Dosimetry, boron estimation and patient positioning have a combined effect on the reliability of the eventual patient dose. The combined implementation scheme is presented in Appendix 4. The total uncertainty of the physical dose is calculated according to the typical dose to normal brain tissue at the reference point (thermal neutron fluence maximum) using a 1 cm^3 volume, 11 cm diameter aperture and 12 μg/g BPA concentration [32]. The uncertainty of each dose component was assessed separately. The total gamma dose is determined experimentally with ionisation chambers and therefore the uncertainty related to the incident beam gamma component is assumed to be 6.3% (1SD) [43]. The beam gammas contribute about 5% of the total gamma dose. Majority (about 95%) of gammas are induced by the radiative hydrogen capture reaction which is relative to thermal fluence. Therefore the uncertainty of the induced gamma dose is the uncertainty of the thermal fluence combined with the uncertainty of the spectral mass energy absorption coefficient which converts the calculated gamma fluence into a gamma dose. The uncertainty of the thermal fluence (4% 1SD) is estimated according to the activation foil measurements which include the uncertainty of the cross sectional data. The uncertainty related to the spectral mass energy absorption coefficient (1% 1SD) is obtained from ICRU [73]. The nitrogen dose is calculated according to the thermal neutron fluence and nitrogen kerma factors and the uncertainty is calculated accordingly. The uncertainty of the nitrogen kerma factors (5% 1SD) is obtained from ICRU [73]. The uncertainty of the fast neutron dose (25% 1SD) is estimated according to the neutron fluence uncertainty combined with the hydrogen kerma factor uncertainty obtained from ICRU [73]. The uncertainty of each dose component is weighted according to its fraction of the total dose. At the last step the uncertainty of the absorbed physical dose due to the uncertainty in patient positioning is taken into account assuming that it is independent of the previous dose uncertainties.

According to this estimation, the combined uncertainty of the physical dose to normal brain at the reference point (thermal maximum) without the boron dose included is 7% (1SD) due to the uncertainties in positioning and in neutron and gamma dose determinations. When the boron dose is included the same uncertainty is 18% (1SD). The uncertainty of the boron dose is estimated according to the uncertainties involved in the thermal neutron fluence, boron kerma factors, blood boron estimation and brain-to-blood boron concentration ratio. The uncertainties of the boron brain-to-blood and tumour/target-to-blood ratios are estimated based on the data from literature [105, 132]. According to the existing published data of the boron tissue-to-blood ratios the uncertainties are very large and there are no generally accepted reference values for the boron brain-to-blood and tumour/target-to-blood ratios [107, 112, 132, 133]. When the boron dose is included and the dose is quoted to target tissue (tumour) which has 3.5:1 as the tumour/target-to-blood ratio the corresponding uncertainty is 15% (1SD). The data used for the combined total dose uncertainty estimation is summarised in Appendix 7.

According to the uncertainty estimations of this study the level of dose accuracy recommended by ICRU is not achieved with the current methods in BNCT. Considering the uncertainties related to the existing neutron interaction data it should be questioned whether the ICRU recommendations should be applied at all to the dose involved in epithermal neutron beams. The accuracy of the neutron interaction data should improve to enable smaller uncertainties in the physical dosimetry in BNCT. However, there are obvious factors also within the current treatment methods that should be improved in order to gain higher accuracy of the doses. The dosimetry system provides functional means for dose assessment but the

accuracy of the total dose should improve. The large uncertainty related to the fast neutron dose is a special area of concern although it has generally only a modest impact on the total dose. Reciprocal verifications between the measurements and calculations are important to ascertain reliable dosimetry in complex geometries. The blood boron estimation performs efficiently and with appropriate reliability but the boron concentrations in other tissues have huge uncertainties which require additional research. The developed patient positioning system applying the beam entry/exit mark alignment as a default positioning method provides the best selectable accuracy for patient positioning. However, the head fixation methods should be further developed to improve the accuracy of the final position. The proposed arc fixation concept could provide such improvement and create valuable openness in the head fixation scheme. Still, the static fixation of the patient with the existing planar beam aperture geometry will remain a challenging task irrespective of the possible developments in the positioning methods.

6.4 Future of BNCT

One of the greatest premises for BNCT to prevail is to find better carrier compounds to bring boron efficiently and selectively to the target cells [25]. Parallel effort is to optimise the delivery strategies of boron compounds. The development of new invasive, pharmacological and physiological methods elaborating the drug delivery is of great importance for BNCT. Different schemes to disrupt the blood brain barrier (BBB) would expose the tumour more effectively to the drug and hence improve the distribution between the healthy tissue and the tumour at the time of the irradiation. According to emerging results elaborating the boron delivery schemes may have potential to enhance the therapeutic efficacy significantly also with the existing boron carriers [12, 25, 134].

Hence the optimal way to implement BNCT is developing. The new boron carrier development, knowledge of the boron biodistribution and more elaborate beam facilities with increasing possibilities to manage the epithermal field intensities and energy distributions are obvious directions in improvement of the methods and tools [24, 25]. In parallel the widening clinical knowledge and initiation of new phase I-II clinical trials, and eventually also randomised trials should further prove the efficacy of BNCT compared with conventional photon radiotherapy in the treatment of brain tumours [63]. Obviously no single research group is likely to accomplish these developments alone. The steady incremental progress of knowledge from multiple research teams is an obvious path to a long-term success. The need for international and interdisciplinary co-operation is therefore as pronounced today than it has been before.

General success in the methods preventing or treating cancer requires an extensive and time-consuming research in many frontiers including the technical and clinical studies and implementations. Probably the focus will be more or less concentrated on the section of molecular biology to bridge the gap between the clinical observations and the physico-chemical developments [135]. However, the technological implementation aspects of the treatments become continuously more important area of research as the treatment modalities become more elaborate and more dependent on multidisciplinary methods.

7 CONCLUSIONS

In this work different methods involved in the implementation of the BNCT treatments in Finland have been presented.

The methods used in the epithermal neutron beam dosimetry based on twin ionisation chambers and TLD's are functional but the accuracy of these methods should be improved. The activation and Si(Li) diode methods produce satisfying accuracy for the neutron fluence measurements. Semiconductor based dosimetry has particular potential in future applications because of its technical and functional benefits. Generally, the dosimetry measurements agree fairly well with the radiation transport calculations. However, near the curvature boundary regions the discrepancy between the calculated and the measured dose is potentially greater. Therefore the importance of reciprocal verification of the measurements and calculations is emphasised as the geometry becomes more complex. Further studies should be conducted with more realistic antropomorphic phantoms. The ICRU recommendation of the dose uncertainty is not directly applicable in BNCT where already the neutron interaction data introduces relatively large uncertainties in the dose determination.

The uncertainty of the boron dose lies mostly in the boron concentrations in other tissues than blood. The blood boron estimation code based on the bi-exponential function fit produce average boron concentration values for the BNCT irradiation fields efficiently and with appropriate reliability. The treatment log combining the beam and the boron data serves well as a practical application for clinical BNCT and as a coherent interface for operational and documentational use.

The Finnish patient positioning system has proven to be a functional solution in BNCT where the conventional methods for positioning are not applicable. The spatial accuracy of the positioning system and the alternative positioning methods is considered currently acceptable. The spatial accuracy of 5 mm using the default beam entry/exit mark alignment method may serve as an initiative reference level of the positioning uncertainty in BNCT. However, technical improvements should be developed especially for more accurate head fixation methods in order to gain consecutive accuracy in the patient dose. The static fixation of the patient with the existing planar beam aperture will remain a considerable challenge to any positioning solution. In that respect, the existing system has performed well and the learning curve of the positioning procedure has revealed that the positioning timeline can be reduced significantly.

The developments presented in this study facilitate the overall treatment process and together they form basic functional prerequisites for the clinical implementation of BNCT in Finland.

ACKNOWLEDGEMENTS

This thesis describes the work of the author in the Finnish BNCT project during 1997-2002. Department of Physical Sciences of the University of Helsinki, Clinical Research Institute, NC-Treatment Ltd. and VTT Processes are acknowledged for providing working facilities for the studies. During these five years many people, colleagues and co-authors have substantially contributed to this work and I would like to express my gratitude to all of them.

I am especially grateful to Docent Sauli Savolainen, Ph.D., and Antti Kosunen, Ph.D., for excellent supervision of this work. Their guidance and consistent support has been lightening many burdens on my shoulders during this effort. Sauli Savolainen has also been my superior for many years in different medical physics and clinical dosimetry fields. He has given irreplaceable support in hospital physics training to me among so many others.

I am greatly indebted to Docent Mikko Tenhunen, Ph.D., and Docent Maunu Pitkänen, Ph.D., for their professional reviews of the manuscript and constructive comments that have markedly improved this thesis.

I am very grateful to Docent Seppo Pakkala, M.D., Ph.D., the managing director of the Clinical Research Institute HUCH Ltd., for encouragement as an employer during the main part of my work in the Finnish BNCT project.

My sincere gratitude to

Professor Juhani Keinonen, Ph.D., Head of the Department of Physical Sciences of the University of Helsinki, for his valuable advice on the manuscript. His brief audience in 1996 was the starting point of my working career in medical physics. Since then he has been supporting my work on behalf of the University of Helsinki.

Iiro Auterinen, M.Sc. (Tech), for his generous advice and co-operation from the beginning of my activities at the Finnish BNCT facility.

Tiina Seppälä, M.Sc., for her continuous help and co-operation during the years. Her wide interest in BNCT has brought up many elucidative discussions which have motivated my work many times.

Professor Emeritus Pekka Hiismäki, D.Tech., Petri Kotiluoto, M.Sc., Tom Serén, Lic.Tech., Pertti Niskala and many others for their kind co-operation at the Finnish BNCT facility on behalf of VTT Processes.

Päivi Ryynänen, M.Sc., Hanna Koivunoro, M.Sc., Petteri Välimäki, M.Sc., Carita Aschan, Ph.D., Johanna Karila, M.Sc., Juha Laakso, M.Sc., Juha Lampinen, Ph.D., Ritva Parkkinen, Lic.Phil., Inkeri Ruokonen, B.A., Matti Toivonen, Ph.D., Jouni Uusi-Simola, M.Sc., Jyrki Vähätalo, Lic.Phil., Hanna Ylä-Mella, M.Sc., and other co-authors and colleagues from the University of Helsinki, STUK, Clinical Research Institute Ltd. and HUS.

Docent Markus Färkkilä, M.D., Ph.D., Professor Heikki Joensuu, M.D., Ph.D., Merja Kallio, M.D., Ph.D., Leena Kankaanranta, M.D. and Martti Kulvik, M.D., for their generous consultancy in various clinical issues.

Kirsti Ahlroos and other nurses for proficient co-operation in patient positioning.

Jyrki Mäkeläinen, the general director of the TE-PA Medical Ltd., for initiative and helpful co-operation in manufacturing the patient coach and the beam aperture simulator.

Fellow workers in HUS Department of Radiology for their assistance and support.

Finally, my warmest thanks to my wife, Ulla, for her lasting encouragement and support that helped me to complete my thesis. Also, her bright comments and elaborate help in proofreading the manuscript has been a touching contribution to this work.

The financial support from the Technology Development Centre, the Finnish Academy, the State Subsidy for University Hospitals, University of Helsinki, Helsinki University Central Hospital and A Code of Practice for Dosimetry of Boron Neutron Capture Therapy (BNCT) in Europe (Contract no. SMT4-CT98-2145) is gratefully acknowledged.

May 2002 Mika Kortesniemi

REFERENCES

1. International Commission of Radiation Measurements and Units (ICRU), *Determination of absorbed dose in a patient irradiated by beams of X or gamma rays in radiotherapy procedures*. ICRU Report 24. 1976, Bethesda, Maryland: ICRU Publications.

2. Brahme, A., *Dosimetric precision requirements in radiation therapy.* Acta Radiol Oncol, 1984. 23(5): p. 379-391.

3. International Atomic Energy Agency (IAEA), *Absorbed dose determination in photon and electron beams*. An international code of practice. 1987, IAEA Tech. Rep. Series 277: Wien.

4. International Commission of Radiation Measurements and Units (ICRU), *Prescribing, Recording and Reporting Photon Beam Therapy*. ICRU Report 50. 1993, Bethesda, Maryland: ICRU Publications.

5. International Commission of Radiation Measurements and Units (ICRU), *Prescribing, Recording and Reporting Photon Beam Therapy, Supplement to ICRU Report 50*. ICRU Report 62. 1999, Bethesda, Maryland: ICRU Publications.

6. *Radiation Therapy Planning*, ed. N. Bllehen, E. Glatstein, and J. Haybittle. 1983, New York: Marcel Dekker.

7. Khan, F., *The Physics of Radiation Therapy*. 2 ed. 1984, Maryland: Williams & Wilkins.

8. Brahme, A., *Accuracy requirements and quality assurance of external beam radiotherapy with photons and electrons.* Acta Oncologica, 1988. Supplementum 1.

9. Mijnheer, B., J. Battermann, and A. Wambersie, *What degree of accuracy is required and can be achieved in photon and neutron therapy?* Radiother Oncol, 1987. 8: p. 237-252.

10. Kosunen, A., *Metrology and quality of radiation therapy dosimetry of electron, photon and epithermal neutron beams*, Ph.D. Thesis in *Department of Physics*. 1999, University of Helsinki: Helsinki, Finland.

11. United Nations Scientific Committee on the Effects of Atomic Radiation (UNSCEAR), *Sources and effects of ionizing radiation*, 1993, United Nations Publications.

12. International Atomic Energy Agency (IAEA), *Current status of neutron capture therapy*, in *IAEA-Tecdoc-1223*. 2001, IAEA: Wien.

13. Laramore, G. and K. Stelzer, *Neutron capture therapy (NCT) enhancement of fast neutron radiotherapy at the University of Washington*, in *Frontiers in Neutron Capture Therapy*, M.F. Hawthorne, K. Shelly, and R.J. Wiersema, Editors. 2001, Kluwer Academic / Plenum Publishing Corporation: New York. p. 695-702.

14. Miller, D.W., *A review of proton beam radiation therapy.* Med Phys, 1995. 22(11 Pt 2): p. 1943-1954.

15. Lomax, A., *Intensity modulation methods for proton radiotherapy.* Phys Med Biol, 1999. 44(1): p. 185-205.

16. Yeboah, C., G.A. Sandison, and A.V. Chvetsov, *Intensity and energy modulated radiotherapy with proton beams: variables affecting optimal prostate plan.* Med Phys, 2002. 29(2): p. 176-189.

17. Webb, S., *The Physics of Conformal Radiotherapy, Advances in Technology*. 1997, London: IOP Publishing.

18. *Intensity-modulated radiotherapy: current status and issues of interest.* Int J Radiat Oncol Biol Phys, 2001. 51(4): p. 880-914.

19. Cheng, C.W. and I.J. Das, *Comparison of beam characteristics in intensity modulated radiation therapy (IMRT) and those under normal treatment condition.* Med Phys, 2002. 29(2): p. 226-230.

20. Barth, R.F., A.H. Soloway, R.G. Fairchild, *et al.*, *Boron neutron capture therapy for cancer. Realities and prospects.* Cancer, 1992. 70(12): p. 2995-3007.

21. Locher, G.L., *Biological effects and therapeutic possibilities of neutrons.* Am J Roentgenol/ Radium Ther, 1936. 36(1): p. 1-13.

22. Busse, P., R. Zamenhof, O. Harling, *et al.*, *The Harward-MIT BNCT program*, in *Frontiers in Neutron Capture Therapy*, M.F. Hawthorne, K. Shelly, and R.J. Wiersema, Editors. 2001, Kluwer Academic / Plenum Publishing Corporation: New York. p. 37-60.

23. Nakagawa, Y., *Boron neutron capture therapy. Recent aspect and new protocol in Japan*, in *Frontiers in Neutron Capture Therapy*, M.F. Hawthorne, K. Shelly, and R.J. Wiersema, Editors. 2001, Kluwer Academic / Plenum Publishing Corporation: New York. p. 73-79.

24. Nigg, D., *Current trends and progress in the physics of BNCT*, in *Frontiers in Neutron Capture Therapy*, M.F. Hawthorne, K. Shelly, and R.J. Wiersema, Editors. 2001, Kluwer Academic / Plenum Publishing Corporation: New York. p. 13-21.

25. Feakes, D., *Chemistry and pharmacology of agents for BNCT*, in *Frontiers in Neutron Capture Therapy*, M.F. Hawthorne, K. Shelly, and R.J. Wiersema, Editors. 2001, Kluwer Academic / Plenum Publishing Corporation: New York. p. 23-34.

26. Diaz, A.Z., J.A. Coderre, A.D. Chanana, *et al.*, *Boron neutron capture therapy for malignant gliomas.* Ann Med, 2000. 32(1): p. 81-85.

27. Aizawa, O., *Research on neutron beam design for BNCT at the Musashi Reactor.* Basic Life Sci, 1990. 54: p. 109-124.

28. Allen, D.A. and T.D. Beynon, *A design study for an accelerator-based epithermal neutron beam for BNCT.* Phys Med Biol, 1995. 40(5): p. 807-821.

29. Allen, D.A., T.D. Beynon, S. Green, *et al.*, *Toward a final design for the Birmingham boron neutron capture therapy neutron beam.* Med Phys, 1999. 26(1): p. 77-82.

30. Allen, D.A., T.D. Beynon, and S. Green, *Design for an accelerator-based orthogonal epithermal neutron beam for boron neutron capture therapy.* Med Phys, 1999. 26(1): p. 71-76.

31. Allen, D.A. and T.D. Beynon, *What is the best proton energy for accelerator-based BNCT using the 7Li(p,n)7Be reaction?* Med Phys, 2000. 27(5): p. 1113-1118.

32. Seppälä, T., S. Savolainen, I. Auterinen, *et al.*, *Determining and reporting the doses in the treatments of glioma patients in the epithermal neutron beam at the Finnish BNCT facility (FiR 1)*, in *Current status of neutron capture therapy (IAEA Tecdoc-1223)*. 2001, IAEA: Wien. p. 275-287.

33. Rorer, D., F. Patti, R. Ma, *et al.*, *Upgrade of the epithrmal neutron beam using U-235 fission plates at Brookhaven Medical Research Reactor (BMRR)*, in *Frontiers in Neutron Capture Therapy*, M.F. Hawthorne, K. Shelly, and R.J. Wiersema, Editors. 2001, Kluwer Academic / Plenum Publishing Corporation: New York. p. 289-294.

34. Auterinen, I., P. Hiismäki, P. Kotiluoto, *et al.*, *Metamorphosis of a 35 years old TRIGA reactor into a modern BNCT facility*, in *Frontiers in Neutron Capture Therapy*, M.F. Hawthorne, K. Shelly, and R.J. Wiersema, Editors. 2001, Plenum Publishing Corporation: New York. p. 267-275.

35. Wheeler, F.J., D.W. Nigg, J. Capala, *et al.*, *Boron neutron capture therapy (BNCT): implications of neutron beam and boron compound characteristics.* Med Phys, 1999. 26(7): p. 1237-1244.

36. Harling, O., G. Kohse, and K. Riley, *The use of polutetrafluoroethylene (teflon) containing filter/moderators for epithermal neutron beam production*, in *Frontiers in Neutron Capture Therapy*, M.F. Hawthorne, K. Shelly, and R.J. Wiersema, Editors. 2001, Kluwer Academic / Plenum Publishing Corporation: New York. p. 363-367.

37. Auterinen, I., T. Seppälä, S. Salmenhaara, *et al.*, *Improving the performance of the FiR 1 BNCT facility*, in *Program and abstracts of 9th International Symposium on Neutron Capture Therapy for Cancer, October 2-6, 2000*. 2000, ISNCT: Osaka. p. 43-44.

38. Solares, G., D. Katz, O. Harling, *et al.*, *On-line dosimetry for boron neutron capture therapy at the MIT Research Reactor*, in *Advances in Neutron Capture Therapy*. 1997, Elsevier Science B. V. p. 147-152.

39. Auterinen, I., P. Hiismäki, S. Salmenhaara, *et al.*, *Operation and on-line beam monitoring of the Finnish BNCT station*, in *Advances in Neutron Capture Therapy*. 1997, Elsevier Science B. V. p. 348-352.

40. Watkins, P., R. Moss, F. Stecher-Rasmussen, *et al.*, *Dosimetry for BNCT in theory and practice*, in *Advances in Neutron Capture Therapy*. 1997, Elsevier Science B. V. p. 141-146.

41. Kaita, K., T. Serén, and I. Auterinen, *First characterisation of the Finnish epithermal beam using activation detectors*, in *Advances in Neutron Capture Therapy*. 1997, Elsevier Science B. V. p. 353-356.

42. Kortesniemi, M., A. Kosunen, C. Aschan, *et al.*, *Measurements of phantom dose distributions at the Finnish BNCT facility*, in *Frontiers in Neutron Capture Therapy*, M.F. Hawthorne, K. Shelly, and R.J. Wiersema, Editors. 2001, Kluwer Academic / Plenum Publishing Corporation: New York. p. 659-664.

43. Kosunen, A., M. Kortesniemi, H. Ylä-Mella, *et al.*, *Twin ionisation chambers for dose determinations in phantom in an epithermal neutron beam.* Radiat Prot Dosim, 1999. 81(3): p. 187-194.

44. Knoll, G., *Radiation detection and measurement*. 3rd edition ed. 2000, USA: John Wiley & Sons.

45. Rogus, R.D., O.K. Harling, and J.C. Yanch, *Mixed field dosimetry of epithermal neutron beams for boron neutron capture therapy at the MITR-II research reactor.* Med Phys, 1994. 21(10): p. 1611-1625.

46. Verbakel, W.F. and F. Stecher-Rasmussen, *On-line reconstruction of low boron concentrations by in vivo gamma-ray spectroscopy for BNCT.* Phys Med Biol, 2001. 46(3): p. 687-701.

47. Munck af Rosenschold, P.M., W.F. Verbakel, C.P. Ceberg, *et al.*, *Toward clinical application of prompt gamma spectroscopy for in vivo monitoring of boron uptake in boron neutron capture therapy.* Med Phys, 2001. 28(5): p. 787-795.

48. Aschan, C., M. Toivonen, S. Savolainen, *et al.*, *Epithermal neutron beam dosimetry with thermoluminescent dosemeters for boron neutron capture therapy.* Radiat Prot Dosim, 1999. 81(1): p. 47-56.

49. Kota, C. and R.L. Maughan, *A dosimetry system for boron neutron capture therapy based on the dual counter microdosimetric technique.* Bull Cancer Radiother, 1996. 83 Suppl: p. 173s-175s.

50. Bradley, P., A. Rosenfeld, B. Allen, *et al.*, *Application of silicon diode arrays for microdosimetry for BNCT and FNT*, in *Frontiers in Neutron Capture Therapy*, M.F. Hawthorne, K. Shelly, and R.J. Wiersema, Editors. 2001, Kluwer Academic / Plenum Publishing Corporation: New York. p. 615-621.

51. Burmeister, J., C. Kota, and R.L. Maughan, *Dosimetry of the boron neutron capture reaction for BNCT and BNCEFNT.* Strahlenther Onkol, 1999. 175 Suppl 2: p. 115-118.

52. Burmeister, J., C. Kota, R. Maughan, *et al.*, *Microdosimetry studies at the BMRR and the MITR-II using miniature tissue-equivalent proportional counters*, in *Frontiers in Neutron Capture Therapy*, M.F. Hawthorne, K. Shelly, and R.J. Wiersema, Editors. 2001, Kluwer Academic / Plenum Publishing Corporation: New York. p. 581-586.

53. Rosenfeld, A.B., *Semiconductor dosimetry in BNCT*, in *Frontiers in Neutron Capture Therapy*, M.F. Hawthorne, K. Shelly, and R.J. Wiersema, Editors. 2001, Kluwer Academic / Plenum Publishing Corporation: New York. p. 557-563.

54. Pospisil, S., B. Sopko, E. Havránková, *et al.*, *Si diode as a small detector of slow neutrons.* Radiat Prot Dosim, 1993. 46(2): p. 115-118.

55. Kaplan, G.I., A.B. Rosenfeld, B.J. Allen, *et al.*, *Semiconductor detectors for in-phantom thermal neutron flux and boron dose measurements in BNCT and fast neutron therapy*, in *Frontiers in Neutron Capture Therapy*, M.F. Hawthorne, K. Shelly, and R.J. Wiersema, Editors. 2001, Kluwer Academic / Plenum Publishing Corporation: New York. p. 1175-1180.

56. Chadwick, M.B., H.H. Barschall, R.S. Caswell, *et al.*, *A consistent set of neutron kerma coefficients from thermal to 150 MeV for biologically important materials.* Med Phys, 1999. 26(6): p. 974-991.

57. Aschan, C., M. Toivonen, S. Savolainen, *et al.*, *Experimental correction for thermal neutron sensitivity of gamma ray TL dosimeters irradiated at BNCT beams.* Radiat Prot Dosim, 1999. 82(1): p. 65-69.

58. Kessler, C., F. Stecher-Rasmussen, J. Rassow, *et al.*, *Application of thermoluminescent dosimeters to mixed neutron-gamma dosimetry for BNCT*, in *Frontiers in Neutron Capture Therapy*, M.F. Hawthorne, K. Shelly, and R.J. Wiersema, Editors. 2001, Kluwer Academic / Plenum Publishing Corporation: New York. p. 1165-1173.

59. International Commission of Radiation Measurements and Units (ICRU), *Clinical neutron dosimetry part I: Determination of absorbed dose in a patient treated by external beams of fast neutrons*. ICRU Report 45. 1989, Bethesda, Maryland: ICRU Publications.

60. Attix, F., *Introduction to radiological physics and radiation dosimetry*. 1986, New York: John Wiley & Sons.

61. Raaijmakers, C.P., P.R. Watkins, E.L. Nottelman, *et al.*, *The neutron sensitivity of dosimeters applied to boron neutron capture therapy.* Med Phys, 1996. 23(9): p. 1581-1589.

62. Brooks, R.A., G. Di Chiro, and M.R. Keller, *Explanation of cerebral white--gray contrast in computed tomography.* J Comput Assist Tomogr, 1980. 4(4): p. 489-491.

63. Joensuu, H., L. Kankaanranta, T. Seppälä, *et al.*, *Boron Neutron Capture Therapy of Brain Tumors: Clinical Trials at the Finnish Facility Using Boronophenylalanine.* J Neurooncol, 2002. Submitted.

64. Coderre, J.A., E.H. Elowitz, M. Chadha, *et al.*, *Boron neutron capture therapy for glioblastoma multiforme using p-boronophenylalanine and epithermal neutrons: trial design and early clinical results.* J Neurooncol, 1997. 33(1-2): p. 141-152.

65. Laakso, J., M. Kulvik, I. Ruokonen, *et al.*, *Atomic emission method for total boron in blood during neutron-capture therapy.* Clin Chem, 2001. 47(10): p. 1796-1803.

66. Ryynänen, P.M., M. Kortesniemi, J.A. Coderre, *et al.*, *Models for estimation of the (10)B concentration after BPA-fructose complex infusion in patients during epithermal neutron irradiation in BNCT.* Int J Radiat Oncol Biol Phys, 2000. 48(4): p. 1145-1154.

67. Seppälä, T., M. Kortesniemi, L. Kankaanranta, *et al. Patient positioning according to dose planning in BNCT at FiR 1*. in *Medical & Biological Engineering & Computing*. 1999. Tallinn: IFMBE. p. 402-403.

68. Sauerwein, W., R. Moss, J. Rassow, *et al.*, *Quality management at the European BNCT center in Petten*, in *Frontiers in Neutron Capture Therapy*, M.F. Hawthorne, K. Shelly, and R.J. Wiersema, Editors. 2001, Kluwer Academic / Plenum Publishing Corporation: New York. p. 113-121.

69. Auterinen, I., P. Hiismäki, P. Kotiluoto, *et al. The new boron neutron capture therapy facility at the Finnish nuclear research reactor (FiR 1)*. in *Medical & Biological Engineering & Computing*. 1999. Tallinn: IFMBE. p. 398-399.

70. Benczik, J., *Relative biological effectiveness of reactor produced epithermal neutrons for the canine brain*, Ph.D. Thesis. 2000, Helsinki University: Helsinki.

71. Sandberg-Wollheim, M., P. Malmstrom, L.G. Stromblad, *et al.*, *A randomized study of chemotherapy with procarbazine, vincristine, and lomustine with and without radiation therapy for astrocytoma grades 3 and/or 4.* Cancer, 1991. 68(1): p. 22-29.

72. Diaz, A., A. Chanana, J. Capala, *et al.*, *Boron neutron capture therapy for glioblastoma multiforme. Results from the initial phase I/II dose escalation studies*, in *Frontiers in Neutron Capture Therapy*, M.F. Hawthorne, K. Shelly, and R.J. Wiersema, Editors. 2001, Kluwer Academic / Plenum Publishing Corporation: New York. p. 61-72.

73. International Commission of Radiation Measurements and Units (ICRU), *Photon, electron, proton and neutron interaction data for body tissues*. ICRU Report 46. 1992, Bethesda, Maryland: ICRU Publications.

74. Serén, T., I. Auterinen, T. Seppälä, *et al.*, *Experimental and calculated neutron spectra at the Finnish epithermal BNCT facility.* Clin Physiol, 1998. 18(3): p. 291.

75. Serén, T., I. Auterinen, T. Seppälä, *et al. Spectrum measurements and calculations in the epithermal neutron beam at the FiR 1 BNCT facility*. in *15th European TRIGA Conference*. 1998. Espoo, Finland.

76. Nigg, D., Y. Harker, J. Hartwell, *et al.*, *Collaborative neutronic performance characterization of the FiR 1 clinical epithermal neutron beam facility for BNCT*, in *INEEL BNCT Research Program, Annual Report 1998*, J.R. Venhuizen, Editor. 1999, INEEL-EXT-99-00293 April 1999. p. 12-38.

77. Nigg, D., Y. Harker, J. Hartwell, *et al.*, *Collaborative spectral characterization of the Finnish epithermal-neutron beam facility for BNCT*, in *INEEL BNCT Research Program, Annual Report 1996*. 1997, INEEL-EXT-97-00319 April 1997. p. 12-38.

78. Kortesniemi, M., T. Serén, T. Seppälä, *et al.*, *Position displacement effect on the doses in the epithermal head regions*, in *Program and abstracts of 9th International Symposium on Neutron Capture Therapy for Cancer, October 2-6, 2000*. 2000: Osaka. p. 283-284.

79. Toivonen, M., V. Chernov, H. Jungner, *et al.*, *The abilities of LiF thermoluminescent detectors for dosimetry at boron neutron capture therapy beams.* Radiat Meas, 1998. 29(3-4): p. 373-377.

80. Mäenpää, T., *Building a small thermal neutron detector*, 1996, Helsinki University of Technology: Espoo, Finland.

81. Raaijmakers, C.P., M. Konijnenberg, H. Verhagen, *et al.*, *Determination of dose components in phantoms irradiated with an epithermal neutron beam for boron neutron capture therapy.* Med Phys, 1995. 22: p. 321-329.

82. Kosunen, A., H. Ylä-Mella, and S. Savolainen, *The twin ionisation chamber technique in quality control of a mixed epithermal neutron and gamma beam for NCT*, in *Advances in Neutron Capture Therapy*. 1997, Elsevier Science B. V. p. 182-187.

83. Jansen, J., C. Raaijmakers, B. Mijnheer, *et al.*, *Relative Neutron Sensitivity of Tissue-Equivalent Ionisation Chambers in an Epithermal Neutron Beam for Boron Neutron Capture Therapy.* Radiat. Prot. Dosim., 1997. 70(1-4): p. 27-32.

84. Seppälä, T., J. Vähätalo, I. Auterinen, *et al.*, *Brain tissue substitutes for phantom measurements in NCT*, in *Advances in Neutron Capture Therapy*. 1997, Elsevier Science B. V. p. 188-191.

85. Raaijmakers, C.P., E.L. Nottelman, and B.J. Mijnheer, *Phantom materials for boron neutron capture therapy.* Phys Med Biol, 2000. 45(8): p. 2353-2361.

86. Snyder, W.S., H.L. Fisher, Jr., M.R. Ford, *et al.*, *Estimates of absorbed fractions for monoenergetic photon sources uniformly distributed in various organs of a heterogeneous phantom.* J Nucl Med, 1969: p. Suppl 3:7-52.

87. *CADSCAN Water Phantom System, User's Manual Version 1.2*, 1990, Dosetek Oy: Espoo.

88. Stallmann, F., *LSL-M2: a computer program for least-squares logarithmic adjustment of neutron spectra*, 1986, Oak Ridge National Laboratory.

89. Serén, T., M. Kortesniemi, C. Aschan, *et al. A tale of two beams - comparison of the radiation fields at the BMRR and FiR 1 epithermal BNCT facilities*. in *Medical & Biological Engineering & Computing*. 1999. Tallinn: IFMBE. p. 396-397.

90. Rhoades, W. and R. Childs, *The DORT Two-Dimensional Discrete Ordinates Transport Code.* Nucl Sci Engr, 1988. 99: p. 88-89.

91. Roussin, R., *BUGLE-80, Coupled 47-Neutron, 20-Gamma Ray, P3, Cross Section Library for LWR Shielding Calculations*, 1980, Radiation Shielding Information Center, Oak Ridge National Laboratory: Oak Ridge.

92. Serén, T. *PC programs for the conversion of neutron spectra and cross sections between different group and point representations*. in *Seventh ASTM-EURATOM Symp on Reactor Dosimetry*. 1992. Strasburg, France: Kluver Academic.

93. International Commission of Radiation Measurements and Units (ICRU), *Tissue Substitutes in Radiation Dosimetry and Measurement*. ICRU Report 44. 1989, Bethesda, Maryland: ICRU Publications.

94. Wojnecki, C. and S. Green, *Reference phantom design for the Birmingham BNCT project*, in *Frontiers in Neutron Capture Therapy*, M.F. Hawthorne, K. Shelly, and R.J. Wiersema, Editors. 2001, Kluwer Academic / Plenum Publishing Corporation: New York. p. 681-686.

95. Bradley, P.D., A.B. Rosenfeld, B. Allen, *et al.*, *Performance of silicon microdosimetry detectors in boron neutron capture therapy.* Radiat Res, 1999. 151(3): p. 235-243.

96. Kota, C., *Microdosimetric considerations in the use of the boron neutron capture reaction in radiation therapy*, Ph.D. Thesis. 1996, Wayne State University: Detroit, USA.

97. Kota, C., R.L. Maughan, D. Tattam, *et al.*, *Use of low-pressure tissue equivalent proportional counters for the dosimetry of neutron beams used in BNCT and BNCEFNT.* Med Phys, 2000. 27(3): p. 535-548.

98. Kota, C., J. Burmeister, and R. Maughan, *Utility of measured microdosimetric single event spectra in interpreting quality of radiation fields used in BNCT*, in *Frontiers in Neutron Capture Therapy*, M.F. Hawthorne, K. Shelly, and R.J. Wiersema, Editors. 2001, Kluwer Academic / Plenum Publishing Corporation: New York. p. 647-651.

99. Burmeister, J., C. Kota, and R. Maughan, *Paired miniature TEPCs for dosimetry in high flux epithermal neutron capture therapy beams.* Nuc Inst and Meth in Phys Res, 1999. A422: p. 606-610.

100. Stecher-Rasmussen, F., I. Auterinen, E. Beddoe, *et al.*, *A code of practice for the dosimetry of BNCT in Europe*, in *Advances in Neutron Capture Therapy*. 1997, Elsevier Science B. V. p. 237-240.

101. Oldham, M., J.H. Siewerdsen, A. Shetty, *et al.*, *High resolution gel-dosimetry by optical-CT and MR scanning.* Med Phys, 2001. 28(7): p. 1436-1445.

102. Savolainen, S., *Polymer gel (BANG3) in the BNCT dosimetry*, 2002, Personal communication.

103. Raaijmakers, C.P., I.A. Bruinvis, E.L. Nottelman, *et al.*, *A fast and accurate treatment planning method for boron neutron capture therapy.* Radiother Oncol, 1998. 46(3): p. 321-332.

104. Chadwick, M.B., *Neutron, proton, and photonuclear cross-sections for radiation therapy and radiation protection.* Radiat Environ Biophys, 1998. 37(4): p. 235-242.

105. Coderre, J.A. and G.M. Morris, *The radiation biology of boron neutron capture therapy.* Radiat Res, 1999. 151(1): p. 1-18.

106. Yoshino, K., A. Suzuki, Y. Mori, *et al.*, *Improvement of solubility of p-Boronophenylalanine by complex formation with monosaccharides.* Strahlenther Oncol, 1989(165): p. 127-129.

107. Elowitz, E.H., R.M. Bergland, J.A. Coderre, *et al.*, *Biodistribution of p-boronophenylalanine in patients with glioblastoma multiforme for use in boron neutron capture therapy.* Neurosurgery, 1998. 42(3): p. 463-8; discussion 468-469.

108. Chanana, A.D., J. Capala, M. Chadha, *et al.*, *Boron neutron capture therapy for glioblastoma multiforme: interim results from the phase I/II dose-escalation studies.* Neurosurgery, 1999. 44(6): p. 1182-1192; Discussion 1192-1193.

109. Imahori, Y., S. Ueda, Y. Ohmori, *et al.*, *Positron emission tomography-based boron neutron capture therapy using boronophenylalanine for high-grade gliomas: part II.* Clin Cancer Res, 1998. 4(8): p. 1833-1841.

110. Imahori, Y., S. Ueda, Y. Ohmori, *et al.*, *Positron emission tomography-based boron neutron capture therapy using boronophenylalanine for high-grade gliomas: part I.* Clin Cancer Res, 1998. 4(8): p. 1825-1832.

111. Imahori, Y., S. Ueda, Y. Ohmori, *et al.*, *Fluorine-18-labeled fluoroboronophenylalanine PET in patients with glioma.* J Nucl Med, 1998. 39(2): p. 325-333.

112. Kabalka, G.W., G.T. Smith, J.P. Dyke, *et al.*, *Evaluation of fluorine-18-BPA-fructose for boron neutron capture treatment planning.* J Nucl Med, 1997. 38(11): p. 1762-1767.

113. Kabalka, G.W., C. Tang, and P. Bendel, *The role of boron MRI in boron neutron capture therapy.* J Neurooncol, 1997. 33(1-2): p. 153-161.

114. Zuo, C.S., P.V. Prasad, P. Busse, *et al.*, *Proton nuclear magnetic resonance measurement of p-boronophenylalanine (BPA): a therapeutic agent for boron neutron capture therapy.* Med Phys, 1999. 26(7): p. 1230-1236.

115. Kabalka, G.W., M. Davis, and P. Bendel, *Boron-11 MRI and MRS of intact animals infused with a boron neutron capture agent.* Magn Reson Med, 1988. 8(2): p. 231-237.

116. Kiger, W.S., M.R. Palmer, K.J. Riley, *et al.*, *A Pharmacokinetic Model for the Concentration of 10B in Blood after Boronophenylalanine-Fructose Administration in Humans.* Radiat Res, 2001. 155(4): p. 611-618.

117. Burden, R. and J. Faires, *Numerical Analysis*. 5 ed. 1993, Boston, USA: PWS Publishing Company.

118. Bevington, P. and D. Robinson, *Data reduction and error analysis for the physical sciences*. 2 ed. 1992, New York: McGraw-Hill Book Company.

119. Kallio, M., M. Kulvik, J. Laakso and J. Vähätalo, *Secondary peak in blood boron clearance curve*, 2001, Personal communication.

120. Kiger, W., M. Palmer, R. Zamenhof, *et al.*, *A pharmacokinetic model for the concentration of boron-10 in blood following boronophenylalanine-fructose administration in humans*, in *Frontiers in Neutron Capture Therapy*, M.F. Hawthorne, K. Shelly, and R.J. Wiersema, Editors. 2001, Kluwer Academic / Plenum Publishing Corporation: New York. p. 249-255.

121. Ryynänen, P.M., A. Kangasmäki, P. Hiismäki, *et al.*, *Non-linear models for the kinetics of 10B in blood after BPA-fructose complex infusion.* Phys Med Biol, 2002. 47: p. 737-745.

122. Kortmann, R.D., G. Becker, J. Perelmouter, *et al.*, *Geometric accuracy of field alignment in fractionated stereotactic conformal radiotherapy of brain tumors.* Int J Radiat Oncol Biol Phys, 1999. 43(4): p. 921-926.

123. Pilipuf, M.N., J.C. Goble, and N.F. Kassell, *A noninvasive thermoplastic head immobilization system. Technical note.* J Neurosurg, 1995. 82(6): p. 1082-1085.

124. Theodorou, K., C. Kappas, and C. Tsokas, *A new non-invasive and relocatable immobilization frame for fractionated stereotactic radiotherapy.* Radiother Oncol, 1998. 47(3): p. 313-317.

125. Wielopolski, L., J. Capala, M. Chadha, *et al.*, *Considerations for patient positioning in static beams for BNCT*, in *Advances in Neutron Capture Therapy*. 1997, Elsevier Science B. V. p. 357-359.

126. Watkins, P., C. Vroegindeweij, S. Garbe, *et al.*, *Patient positioning at the HFR Petten*, in *Frontiers in Neutron Capture Therapy*, M.F. Hawthorne, K. Shelly, and R.J. Wiersema, Editors. 2001, Plenum Publishing Corporation: New York. p. 179-183.

127. Palmer, M., W. Kiger, C. Zuo, *et al.*, *Integrated medical imaging registration, patient positioning, and patient monitoring for cranial BNCT*, in *Frontiers in Neutron Capture Therapy*, M.F. Hawthorne, K. Shelly, and R.J. Wiersema, Editors. 2001, Kluwer Academic / Plenum Publishing Corporation: New York. p. 195-199.

128. Hendee, E., W. Tomé, and W. Hendee, *In stereotactic radiosurgery, implanted fiducials are superior to an external coordinate system.* Med Phys, 2002. 29(1): p. 100-102.

129. Michiels, J., H. Bosmans, P. Pelgrims, *et al.*, *On the problem of geometric distortion in magnetic resonance images for stereotactic neurosurgery.* Magn Reson Imaging, 1994. 12(5): p. 749-765.

130. Sumanaweera, T.S., J.R. Adler, Jr., S. Napel, *et al.*, *Characterization of spatial distortion in magnetic resonance imaging and its implications for stereotactic surgery*. Neurosurgery, 1994. 35(4): p. 696-703; discussion 703-704.

131. Bjugg, H., I. Auterinen, P. Kotiluoto, *et al.*, *Quality control procedure of the BNCT patient dose determination*, in *Program and abstracts of 9th International Symposium on Neutron Capture Therapy for Cancer, October 2-6, 2000*. 2000, ISNCT: Osaka. p. 195-196.

132. Palmer, M., C. Chuang, W. Kiger, *et al.*, *Predicting boron-10 concentrations in normal brain and GBM from blood measurements*, in *Frontiers in Neutron Capture Therapy*, M.F. Hawthorne, K. Shelly, and R.J. Wiersema, Editors. 2001, Kluwer Academic / Plenum Publishing Corporation: New York. p. 243-247.

133. Coderre, J.A., A.D. Chanana, D.D. Joel, *et al.*, *Biodistribution of boronophenylalanine in patients with glioblastoma multiforme: boron concentration correlates with tumor cellularity*. Radiat Res, 1998. 149(2): p. 163-170.

134. Barth, R.F., W. Yang, J.H. Rotaru, *et al.*, *Boron neutron capture therapy of brain tumors: enhanced survival and cure following blood-brain barrier disruption and intracarotid injection of sodium borocaptate and boronophenylalanine.* Int J Radiat Oncol Biol Phys, 2000. 47(1): p. 209-218.

135. Larsson, B. and N. Crompton, *Monochromatic X-rays, slow neutrons, and radionuclides for targeted radiotherapy*, in *Frontiers in Neutron Capture Therapy*, M.F. Hawthorne, K. Shelly, and R.J. Wiersema, Editors. 2001, Kluwer Academic / Plenum Publishing Corporation: New York. p. 5-12.

LIST OF FIGURES

Figure 1. The optimal dose for the radiotherapy application. The tumour tissue suffers from the radiation dose which is still tolerated by the healthy tissue. The width of the window sets the upper and the lower limit for the dose which is applied to the target volume. ... 10
Figure 2. The concept of boron neutron capture therapy presented in two levels. In A) the boron neutron capture reaction occurs where a neutron activates the boron-10 atom fission into highly lethal alpha and lithium particles with tissue track lengths of 9 and 5 μm, respectively. In B) the patient head is positioned into the planned location and angle with respect to the collimated epithermal neutron beam. The tumour has a higher boron concentration and is presented lighter than the surrounding healthy tissue which is presented darker. The intracranial vasculature functions as a channel for the intravenously infused boron carrier on its way to the tumour. ... 12
Figure 3. The FiR (K63) BNCT beam components presented as the relative neutron field contributions to total neutron fluence (A), relative dose components of the total dose (B) and absolute dose values (C) in free beam and in three depths in the central axis of the cylindrical Liquid B phantom. The component colors are explained in C. ... 24
Figure 4. The schematic structure of the Si(Li) diode detector used for the thermal neutron fluence measurements. ... 25
Figure 5. The pulse spectrum of the Si(Li) diode detector in the central depth axis of the cylindrical PMMA phantom in the depth of 21 mm. ... 26
Figure 6. The phantom materials and the ICRU brain elemental composition [84]. ... 28
Figure 7. The phantoms used in dosimetry studies at the Finnish BNCT facility; A) the liquid cylinder attached to the tank phantom, B) the solid PMMA cylinder, C) the ellipsoidal phantom and D) the doghead phantom. ... 29
Figure 8. The Finnish BNCT beam construction and the measurement set-up. The epithermal neutron beam is produced as the radiation from the reactor core and the graphite reflector is filtered through the boral plate, the 63 cm thick Fluental moderator and the bismuth shield. Finally, the beam is collimated by the ^{6}Li enriched aperture cone rings before the resulting neutron and gamma field is distributed and detected in the phantom (P). The phantom (not in scale) is attached to the large liquid pool (LP) and the detector (D) is moved in three dimensions using the computer controlled transport mechanism (TM). . 30
Figure 9. The relative neutron sensitivity (k_t) of the TE(TE) ionisation chamber determined in the central beam axis according to the depth in the elliptical water filled phantom. The beam aperture diameter was Ø14 cm. ... 32
Figure 10. The measured absorbed gamma (circles) and neutron (triangles) dose rate as a function of depth along the beam central axis in the water filled ellipsoidal phantom. The calculated dose from the SERA (solid line) and MCNP (dashed line) simulations are presented, respectively. The beam aperture was Ø14 cm. Error bars represent the uncertainty (1SD) of the measured dose. ... 33
Figure 11. The absorbed gamma dose rates at the perpendicular direction of the water filled ellipsoidal phantom. Distance is from the beam central axis. The calculated gamma doses from the SERA and MCNP simulations are presented as lines (SERA=solid, MCNP=dashed) and measured (IC) doses are marked individually as circles. Thicker lines and solid circles correspond to 30 mm depth. Thinner lines and empty circles correspond to 60 mm depth. The beam aperture was Ø14 cm. Error bars represent the uncertainty (1SD) of the measured dose. ... 33
Figure 12. The absorbed total neutron dose rates at the perpendicular axis of the water filled ellipsoidal phantom. The distance is from the beam central axis. The calculated neutron

doses from the SERA and MCNP simulations are presented as lines (SERA=solid, MCNP=dashed) and measured (IC) doses are marked individually as triangles. Thicker lines and solid triangles correspond to 30 mm depth. Thinner lines and empty triangles correspond to 60 mm depth. The beam aperture was Ø14 cm. Error bars represent the uncertainty (1SD) of the measured dose. 34
Figure 13. The measured (IC) gamma (circles) and neutron (triangles) dose rates in the beam central depth axis in the water filled ellipsoid (solid symbols) and cylinder (empty symbols) phantom. The data from Kosunen et al. is used for the doses in the cylindrical water phantom [43]. The beam aperture was Ø14 cm. Error bars represent the uncertainty (1SD) of the measured dose. 35
Figure 14. The measured (solid line) and calculated (dashed line) relative lithium reaction rates, calculated thermal neutron fluence (diamonds) and measured Mn reaction rates (empty circles) at the beam central depth axis in the water filled ellipsoidal phantom. The beam aperture diameter was Ø14 cm. 36
Figure 15. The measured (lines) and calculated (diamonds) relative lithium reaction rates at the beam central depth axis in the ellipsoidal (solid line and diamonds) and cylindrical (dashed line and empty diamond) water filled phantoms. The beam aperture diameter was Ø14 cm. 36
Figure 16. The IC measurement points inside the ellipsoidal phantom. Two phantom positions were used for all the measurement points. The eye plane points were used in this study to determine the doses near the edge of the phantom with and without the beam asymmetry caused by the lateral phantom displacement of 35 mm [78]. The beam direction is schematically presented as an arrow. 37
Figure 17. The measured (IC, circles) and calculated (SERA, triangles) gamma dose rates in the specific locations in the water filled ellipsoidal phantom with two studied phantom positions (solid symbol for centre and empty symbol for displacement) in the translated sagittal plane points of the ellipsoidal phantom. The beam aperture was Ø11 cm [78]. . 38
Figure 18. The distribution of the relative neutron sensitivity k_t of the tissue equivalent ionisation chamber as a function of neutron energy presented in the BUGLE energy structure with 47 energy groups using the data of Jansen [83]. The thermal (T), epithermal (E) and fast (F) energy ranges are separated with dash lines. 39
Figure 19. The average blood ^{10}B concentration curve showing the BPA-F infusion and BNCT irradiation field phases of the Finnish clinical phase I trials. Standard (dashed line) and iterated fit (solid line) are presented with start and end indicators of the fields (vertical lines). Measured values during the infusion (empty circles), initial phase (solid circles) and intermediate phase (solid triangles), and after the treatment (empty square) are presented with individual symbols. Error bars represent the uncertainty of the measured values. 46
Figure 20. The average blood boron concentrations of the 12 protocol-1 patients with 290 mg/kg of BPA infusions according to the interpolated boron data. Error bars represent the uncertainty (1SD) of the interpolated values. 47
Figure 21. The fitted half lives of the protocol 1 patients with 290 mg/kg infusions (black circles), protocol 1 patients with 330-400 mg/kg infusions (white circles), protocol 3 patients with 290 mg/kg infusions (triangles). The average half lives of the protocol 1 patients with 290 mg/kg infusions (excluding the two ringed circles) were used as defaults (cross and arrows). The BPA-F infusion time was 120 min. The regression line (solid) is plotted with the correlation coefficient R. 49
Figure 22. The bi-exponential function fitting solutions for 1 (A), 3 (B), 5 (C), and 7 (D) blood boron values after the BPA-F infusion, determined from the interpolated average

boron measurement data of the protocol 1 patients with 120 min (290 mg/kg BPA-F) infusions. 50
Figure 23. The increasing accuracy of the boron estimation described by the relative uncertainty (1SD) between the updating fitting curves and the final measured (ICP-AES) boron concentrations determined from the interpolated average boron measurement data of the protocol 1 patients with 120 min (290 mg/kg BPA) infusions. 51
Figure 24. An example of a clearance phase with a transient plateau. The measured (ICP-AES) blood boron concentrations (solid circles) and the bi-exponential fit (solid line) calculated from the clearance phase data points. Start and end indicators of the fields are presented as vertical lines. Error bars represent the uncertainty of the measured values. 53
Figure 25. The floor plan showing the irradiation room and the simulation room of the Finnish BNCT facility. 55
Figure 26. The coordinate system with respect to the beam aperture. The transaxial plane is defined with the x/z-axis, the coronal plane is defined with the x/y-axis and the sagittal plane is defined with the y/z-axis if the patient is located on the y axis in a supine position. The y axis is located on the beam central axis. 57
Figure 27. A) The sagittal MRI head image and three image stacks covering the head and B) the locations of the fiducial marks on the head model. 58
Figure 28. A) The beam alignment with two angular settings. The transaxial plane corresponding to head turn is rotated α degrees. The coronal plane corresponding to coach rotation on the lateral plane is moved β degrees. B) The beam alignment with three distance settings (a, b, c) of the beam side fiducial marks with respect to the aperture plane. 59
Figure 29. The final positioning in an actual patient treatment. 61
Figure 30. The antropomorphic head phantom (RSVP) with a part of the E-vitamin capsules shown on the fiducial mark locations corresponding to the transaxial, vertex and six beam entry/exit points used in the spatial accuracy study. 62
Figure 31. In A, the ellipsoidal phantom is positioned laterally on the beam central axis and at 5 mm off-axis. The spherical target volume and the tumour were positioned near the beam side surface of the phantom at the location of thermal fluence maximum. In B, the SERA simulation image shows the central position and the dose profile lines in the lateral depth axis (solid line) and in the perpendicular axis at three depths (dash lines). 63
Figure 32. The treatment coach dimensions and movement ranges in x, y, and z directions. 64
Figure 33. The coach and the anthropomorphic model positioned for the lateral field. In practical positioning the semi-lateral body posture is used to fit patient shoulders on the beam side. 65
Figure 34. The coach and the human model positioned for the posterior field. 65
Figure 35. The treatment coach (A) and the beam simulator system (B). The coach is attached to the docking base (C). In the small image the head model has been positioned for the vertex field using vacuum cushion fixation. 66
Figure 36. The total dose in the lateral depth axis directed through the ellipsoidal phantom, the target volume and the tumour centre points. The solid line represents the central dose profile whereas the crosses represent the doses in the same points but at the 5 mm displaced beam position. 67
Figure 37. The total doses in the perpendicular axis at three depths corresponding to the ellipsoidal phantom (8 cm), the target volume (6 cm) and the tumour (4 cm) centre points. The solid lines represent the central position dose profiles whereas the dash lines represent the 5 mm displaced position dose profiles. 68

Figure 38. The arc method for head fixation in BNCT. Soft anatomically shaped wedges are used to secure the head fixation. The arc can be turned aside to allow various beam alignments. The medial and transaxial adjustments provide accurate angular settings of the head while maintaining the fixation. In the small image the head is included in the fixation scheme. 71

LIST OF TABLES

Table 1. The Exradin thimble TE(TE) and Mg(Ar) ionisation chamber characteristics. 27
Table 2. The phantom materials and dimensions. 29
Table 3. Summary of the studied cases including the patient and protocol number, the infusion amount (BPA of total body weight), the normalised χ^2, the intrinsic standard deviation of the fit in ppm of boron and the half life values (fast and slow) of the bi-exponential fit. 50
Table 4. The spatial and directional uncertainties of the three positioning methods: the entry-exit mark alignment (EMA), the mark angle to plane (MAP), and the mark distance to aperture (MDA). 66
Table 5. The realised positioning schedule for an immobile 64-year-old male patient. 69

APPENDICES

Appendix 1 - Beam dosimetry chain

Appendix 2 - Boron dosimetry chain

Appendix 3 - Patient positioning chain

Appendix 4 - Implementation model

Appendix 5 - Treatment process

Appendix 6 - Quality control chain

Appendix 7 - Uncertainty of the dose

Appendix 8 - Treatment log (Positioning data)

Appendix 9 - Treatment log (Beam data)

Appendix 10 - Treatment log (Boron data)

Appendix 11 - Treatment log (Summary)

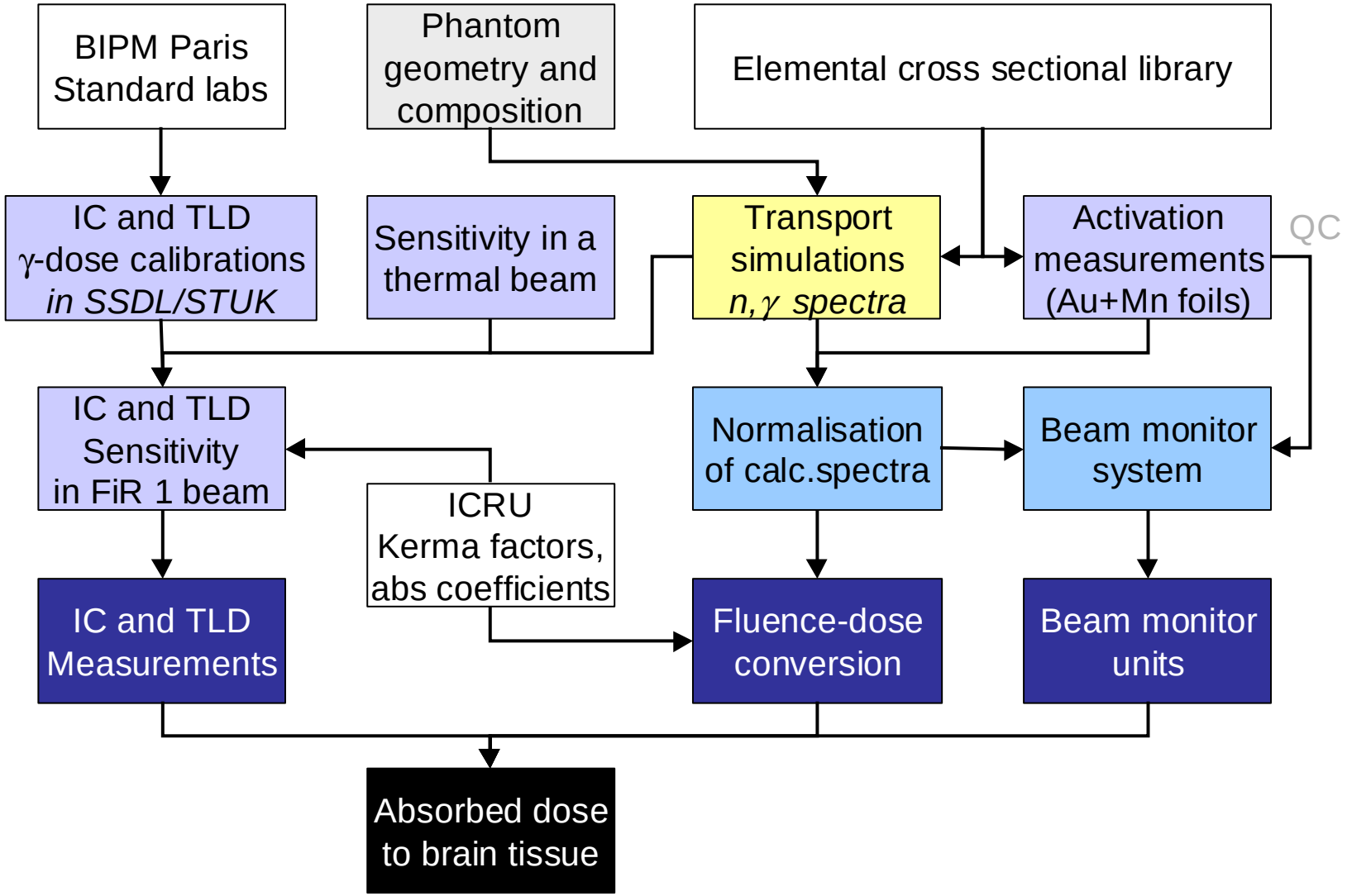

Appendix 1 - Beam dosimetry chain

Appendix 2 - Boron dosimetry chain

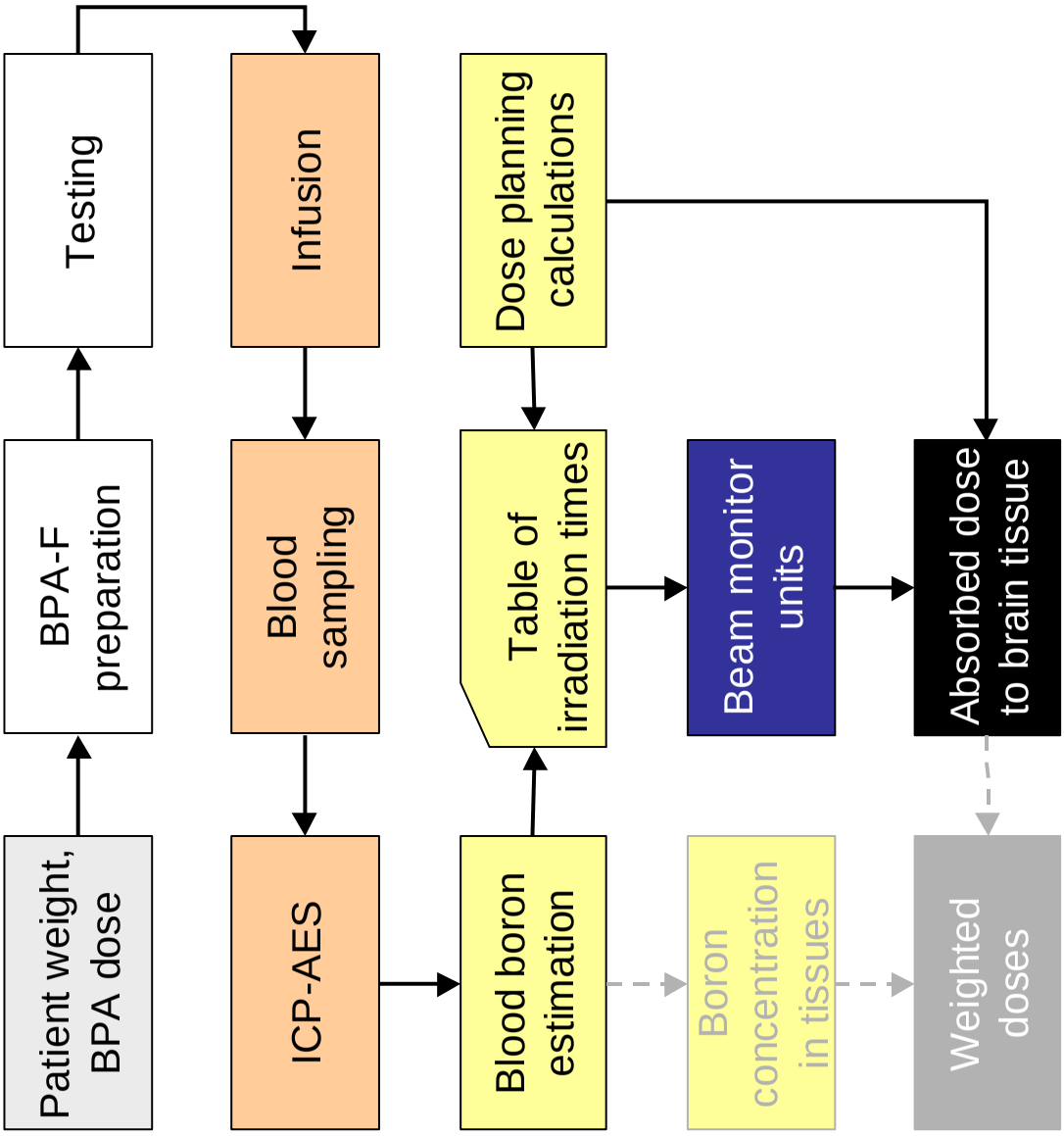

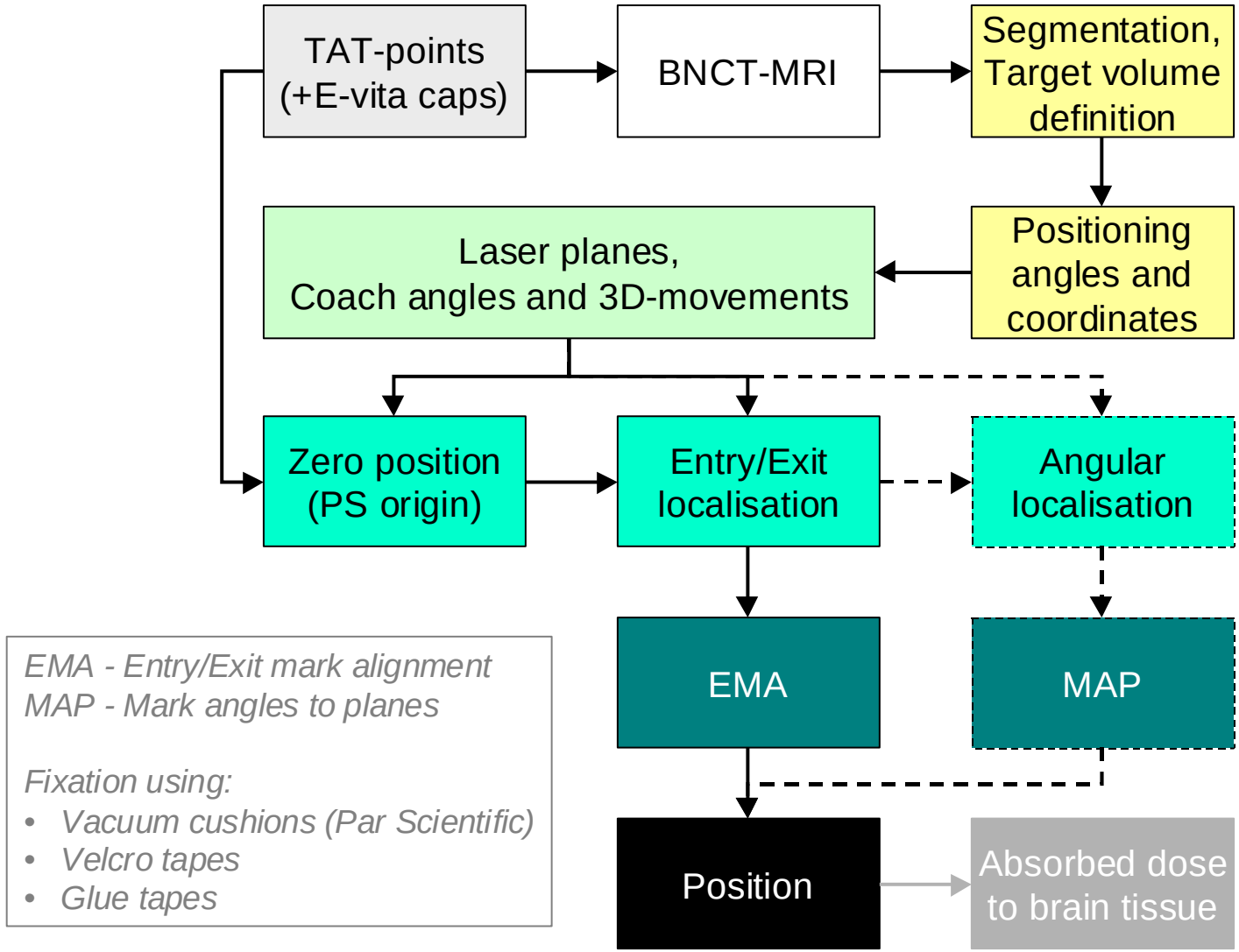
TAT-points
(+E-vita caps)
BNCT-MRI
Segmentation,
Target volume
definition
Laser planes,
Coach angles and 3D-movements
Positioning
angles and
coordinates
Zero position
(PS origin)
Entry/Exit
localisation
Angular
localisation
EMA
MAP
Position
Absorbed dose
to brain tissue
EMA - Entry/Exit mark alignment
MAP - Mark angles to planes
Fixation using:
• Vacuum cushions (Par Scientific)
• Velcro tapes
• Glue tapes

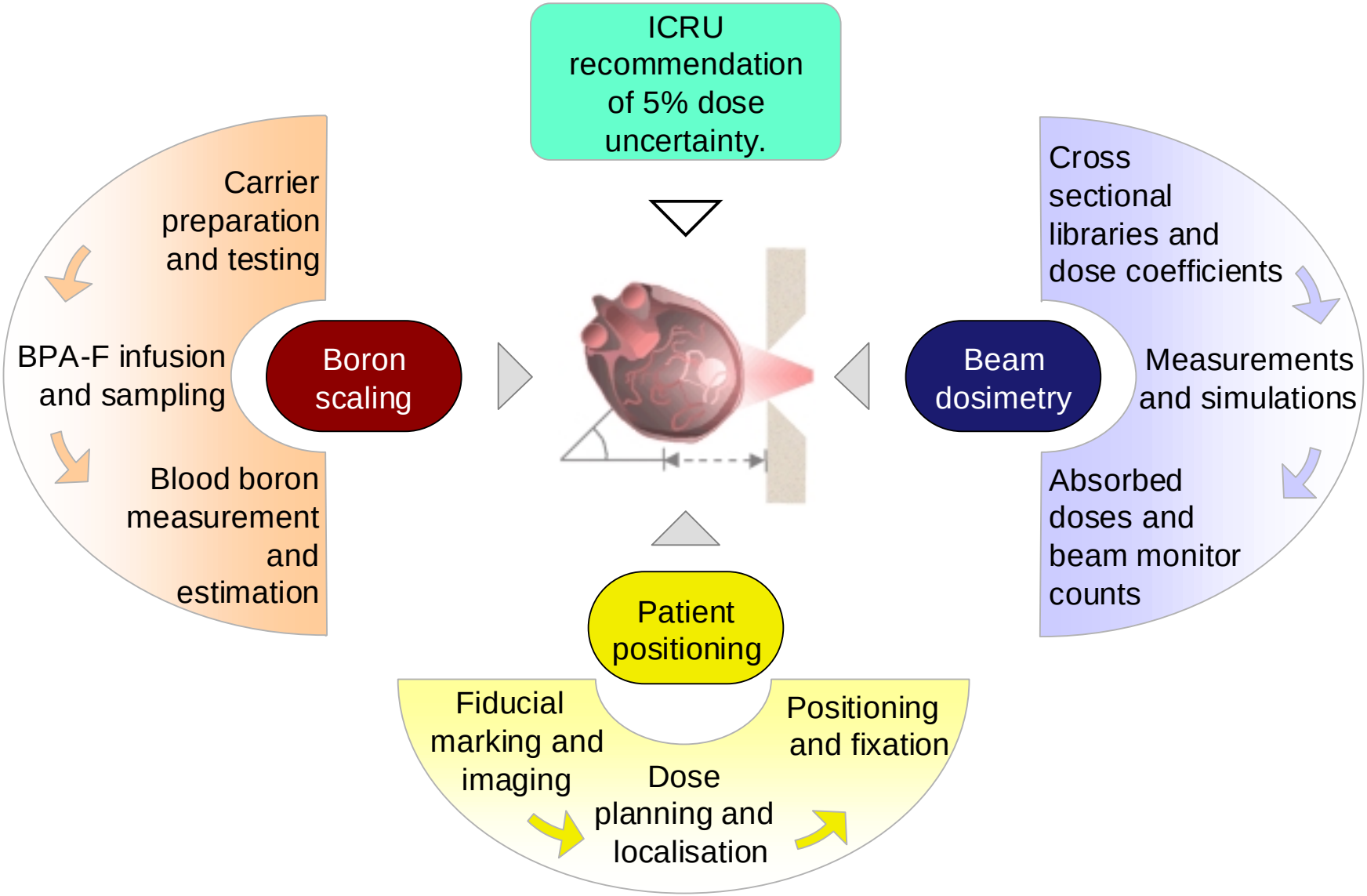

Appendix 4 - Implementation model

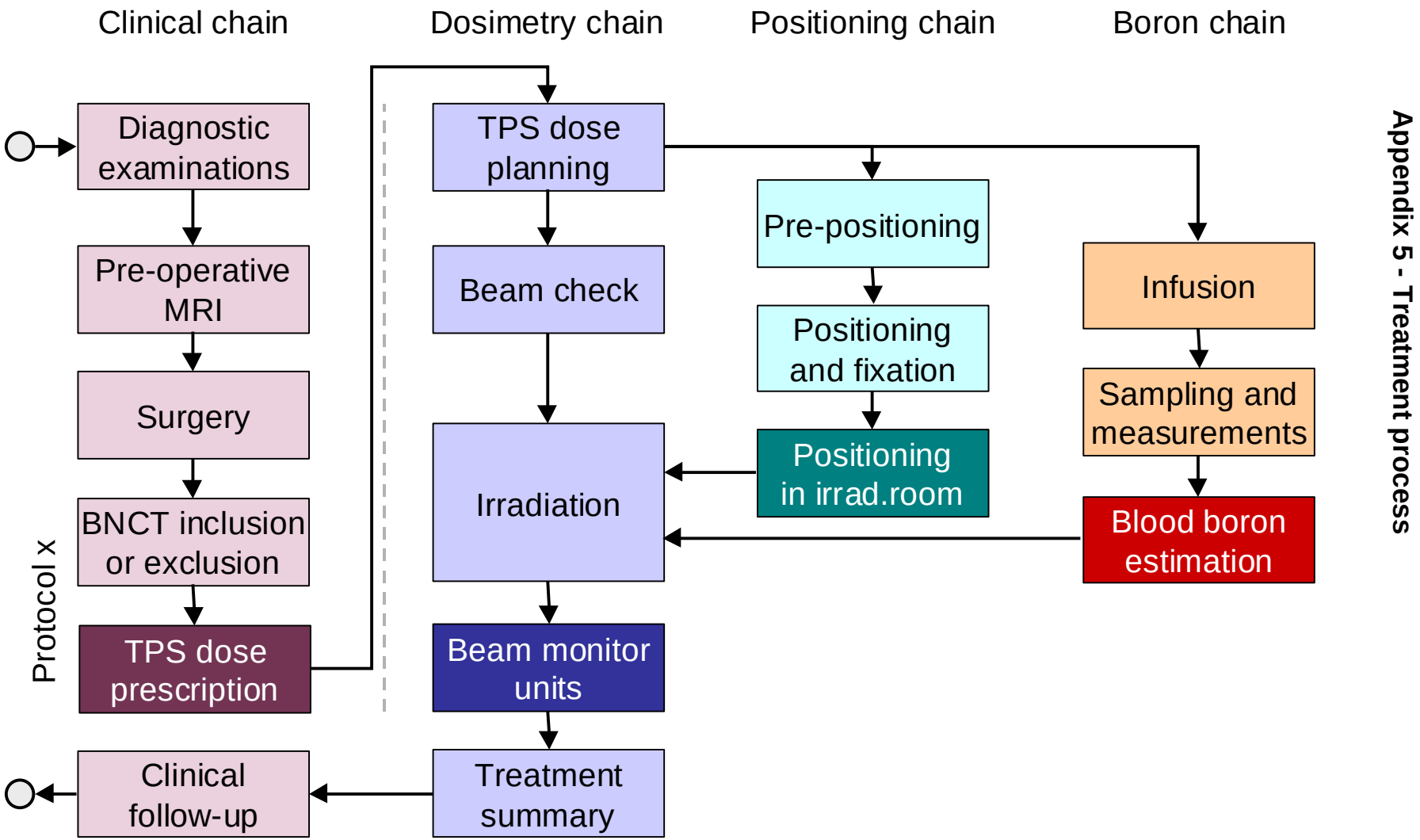
Clinical chain
Dosimetry chain
Positioning chain
Boron chain
Diagnostic examinations
Pre-operative MRI
Surgery
BNCT inclusion or exclusion
TPS dose prescription
Protocol x
Clinical follow-up
TPS dose planning
Beam check
Irradiation
Beam monitor units
Treatment summary
Pre-positioning
Positioning and fixation
Positioning in irrad.room
Infusion
Sampling and measurements
Blood boron estimation
Appendix 5 - Treatment process

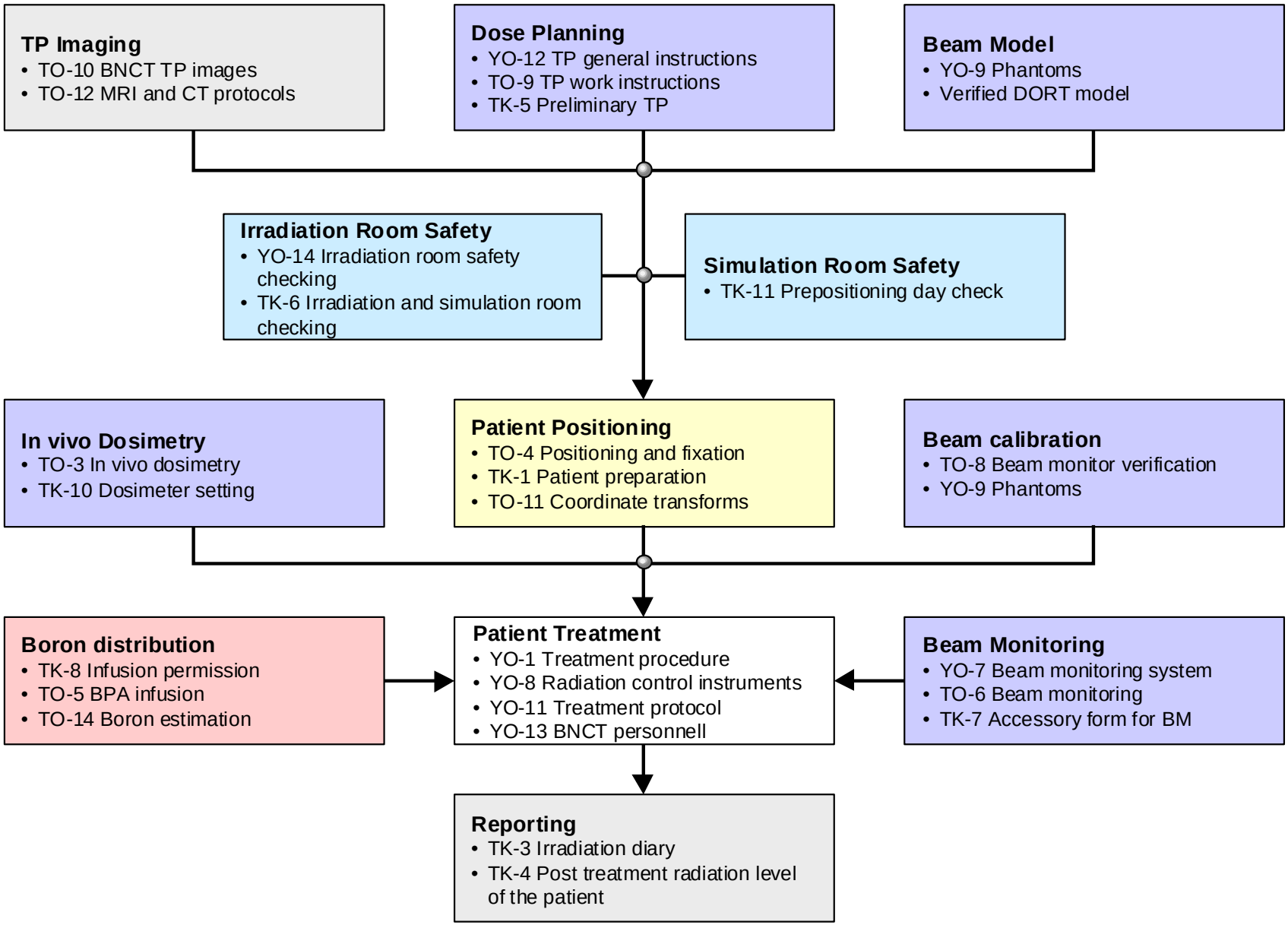

Appendix 6 - Quality control chain

Appendix 7 - Uncertainty of the dose

Radiation interaction uncertainties	Photons mass energy absorption coef	Nitrogen kerma factor	Hydrogen kerma factor	Boron kerma factor
	1 %	5 %	1 %	5 %
Ref			ICRU 46	Estimated

Gamma dose and neutron fluence uncertainties	Total gamma	Thermal	Epithermal	Fast
	4 %	4 %	4 %	25 %
Ref			Kortesniemi 2001	Estimated

Dose rates (Gy/h) in reference point (thermal maximum)	Gamma	Nitrogen	Fast	Boron
Target	5.0	0.9	0.2	18.6
Normal brain	5.0	0.9	0.2	5.3
Ref				IAEA Tecdoc 2001

Components	Positioning	Boron	B-ratio
	max dose effect	*in blood*	*in tissue*
Uncertainty (target)	*from 5mm displ.*		15.0 %
Uncertainty (brain)			30.0 %
Uncertainty (brain+target)	5.0 %	3.0 %	23.8 %
Ref	Simulation	Bi-exp est.	Palmer 2001

Components	Gamma	Nitrogen	Fast	Boron
Share (target)	20.3 %	3.7 %	0.8 %	75.3 %
Share (normal brain dose)	43.9 %	7.9 %	1.8 %	46.5 %
Share w/o boron dose	82.0 %	14.8 %	3.3 %	void
Uncertainty (target)	4.2 %	6.4 %	25.0 %	16.6 %
Uncertainty (normal brain dose)	4.2 %	6.4 %	25.0 %	30.8 %
Uncertainty (brain+target)	4.2 %	6.4 %	25.0 %	24.8 %
Ref				Kortesniemi 2001, IAEA Tecdoc 2001

Uncertainty factors	brain	target
Physical dose	17.1 %	13.8 %
Physical dose w/o boron	5.2 %	
Positioning	5.0 %	

Combined uncertainty	brain	target
Total physical dose	**18 %**	**15 %**
Total phys dose w/o boron	**7 %**	

Positioning data 12.02.2002 XXP01-02 12344M

Positioning date	11.02.2002

Schedule

Event	Time	Total duration	Event duration
Start	12:00	0:00	0:00
Zero position ready	12:20	0:20	0:20
Beam point localization and marking			0:12
1-Entry	12:25	0:25	0:05
1-Exit	12:27	0:27	0:02
2-Entry	12:30	0:30	0:03
2-Exit	12:32	0:32	0:02
Field positioning			0:48
1-Field position ready	13:00	1:00	0:28
2-Field position ready	13:20	1:20	0:20
Positioning done	13:30	**1:30**	0:10

Settings

1-Field	Coach coordinates	x	-182	mm
		y	-139	mm
		z	-82	mm
Aperture size [cm]	Coach angle	phi	55,0	deg
14	Head rest settings	lateral	106,0	cm
		angular	8,0	cm

Entry deviation	0	mm
Exit deviation	0	mm

in final positioning

2-Field	Coach coordinates	x	64	mm
		y	-125	mm
		z	-43	mm
Aperture size [cm]	Coach angle	phi	52,5	deg
14	Head rest settings	lateral	91,2	cm
		angular	12,5	cm

Entry deviation	1	mm
Exit deviation	0	mm

in final positioning

Beam Data	12.02.2002	XXP01-02	12344M

Field 1	250 kW

Aperture Ø	14	cm
Field ratio	60	%

Dose	Planned	Revised	
Blood boron	17,0	17,5	ppm
Ref duration	28,2	27,8	min
N1	58969584	58133136	cts
N2	260436363	256742230	cts
N3	120971023	119255122	cts
Est duration	25,3	24,9	min

Timing	start	stop	
Clock	14:01:15	14:26:21	hh:mm
Elapsed time	170	195	min
Duration min	25,1	14:26:30	est stop

Results	cts	ratio	
N1	59088278	100,2 %	true/planned
N2	261222681	100,3 %	
N3	121092130	100,1 %	

Ref N1	N1	N2	N3
34852	38900	171800	79800

Field 2	250 kW

Aperture Ø	14	cm
Field ratio	40	%

Dose	Planned	Compensated	
Blood boron	15,0	0,97535	factor
Ref duration	20,0	19,5	min
N1	41822400	40791671	cts
N2	185074899	180154476	cts
N3	85908384	83680601	cts
Est duration	17,9	17,5	min

Timing	start	stop	
Clock	15:05:52	15:23:32	hh:mm
Elapsed time	235	253	min
Duration min	17,7	15:23:20	est stop

Results	cts	ratio	
N1	40879625	100,2 %	true/planned
N2	180711252	100,3 %	
N3	83871444	100,2 %	

N1	N2	N3
38800	171700	79700

Appendix 9 - Treatment log (Beam data)

Appendix 10 - Treatment log (Boron data)

Boron Data	12.02.2002	XXP01-02	12344M

Infusion start	Infusion stop	Infusion start	Infusion stop	Patient weight	BPA infusion	Blood volume	B inf velocity	BPA mass	Boron n	Boron mass	B inf velocity
hh:mm:ss	hh:mm:ss	min	min	kg	mg/kg	litres	μg_B/g/min	g	mol	g	mg/min
11:11:00	13:11:00	0	120	72,0	360	5,3	2,168	25,9	131,8	1,4	11,5

Sample	Time	Time	Boron
#	hh:mm:ss	min	ppm
1	11:11:00	0	0,0
2	11:31:00	20	10,9
3	11:51:00	40	16,0
4	12:11:00	60	22,3
5	12:31:00	80	25,0
6	12:51:00	100	28,2
7	13:11:00	120	29,1
8	13:31:00	140	22,6
9	13:51:00	160	19,2
10	13:57:00	166	18,5
11	14:33:00	202	16,1
12	15:02:00	231	15,0
13	15:32:00	261	14,0
14			
15			
16			
17			
18			
19			
20			
21			
22			
23			
24			
25			
26			
27			
28			
29			
30			

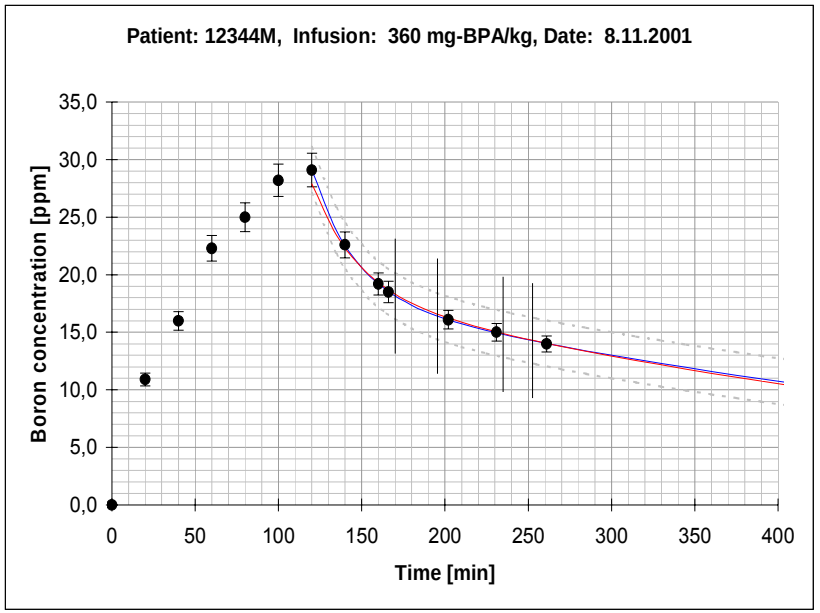

Field 1	Field 2
Average ppm	Average ppm
17,2	14,5
start ppm	start ppm
18,1	14,8
stop ppm	stop ppm
16,4	14,3
start min	start min
170	235
stop min	stop min
195	253
Duration min	Duration min
25,1	17,7

Calculation parameters:	
a1	10,83763
a2	-0,03902
b1	18,27171
b2	-0,00189
T½ fast [min]	18
T½ slow [min]	366
T-50% [min]	135,0
Chi-Square	0,000474527
Iterations	4
Iteration test	0,00000040
Threshold	0,000001
Set T½ fast	x
Set T½ slow	x
Meas B uncert	5
Curve uncert	2

Appendix 11 - Treatment log (Summary)

BNCT-HOIDON YHTEENVETO

	Protokolla	Potilas
Hoitotunniste	XXP01-02	12344M
Hoitopäivä	tiistai, 12.02.2002	

1 - Boori-infuusiotiedot

Infuusiomäärä	360	mg-BPA/kg
Potilaan paino	72	kg
Infuusion kesto	120	min

2 - Boorianalyysi ICP-AES

Näyte	Aika [min]	B [ppm]
1	0	0.0
2	20	10.9
3	40	16.0
4	60	22.3
5	80	25.0
6	100	28.2
7	120	29.1
8	140	22.6
9	160	19.2
10	166	18.5
11	202	16.1
12	231	15.0
13	261	14.0
14	0	0.0
15	0	0.0

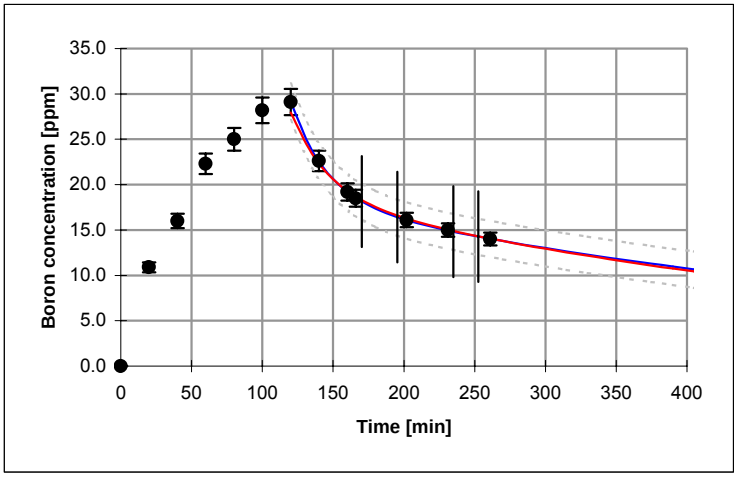

3 - Keskimääräiset booripitoisuudet ja hoitokeilojen ajat

Keila	Arvioitu [ppm]	Toteutunut [ppm]	Alkoi [min]	Loppui [min]
1	17.0	17.2	170	195
2	15	14.5	235	253

4 - Annosyksiköt ja apertuurikoot

Keila	Referenssi säteilytysaika [min]	Määrätyt N1 monitoriyksiköt [cts]	Annetut N1 monitoriyksiköt [cts]	Annettu/Määrätty N1 osuus [%]	Apertuurin halkaisija [cm]
1	28.2	58969584	59088278	100.2 %	14
2	19.5	40791671	40879625	100.2 %	14

5 - Huomautuksia

Alkuperäinen havaintomateriaali on arkistoituna NC-Hoito Oy:n tiloihin FiR 1 BNCT-asemalla.

ISSN 0356-0961
ISBN 951-45-8954-8
ISBN 951-45-8955-6 (pdf-version)
http://ethesis.helsinki.fi/
Helsinki 2002
Yliopistopaino

Errata

No.	Page	Chapter	Erratum
1	13	2	2.6 years
2	24	Figure 3	*Slight distortion in Figure 3C due to rounding of absolute dose values.*
3	40	2	~~incident~~ induced gammas
4	43	2	a spin echo sequence
5	45	1	ratios for the tumour and the healthy tissue
6	48	Equation 6	*The subscript of the denominator ∂a:* ~~1~~ i
7	52	1	~~specificly~~ specifically
8	57	1	a special structure
9	57	2	a T1 weighted imaging sequence
10	68	1	the transaxial rotational laser crosshair

Correction marks: removals (red) striked out, additions (blue) underlined